OPTICAL AND X-RAY DIFFRACTION STUDIES OF POLYNUCLEOTIDES AND THEIR INTERACTION WITH DRUGS

by

HOREA PORUMB, B.Sc. (London)

A Thesis Submitted for the Degree of

Doctor of Philosophy

in the

University of Keele

July 1976

University of Keele,
England.

ABSTRACT

The interactions in solution and the solid state of the antibiotic drugs ethidium bromide, adriamycin and daunomycin with deoxyribonucleic acid have been investigated with the aim of understanding at a molecular level the basis of their chemotherapeutic activity.

Both ethidium bromide and the two related anthracycline drugs adriamycin and daunomycin possess planar aromatic chromophores by virtue of which they can intercalate into the deoxyribonucleic acid helix. A study of the spectroscopic properties of the drugs in solution as a function of concentration, solvent and ionic strength gave an insight into the properties of the drug chromophores, which helped in understanding the spectral changes which take place when complexes form between the drugs and polynucleotides or polyelectrolytes.

A microspectrophotometer was specially constructed to measure the linear dichroism (in the visible range) and the birefringence of oriented fibres and fibre sections of drug-deoxyribonucleic acid complexes and an X-ray diffraction study of the same specimens was carried out in parallel.

It was found that a change in the degree of hydration of the nucleic acid helices results in a redistribution of the drug molecules between the intercalated and non-intercalated states. The intercalation is driven by hydrophobic forces (additional stabilization being gained from specific electrostatic and hydrogen bonding interactions) and is opposed by the hydrophilic nature of some features of the drugs. The helix pitch increases with increasing relative humidity up to a maximum value which may represent the situation in which no nett increase in the fraction of intercalated drug is possible because these two effects counterbalance each other. An estimate of the lower limit to the values of the unwinding angle of the deoxyribonucleic acid

helix at the site of intercalation was made on the basis of the maximum pitch values. This angle ($12^{o} \pm 3^{o}$) fitted the data obtained from both ethidium bromide and the anthracyclines.

Ethidium bromide dissociates completely from the intercalated state at low humidities, whereas a large fraction of the anthracycline molecules remain intercalated even at very low relative humidities. The enhanced chemotherapeutic activity of adriamycin, as compared to daunomycin, was associated with the observed increased stability of the intercalated state of adriamycin under conditions of low hydration and could be justified in terms of an additional hydrogen bond formed by adriamycin with the DNA backbone.

While the X-ray diffraction technique provides information mainly on the drug species which is intercalated, the linear dichroism and birefringence reflect the state of both intercalated and non-intercalated species present in the fibre. A quantitative analysis of the combined X-ray diffraction and optical data, coupled with computer simulations of the fibre dichroism and birefringence, produced on one hand, a picture of the degree of internal alignment of the helices in the fibre and, on the other hand, an estimate of the orientation of the non-intercalated species. It was concluded that in the case of ethidium bromide, and possibly, in the case of the anthracyclines, the non-intercalated drug is externally bound, essentially perpendicular to the deoxyribonucleic acid helix axis. Limits to the possible tilt angles and orientational freedom of the externally bound species were derived.

ACKNOWLEDGEMENTS

I wish to express my thanks to Professor W. Fuller for having closely supervised this project, for provision of excellent research facilities and for his encouragement and guidance throughout my work both as an undergraduate student and as a postgraduate.

I am specially indebted to Dr. W.J. Pigram for consultation and collaboration, and for critically reading this manuscript. I am grateful to Dr. E.F. Slade, who advised me on the construction of the microspectrophotometer, described in Chapter 3, to Dr. P.M. Bayley, from the National Institute for Medical Research, Mill Hill, who stimulated my interest for the spectroscopic investigations from Chapter 4, to Dr. C. Nave, who gave valuable help with the X-ray equipment, and to T. Porumb who assisted me with the computer simulations of the birefringence and dichroism, from Sections 5.2 and 7.1.

The work on anthracycline-DNA complexes, presented in Section 6.2, was carried out as part of a Cancer Research Campaign project. I would like to thank Dr. T. Sundaresan, who prepared the fibres, obtained the X-ray diffraction data and with whom I discussed the subsequent analysis for this section.

I also wish to convey my thanks to the academic staff and my fellow research students from the Physics Department, University of Keele, for many useful discussions, to the technical staff, for mechanical and electrical assistance in the construction of the microspectrophotometer and for all the photographic work, and to Mrs. J. Gill, for having typed this manuscript.

The costs of the microspectrophotometer and Cary spectrophotometer were covered by grants to Professor W. Fuller from the Science

Research Council and the Cancer Research Campaign respectively.

CONTENTS

Page No.

ABSTRACT

ACKNOWLEDGEMENTS

CHAPTER 1 : INTRODUCTION 1

1.1 The interaction of drugs with the deoxyribonucleic acid 1

1.2 The intercalation model 4

1.3 Intercalation and external binding 6

1.4 Outline of the project 9

References 12

CHAPTER 2 : EXPERIMENTAL TECHNIQUES 16

2.1 The materials 16

2.2 A least squares method for the two component analysis of solution spectra 17

2.3 Oriented drug - DNA fibres 20

2.4 The variation of the dimensions and birefringence of the fibres with the relative humidity 20

2.5 Fibre X-ray diffraction 23

2.6 Absorption spectra and dichroic ratios of fibres and fibre sections 25

References 27

CHAPTER 3 : THE CONSTRUCTION OF A MICROSPECTROPHOTOMETER .. 28

3.1 Introduction 28

3.2 The Basic Design 29

3.3 The construction of the microspectrophotometer .. 32

3.4 The performance 35

Page No.

3.5 Practical aspects related to the work with fibres 36

Appendix 39

References 39

CHAPTER 4 : SPECTROSCOPIC STUDY OF DRUGS AND DRUG-POLYNUCLEOTIDE COMPLEXES IN SOLUTION 40

4.1 Experimental Results 40

4.1.1 Absorption spectra of Ethidium Bromide and Ethidium-DNA complexes in solution 40

4.1.2 Adriamycin and Daunomycin 43

4.2 Interpretation of the Experimental Results 45

4.2.1 The Effect of concentration, ionic strength and solvent on the spectra of the free drugs in solution 45

4.2.2 The interpretation of the absorption spectra of the drugs bound to mucleic acids in solution 53

References 58

CHAPTER 5 : THE BIREFRINGENCE OF THE POLYNUCLEOTIDE FIBRES 61

5.1 Introduction 61

5.1.1 The physical basis of the birefringence .. 61

5.1.2 The measurement of the birefringence 62

5.2 The theoretical simulation of the birefringence of a polynucleotide fibre 64

5.2.1 Background 64

5.2.2 The intrinsic birefringence 64

5.2.3 The form birefringence 67

5.3 Experimental Results 69

5.3.1 The fibre dimensions 69

5.3.2 The variation of the birefringence of the polynucleotide fibres 71

Page No.

5.3.3 The birefringence of the drug-DNA fibres .. 74

References 78

CHAPTER 6 : X-RAY DIFFRACTION RESULTS FROM DRUG-POLYNUCLEOTIDE FIBRES 79

6.1 Introduction

X-Ray diffraction patterns from DNA fibres 79

6.2 Fibres of DNA with adriamycin and daunomycin 82

6.2.1 Experimental results 82

6.2.2 Discussion of the experimental results 84

6.2.2A The interpretation of the variation of the helix pitch as a function of relative humidity 84

6.2.2B Considerations related to the external binding of the drug molecules in the fibre .. 88

6.2.2C Considerations related to the possibility of intercalation into the low-humidity form of the DNA 90

6.3 X-ray diffraction results obtained with EB-DNA fibres 92

References 96

CHAPTER 7 : THE OPTICAL DICHROISM OF DRUG - DNA FIBRES .. 98

7.1 Theoretical considerations 98

7.1.1 Introduction 98

7.1.2 Theoretical simulation of the fibre dichroism 99

7.1.3 An analysis of the dichroism in terms of two bound drug species 101

7.2 Experimental results 103

7.2.1 General 103

Page No.

7.2.2 Dichroism of drug-DNA fibres 105

7.2.2A Anthracycline-DNA fibres 105

7.2.2B Ethidium - DNA fibres 109

7.2.3 Dichroism of fibre sections 110

References 114

CHAPTER 8 : CONCLUSIONS 115

References 119

CHAPTER 1

INTRODUCTION

1.1 The interaction of drugs with the deoxyribonucleic acid

A number of drugs interact with the deoxyribonucleic acid (DNA) in such a way as to prevent its participation as a template in nucleic acid synthesis. Among these, are the drugs ethidium bromide (EB), which displays trypanocidal, antiviral and antibacterial properties (Ref. 1), and the anthracyclines: adriamycin (ADM) and daunomycin (DM), which are used in the treatment of acute leukaemia and solid tumours in man (Ref. 2 and Ref. 3). The interaction of these drugs with DNA constitutes the object of the present investigation.

Ethidium bromide and the anthracyclines inhibit both DNA and RNA (ribonucleic acid) synthesis in vitro (Ref. 4 and Ref. 5). In vivo, EB inhibits DNA synthesis (Ref. 1), selectively interferes with RNA synthesis in mitochondria without interfering with the nuclear RNA synthesis (Ref. 6), and converts yeast cells to respiration deficient 'petite' mutants by interaction with the mitochondrial DNA of these cells (Ref. 7). The anthracyclines inhibit both DNA and RNA synthesis in vivo (Ref. 8), prevent repair - replication in X-irradiated cells and have been reported to cause chromosomal damage, such as fragmentation and mitotic aberration (Ref. 9). When compared to daunomycin, adriamycin is more effective in inhibiting tumour growth in experimental cultures and reducing tumour recurrence (for a review, see Ref. 9). Severe toxic side effects are associated with the clinical use of the anthracyclines, and for this reason such chemotherapy is used only in the acute stages of the disease (Ref. 9).

This study aims towards understanding the mode of action of the

drugs at a molecular level, which is not only of direct relevance in pharmacology - eventually leading to the design of drugs with improved selectivity and enhanced chemotherapeutic activity, but, because this study clarifies basic concepts regarding the interaction of small molecules with DNA, it is also a first step towards understanding the interaction between the DNA and more complex systems, such as enzymes and regulatory proteins (Ref. 10).

The chemical structures of ethidium bromide {3,8 diamino - 6 - phenyl - 5 - ethyl phenantridinium bromide}, daunomycin {9 - acetyl - 4 - methoxy - 7, 8, 9 - 10 - tetrahydro - 6, 7, 9, 11 - tetrahydroxy - 5, 12 - naphtacenequinone - 7 - O - (3' - amino - 2',3',6' - trideoxy - α - L - lyxohexopyranoside)} and adriamycin (14 - hydroxydaunomycin) are shown in Fig. 1.1. It will be noted that these drugs possess planar aromatic triple ring systems. The phenantridinium ring of EB carries a positive charge localized on the nitrogen atom in position 5 of the chromophore and, as deduced by X-ray crystallography, the phenyl substituent is oriented at right angles to the main ring (Ref. 11). As regards the crystal structure of daunomycin (Ref. 12), the cyclohexene ring is in the 'half-chair' conformation, the C - 9 atom being displaced towards the C - 9 hydroxyl by about 0.7 Å from the approximate plane of the other atoms of the chromophore; the daunosamine (sugar) substituent, in the 'chair' conformation, is oriented at 100^{o} to this plane. Adriamycin and daunomycin share the same structure, except for an additional hydroxyl group possessed by adriamycin in position 14 of the chromophore. It is challenging to search for an explanation of the different chemotherapeutic activities of these two drugs in terms of the slight difference in their chemical structure.

It is now known that ethidium bromide and the anthracyclines interact with the DNA by the intercalation of their chromophores between

ETHIDIUM BROMIDE

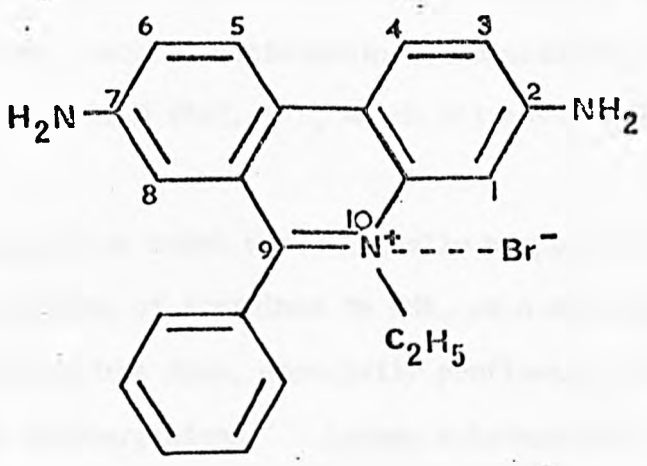

THE ANTHRACYCLINES: DAUNOMYCIN & ADRIAMYCIN

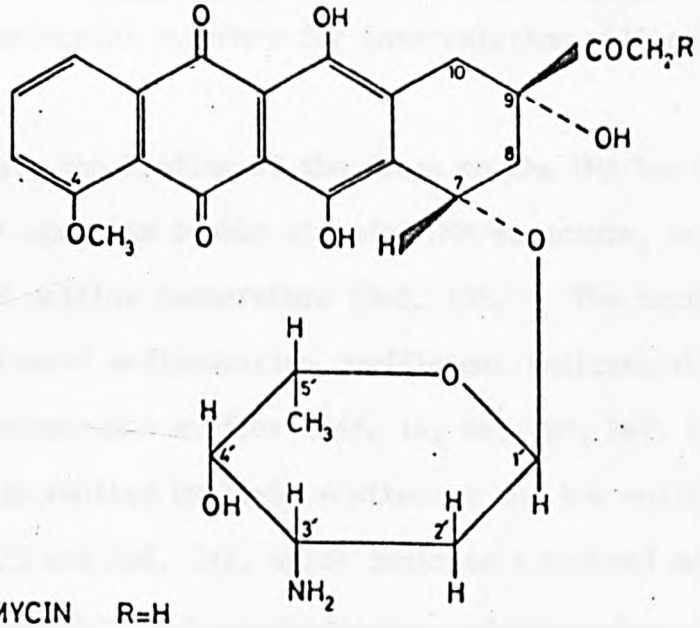

DAUNOMYCIN R=H
ADRIAMYCIN R=OH

FIG. 1.1. CHEMICAL STRUCTURES OF THE DRUGS

adjacent base-pairs of the double helical DNA molecule (Ref. 13 and Ref. 14), in common with a wide range of other antibiotics of clinical and biological importance, such as actinomycin D, nogalamycin, chloroquine, propidium iodide, miracil D (Ref. 15), which all possess planar chormophores.

The intercalation model was originally proposed by Lerman (Ref. 16) for the binding of acridines to DNA, as a molecular basis for the ability of the acridine dyes, especially proflavine, to induce frame shift mutations in microorganisms. Lerman substantiated this hypothesis by a wide range of hydrodynamic, optical and chemical evidence (Ref. 16, Ref. 17 and Ref. 18). Similar evidence was subsequently obtained with other drugs and was subjected to improved quantitative analysis. Detailed reviews on this topic are available elsewhere (see, for example, Ref. 19 for a general discussion; Ref. 9 for the anthracyclines), therefore the experimental evidence for intercalation will only briefly be mentioned here.

In general, the binding of the drugs to the DNA has a stabilizing effect upon the double stranded DNA structure, as deduced from the increased melting temperature (Ref. 18). The increased viscosity and decreased sedimentation coefficient indicate that the DNA becomes longer, thinner and stiffer (Ref. 16, Ref. 20, Ref. 21 and Ref. 22). This is also implied by light scattering and low angle X-ray scattering (Ref. 23 and Ref. 24), which indicate a reduced mass per unit length, and confirmed by electron microscopy and autoradiography (Ref. 25 and Ref. 26), which indicate an increased DNA contour length. Flow dichroism and fluorescence polarization experiments indicate the approximate perpendicularity of the drug chromophores to the DNA axis (Ref. 17, Ref. 21, Ref. 27 and Ref. 28).

Early X-ray diffraction photographs from oriented drug - DNA

fibres (Ref. 16 and Ref. 13) showed the retention of the 3.4 A meridional reflections, due to the stacking of the base-pairs perpendicular to the helix axis, and a change in the positions of the equatorial reflections, indicating a closer packing of the helices in the fibre. Subsequently, better X-ray diffraction patterns were obtained (Ref. 14 and Ref. 29), showing well defined layer lines, the separations of which were usually smaller than in the case of the control DNA, indicating that the helix pitch had become larger.

The binding of the drugs reduces the supercoiling of the closed circular DNA, as detected by a change in sedimentation velocity or banding density in the ultracentrifuge (Ref. 30 and Ref. 31), indicating that in order to accommodate the dye an unwinding of the helix takes place.

1.2 The intercalation model

According to Lerman's intercalation model, a 3.4 A gap is formed in between two successive base-pairs in the B-DNA helix, in which the planar drug chromophore is inserted. The hydrophobic drug molecule, away from the aqueous environment, is stabilized in its intercalated state by stacking interactions resulting from the extensive overlap of the π-electron systems of the chromophore and the nucleic acid bases. Insofar as the 3.4 A meridional repeat in the X-ray diffraction patterns is concerned, the drug is equivalent to an extra base pair. As the sugar-phosphate chain is fully extended in the B-DNA, an unwinding of the helix at the site of intercalation is required in order to enable the formation of the intercalation gap. It may be noted that these factors contribute to the increase in helix pitch and cause a reduction of the helix diameter next to the intercalation site.

Fuller and Waring (Ref. 13) refined Lerman's original model and, on the basis of model building studies, suggested an unwinding angle per intercalated drug of 12°. This value was later confirmed by extensive manual model building and a linked-atom least squares computer analysis by Pigram et al (Ref. 14 and Ref. 32) to represent the minimum unwinding angle for an intercalation gap consistent with satisfactory stereochemistry. Referring primarily to ethidium bromide and proflavine, Fuller and Waring also suggested that, in addition to the hydrophobic stacking, the intercalated state could be stabilized by specific hydrogen bonding between the amino groups at the two extremities of the drug chromophores and phosphate groups on the DNA backbone chains. Subsequently, the existence of hydrogen bonding or electrostatic interactions between the intercalated chromophore (or its substituent groups) and the DNA was also postulated for other drugs, such as daunomycin (Ref. 14), actinomycin (Ref. 33) or the acridines (Ref. 34); (see also next section).

Pursuing the computer analysis of the intercalation model, Alden and Arnott (Ref. 35) point out the necessity for the residues adjacent to the intercalation site to unwind slightly as well, in order to relieve strain in the polynucleotide backbone. Thus, while the local unwinding at the site of intercalation may still be of the order of 12°, as in the classical Fuller and Waring model, the authors predict that the turn angle distributed over three polynucleotide residues (90°) would be equivalent to a total unwinding of about 18°. The propagation of the distortion to adjacent residues may provide a rationale for the observation that the drug uptake by the DNA usually saturates at a level of about one drug bound per two base pairs, a situation known as nearest neighbour exclusion (Ref. 36).

It should be pointed out that the pitch values determined from

X-ray diffraction photographs of daunomycin-DNA fibres by Pigram et al (Ref. 14) fitted the theoretical predictions made on the basis of a model with 12^{o} unwinding if one assumed that all the drug molecules present in the fibre were intercalated. However, it became clear from the observation of the variability of the helix pitch with the relative humidity (Ref. 14, Ref. 29, Ref. 32, Ref. 37) that some of the drug molecules in the fibre might not be intercalated. Thus, the 12^{o} unwinding angle, apparently matching the X-ray diffraction data, might be an underestimate of the true value. Indeed, independent estimates of the unwinding angle by fluorescence anisotropy decay studies of EB bound to DNA (Ref. 38) and by CsCl titration studies of EB bound to closed circular DNA (Ref. 39), suggested 17^{o} and 26^{o} respectively, in both cases larger than 12^{o} and nearer to the value predicted by Alden and Arnott.

1.3 Intercalation and external binding

Waring has performed sedimentation studies of closed circular DNA in the presence of various drugs and compared the ability of these drugs to remove the tertiary superhelical turns of the circular DNA (Ref. 15). This study permitted an estimate to be made of the angle of unwinding associated with each drug, taking EB as standard and assuming that all the drug molecules, detected as 'bound' by a solvent partition method, were actually intercalated. The results showed that in each case the unwinding angle per intercalated molecule was lower than that of EB, which implies that the stereochemistry of the intercalation process varies among drugs. Indeed, such a possibility is justifiable on energetic grounds in view of the fact mentioned above that, in addition to the hydrophobic stacking, the intercalated state is also stabilized

by specific interactions. These are usually hydrogen bonding or electrostatic contacts and could impose a variation in the intercalation geometry. Another possible explanation of the apparent difference in the unwinding angles is that a certain fraction of the 'bound' drug molecules were not intercalated, but were probably attached to the exterior of the DNA molecule, in such a way as not to cause unwinding of the helix. It is also possible that both these effects are present at the same time.

Evidence for the coexistence of two modes of binding has been obtained from equilibrium investigations of the interaction with DNA of EB (Ref. 21 and Ref. 40), DM (Ref. 41) and other drugs (Ref. 42), and from kinetic studies, which enable the sequence of the events involved in the binding process to be determined (Ref. 43 and Ref. 44). Intercalation is the 'strong' mode of binding, predominating at low drug to DNA-phosphate ('D/P') ratios. At large D/P ratios, after the strong binding reaches saturation at about one drug per 4 - 5 bases, a 'weak' mode of binding becomes observable, usually by the distinct change in slope of the corresponding Scatchard plot (Ref. 45).

The 'weak' mode of binding is present on its own in the interaction of the drugs with single stranded polynucleotides (Ref. 46) and polyelectrolytes, such as polyphosphate, polystyren sulphonic acid, polyvinyl alcohol (Ref. 21, Ref. 47 and Ref. 48). Because of the ionic strength sensitivity, it is generally accepted that both in these cases and in the interaction with DNA the 'weak' mode of binding consists in an electrostatic attachment of the cationic drug molecules (the drugs being usually protonated at neutral pH) along the negatively charged backbone of the polymers (Ref. 49).

The determination of the distribution of the drug molecules between the two bound states is a difficult task because both inter-

calated and monomeric externally bound species display the same spectral characteristic, namely a visible absorption band red shifted and hypochromic relative to that of the free molecules (Ref. 44; see also Chapter 4). In the case of EB, the two species can be differentiated on the basis of their fluorescence, since the intercalated drug has an enhanced fluorescence quantum yield (Ref. 21 and Ref. 50). However, in general, fluorescence estimates of the fraction of intercalated drug should be treated with caution, since the fluorescence quantum yield is a highly unpredictable parameter. For example, the fluorescence of the intercalated daunomycin is quenched (Ref. 51), whereas for certain acridines the fluorescence quantum yield is a function of the DNA base composition (Ref. 52). An estimation of the total concentration of bound ligand in a drug-polynucleotide complex raises fewer problems and can be obtained by spectroscopic methods (Ref. 49; see also Section 2.2), equilibrium dialysis (Ref. 53), ultracentrifugation (Ref. 54; see also Section 4.1), or the solvent-partition method (Ref. 55).

A number of simple, planar dye molecules, such as the acridines, are characterized by a tendency to aggregate by stacking in concentrated aqueous solutions, the visible absorption spectrum of the aggregate usually being blue-shifted relative to that of the monomer dye. Similar interactions, with the display of the corresponding blue shifted band of the stacked aggregates, are found to take place among acridine molecules bound at neighbouring sites, at the exterior of the polymer chains in acridine-polyclectrolyte or acridine-DNA complexes of D/P ratios near to unity (Ref. 49 and Ref. 56). Such behaviour is not observed with ethidium bromide and the anthracyclines, probably because of steric restrictions to close contact imposed by their side groups. However, an ethidium derivative devoid of the phenyl substituent gains similar stacking behaviour as the acridines (Ref. 55).

The formation of such stacked drug aggregates substantiates the existence of an external mode of binding of the drugs to the DNA. The coexistence of two modes of drug binding will be one of the central aspects investigated in this thesis.

It should be mentioned that with ethidium-RNA complexes the molecular steps involved in binding are to a large extent similar to those of the ethidium-DNA complexes, for which the 'strong' type of binding is the intercalation. Evidence for this comes from kinetic studies (Ref. 57), the absorption spectra (Ref. 40), the shape of the Scatchard plots and the enhanced fluorescence (Ref. 21 and Ref. 58). However, the existing intercalation models have always referred to B-type DNA and never considered explicitly the case of the polynucleotides confined to an A-type structure, like the RNA. The question thus arises whether an intercalative mode of binding would be possible in a polynucleotide structure other than the B form. This point will be taken up in Chapter 6.

1.4 Outline of the project

The discussion presented in the previous sections has shown that the biological activity of several drugs relies on their interaction with the DNA, in particular on the possibility of intercalation into the DNA helix. The previous investigations in this field were carried out on drug-DNA complexes in two phases: in solution and in solid state. The aim of the present project is to continue these investigations and to draw a link between the properties displayed by these complexes in the two phases.

The solution behaviour of ethidium bromide and the anthracyclines is dominated by drug - drug, drug - solvent, drug - counterion and

drug - DNA interactions, the spectroscopic effects of which are often difficult to differentiate. (The similarity between the absorption spectra of the intercalated and externally bound drug is discussed in the previous section.)

The first aim therefore is to characterize these interactions, searching for common features and differences between the two types of drugs (Chapter 4).

For complexes in the solid state, fibre X-ray diffraction is the most powerful technique to relate the changes in the polynucleotide structure to the presence of the intercalating drugs. However, the previous X-ray diffraction experiments were designed primarily for proving that certain drugs intercalate, rather than for obtaining quantitative estimates of the fraction of drug molecules actually intercalated in the fibre. As for the simultaneous existence of an external mode of binding, the solid state investigations have not considered this possibility explicitly. It is felt that the X-ray diffraction technique is capable of providing much more information in this context. An extensive X-ray diffraction study of the variation of the helix parameters with the relative humidity and the drug content was carried out (Chapter 6), in order to determine quantitatively the distribution of the drug among the different modes of binding and to make estimates of the unwinding angle(s) of the DNA helix at the site of intercalation.

In order to clarify the binding behaviour of the drug in the fibres, it was considered beneficial to complement the fibre X-ray diffraction by linear dichroism (in the visible range) and birefringence studies of the fibres. Although these techniques played a major role in the understanding of intercalation and polynucleotide structure (see Section 1.1), they have hardly been exploited in fibre work (Ref. 59).

The measurement of fibre dichroism requires the accurate

recording of absorption spectra of small selected regions of highly absorbant specimens, for which suitable instruments are not generally available. Thus, to enable the measurement of the dichroism and birefringence of the same fibre specimens which are used in the X-ray diffraction study, it was decided to construct a microspectrophotometer with polarized light facilities (Chapter 3).

While the X-ray diffraction technique provides information mainly on the drug species which is intercalated, the fibre dichroism reflects the state of both intercalated and non-intercalated species present in the fibre. At the same time, the birefringence, which reflects the optical anisotropy of both drug and polynucleotide bases, provides information on the polynucleotide structure and the degree of internal ordering in the specimen, thus complementing both dichroism and X-ray diffraction techniques. It is envisaged that by measuring the dichroism and birefringence of fibres as a function of relative humidity, in parallel with the X-ray diffraction measurements, the combined data will provide information on the orientation of both externally bound and intercalated drug species relative to the fibre axis. Moreover, a study of the absorption spectra recorded from fibres will provide the link between the properties of the complex in solid state and in solution.

It is hoped that by combining information obtained by these techniques, one will be able, on the one hand, to understand better the structure of the polynucleotide fibres and, on the other hand, to characterize the state of the drug in the fibre, both in its intercalated and externally-bound forms.

REFERENCES

1. B.A. NEWTON (in); Advances in Chemotherapy (A. Goldin & F. Hawking ed.), Vol. 1, 35, Academic Press (1964), New York.
2. C. TAN, H. TASAKA, K. YU, M.L. MURPHY, D.A. KARNOFSKY; Cancer (1967) 20, 333.
3. M. BOLRON, C. JAQUILLAR, M. WEIL, J. TANZER, D. LEVY, C. SULTAN, J. BERNARD; Lancet (1969), i, 330.
4. H.J. WARING; Biochim. Biophys. Acta (1964) 87, 358-361.
5. T. TAO, J.H. NELSON, C.R. CANTOR; Biochemistry (1970) 9, 3514-3524.
6. E. ZYLBER, C. VESCO, S. PENMAN; J. Mol. Biol. (1969) 44, 195-207.
7. P.P. SLONIMSKY, G. PERRODIN, J.H. CROFT; Biochem. Biophys. Res. Commun. (1968) 30, 232-239.
8. A. THEOLOGIDES, J.W. YARBRO, B.J. KENNEDY; Cancer (1968) 21, 16.
9. A. DI MARCO, F. ARCAMONE, F. ZUMINO; (in): Antibiotics (J.W. Corcoran & F.E. Hahn ed.), Vol. B, Springer-Verlag (1974), Berlin.
10. H.M. SOBELL; Scientific American (1974) 231, 82-91.
11. SUBRAMANIAN, TROTTER, BUGG; J. Cryst. Mol. Stud. (1971) 1, 3.
12. R. ANGUILI, F. ARCAMONE, E. FORESTI, N.W. ISAACS, O. KENNARD, W.D.S. MOTHERWELL, L. RIVA DI SANSEVERINO, D.L. WAMPLER; Nature New Biol. (1971) 234, 78-80.
13. W. FULLER, M.J. WARING; Ber. Bunsenges. Phys. Chem. (1967) 68, 805-808.
14. W.J. PIGRAM, W. FULLER, L.D. HAMILTON; Nature New Biol. (1972) 53, 17-19.
15. M.J. WARING; Prog. Mol. Subcell. Biol. (1971) 2, 216-231.
16. L.S. LERMAN; J. Mol. Biol. (1961) 3, 18-30.

17. L.S. LERMAN; Proc. Nat. Acad. Sci. U.S. (1963) 49, 94-102.

18. L.S. LERMAN; J. Cell. Comp. Physiol. (1964) 64, Suppl. 1, 1-18.

19. V.A. BLOOMFIELD, D.M. CROTHERS, I. TINOCO JR.; Physical Chemistry of the nucleic acids (1974), Harper and Row, New York.

20. D.S. SRUMMOND, N.J. PRITCHARD, V.F.W. SIMPSON-GILDMEISTER, A.R. PEACOCKE; Biopolymers (1966) 4, 971.

21. J. -B. LE PECO, C. PAOLETTI; J. Mol. Biol. (1967) 27, 87-106.

22. G. COHEN, H. EISENBERG; Biopolymers (1969) 8, 45.

23. Y. MAUSS, J. CHAMBRON, M. DAUNE, H. BENOIT; J. Mol. Biol. (1967) 27, 579.

24. V. LUZZATI, F. MASSON, L.S. LERMAN; J. Mol. Biol. (1961) 3, 634.

25. D. FREIFELDER; J. Mol. Biol. (1971) 60, 401-403.

26. J. CAIRNS; Cold Spring Harbor Symp. Quant. Biol. (1962) 27, 311-318.

27. D. GENEST, P. WAHL; Biochim. Biophys. Acta (1972) 259, 175-188.

28. M. LENG, J. RAMSTEIN, V. DEUBEL, J.L. DROCOURT; Stud. Biophys. (1973) 40, 83-90.

29. D.M. NEVILLE JR., D.R. DAVIES; J. Mol. Biol. (1966) 17, 57-74.

30. L.V. CRAWFORD, M.J. WARING; J. Mol. Biol. (1967) 25, 23.

31. W. BAUER, J. VINOGRAD; J. Mol. Biol. (1968) 33, 141.

32. W.J. PIGRAM; Thesis (1968), London University.

33. S.C. JAIN, H.M. SOBELL; J. Mol. Biol. (1972) 68, 1-20.

34. N.J. PRITCHARD, A. BLAKE, A.R. PEACOCKE; Nature (1966) 212, 1360-1361.

35. C.J. ALDEN, S. ARNOTT; Nucleic Acid Research (1975) 2, 1701-1717.

36. D.M. CROTHERS; Biopolymers (1968) 6, 575-584.

37. W.J. PIGRAM, W. FULLER, M.E. DAVIES; J. Mol. Biol. (1973) 80, 361-365.

38. J.L. TICHADOU, D. GENEST, Ph. WAHL, G. AUBEL-SADRON; Biophysical chemistry (1975) 3, 142-146.

39. J.C. WANG; J. Mol. Biol. (1974) 89, 783-801.

40. M.J. WARING; J. Mol. Biol. (1965) 13, 269-282.

41. F. ZUNINO, R. GAMBETTA, A. DI MARCO, A. ZACCARA; Biochim. Biophys. Acta (1972) 277, 489-498.

42. A. BLAKE, A.R. PEACOCKE; Biopolymers (1968) 6, 1225-1253.

43. J.L. BRESSLOFF, D.M. CROTHERS; J. Mol. Biol. (1975) 95, 103-123.

44. H.J. LI, D.M. CROTHERS; J. Mol. Biol. (1969) 39, 461-477.

45. G. SCATCHARD; Ann. N.Y. Acad. Sci. (1949) 51, 660-672.

46. M.J. WARING; Biochim. Biophys. Acta (1966) 114, 234-244.

47. G. WEILL, M. CALVIN; Biopolymers (1963) 1, 401-417.

48. V. VITAGLIANO, L. COSTANTINO; J. Phys. Chem. (1970), 74, 197-202.

49. A.R. PEACOCKE, J.N.H. SKERRETT; Trans. Faraday Soc. (1956) 52, 261-279.

50. L.M. ANGERER, E.N. MOUDRIANAKIS; J. Mol. Biol. (1972) 63, 505-521.

51. A. DI MARCO, F. ARCAMONE; Drug Research (1975) 25, 368-375.

52. B. WEISBLUM; Cold Spring Harbor Symp. Quant. Biol. (1973) 38, 441-449.

53. M. MULLER, D.M. CROTHERS, M.J. WARING; Eur. J. Biochem. (1974) 39, 223-234.

54. P.H. LLOYD, R.N. PRUTTON, A.R. PEACOCKE; Biochem. J. (1968) 107, 353-359.

55. L.P.G. WAKELIN, M.J. WARING; Molecular Pharmacology (1974) 9, 544-561.

56. D.F. BRADLEY, G. FELSENFELD; Nature (1959) 184, 1920.

57. D.E.V. SCHMECHEL, D.M. CROTHERS; Biopolymers (1971) 10, 465-480.

58. BITTMAN; J. Mol. Biol. (1969) 46, 251-268.

59. W.E. SEEDS; Thesis (1951), London University.

CHAPTER 2

EXPERIMENTAL TECHNIQUES

2.1 The materials

The DNA was highly polymerised Calf Thymus DNA (sodium salt) obtained from Miles. The double stranded synthetic RNA poly I poly C was obtained from Sigma. The drugs Adriamycin and Daunomycin (Farmitalia, Milan) were a gift from Professor A. Di Marco. Ethidium bromide was obtained from Boots and Toluidine Blue from Gurr. All the reagents were of analytic grade. Glass - distilled water was used throughout.

The DNA was deproteinized according to the following procedure (Ref. 1): the DNA was first dissolved at 1 mg/ml in 0.001M NaCl after which the salt concentration was increased to 0.1M. It was then mixed with an equal volume of freshly distilled phenol, saturated with a NaCl solution of the same ionic strength. After 20 minutes of gentle shaking the mixture was separated in the centrifuge, the aqueous layer from the top recovered and poured over an equal volume of propanol. The precipitated DNA was collected with a glass rod, washed in 80% ethanol, acetone and then dried. The purification procedure was repeated 1 - 3 times. Finally, the DNA was dissolved in 0.001M NaCl at 1 mg/ml concentration (approx. 3mM, the average molecular weight per nucleotide being 330). The molar absorptivity at 260μm was taken as 6600 $(M\,cm)^{-1}$ representing an average of several published values (Ref. 2). To obtain the lithium salt of the DNA, LiCl was used throughout the purification in place of NaCl.

The synthetic RNA was used without purification. An ionic strength greater than 0.03M had to be used in order to ensure that it

remained double stranded (Ref. 3).

The drugs were dissolved in water. The molecular weight of EB is 395 and the absorptivity at 480μm is equal to 5600 $(Mcm)^{-1}$ (Ref. 4). The molecular weights of ADM HCl and DM HCl are 580.0 and 563.5 (Ref. 5). It was assumed that the absorptivity value of 9860 $(Mcm)^{-1}$, at 480nm, quoted in the literature for DM (Ref. 6), also held for ADM.

No buffer was used in this work, except where indicated (see section 4.1.1). Occasionally, the pH of the samples was measured and found to be close to neutrality.

Solutions of drug - DNA complexes were prepared by gently pouring drug solutions over an approximately equal volume of DNA solution and stirring. This ensured uniform mixing without precipitating. The ionic strength of the components was adjusted to the desired value prior to mixing. Control samples of DNA without drug were prepared for every mixture.

The absorption spectra of the mixtures were recorded on a Cary 118C Spectrophotometer having the DNA control samples in the reference cell. In the visible range, this arrangement cancelled out the effect of light scattering due to the macromolecular phase, and in the UV it enabled the contribution of the drug to the absorption of the mixture to be recorded separately (see section 4.2.2).

2.2 A least squares method for the two component analysis of solution spectra

A computer program based on a least squares method was developed to analyse the visible absorption spectra of drug - DNA mixtures in terms of two given library spectra. The library spectra belong to the two components present in the complex : the free and the bound drug. (The validity of this assumption will be discussed in section 4.2). The

spectrum of the free drug is obtained from a pure drug solution of known concentration. The spectrum of the bound drug is that of a mixture of very large phosphate-to-drug, P/D, ratio in which all the drug may be assumed bound (Ref. 7).

In principle, the function

$$\phi = \sum_{j=1}^{m} (A^{o}j - A^{c}j)^2 \qquad (2.1)$$

is obtained where $A^{o}j$ are the observed absorbances (the spectrum of the mixture), and $A^{c}j$ are the absorbances 'calculated' in terms of the known absorptivities a_1, a_2 and the unknown concentrations c_1, c_2 of the two components according to the formula:

$$A = a_1c_1 + a_2c_2 \qquad (2.2)$$

The sum runs over the points corresponding to m wavelengths.

The 'best' values for c_1 and c_2 are those for which ϕ is minimum, situation which is achieved when the derivatives of ϕ with respect to c_1 and c_2 vanish:

$$\sum_{j=1}^{m} (A^{o}j - A^{c}j) \frac{dA^{c}j}{dC_i} = 0, \quad i = 1,2 \qquad (2.3)$$

By solving the two equations (2.3), the concentrations of free and bound drug in the mixture are obtained.

It may be noted that this treatment can be regarded as an extension of Peacocke and Skerrett's method (Ref. 7) for obtaining the fraction of bound drug, f, based on measuring the absorbances at one wavelength only:

$$f = \frac{A_1 - A}{A_1 - A_2} \qquad (2.4)$$

Indeed, making the notations:

$$f = C_2/(C_1 + C_2),\ A_1 = a_1c_1,\ A_2 = a_2c_2\ , \quad (2.5)$$

it is easy to verify that the equations (2.2) and (2.4) are equivalent.

The advantage of the least squares method is that it relies on the entire absorption spectrum, thus compensating for random errors. It can be easily extended to take into account more components, in the UV for example. The departure from Beer's Law of one component (or both) may not be a problem if an iterative procedure is adopted. For example, in the case of the acridines (Ref. 8, 9), which display a marked redistribution of the band intensities as a result of aggregation at high concentrations, a library of spectra of the dyes at different concentrations should be available. In each cycle of refinement one would use the library corresponding to the concentration obtained in the previous stage.

The computer program received the input spectra digitized with the aid of a "D-mac" pencil-follower. In addition to determining the concentrations C_1 and C_2, the computer program also calculated and plotted against wavelength the 'discrepancies', ΔA, defined by:

$$\Delta Aj = A^Oj - A^Cj \quad (2.6)$$

The program was tested on spectra consisting of two gaussians added in various proportions accompanied by various levels of noise. The concentrations obtained were the expected ones in all the cases, only the ΔA values fluctuated over a wider band if the noise was greater. However, by shifting the baseline of one of the input spectra, the ΔA plot looked like a reduced image of this spectrum. On the basis of this finding, the plot of ΔA was used as a check of the compatibility of the library spectra with the spectrum to be analyzed.

2.3 Oriented drug - DNA fibres

The drug - DNA complexes were concentrated by spinning for about 10 hours in an MSE ultracentrifuge at 40,000 rpm. Each 10ml centrifuge tube contained 1mg of DNA (the P/D ratios ranged over up to two orders of magnitude). With an ionic strength around 0.005M NaCl an excellent pellet was obtained. With lower ionic strengths (0.001) the sedimentation was not complete and with larger ionic strengths (over 0.02) the pellet was too compact. For mixtures more dilute than 1mg DNA in 10ml, filtration through Diaflo membranes was found more convenient than the ultracentifugation.

A drop of the concentrated drug - DNA mixture from the pellet was placed in between the rounded tips of two glass rods about 1mm apart. As the evaporation proceeded, the DNA helices tended to align along the direction joining the two tips, resulting in an oriented fibre. In order to prevent the crystallization of the salt in the fibre, the fibres of high ionic strength were made in the cold room, where they dried over a period of days.

The dry fibres were cut at one end and stored at room temperature and humidity.

2.4 The variation of the dimensions and birefringence of the fibres with the relative humidity

A 3mm thick disc-shaped humidity cell was made to hold the fibre with its glass rod support and to fit onto the specimen stage of the polarizing microscope (Fig. 3.3).

The cell was flushed with nitrogen gas of controlled relative humidity. The gas was humidified by bubbling it through water and then through a saturated solution of an appropriate salt (Ref. 10). The gas

flow was adjusted so that the cell volume was replaced several times in one minute. The relative humidity (RH) was monitored with a paper hygrometer connected at the exit of the cell. (All the hygrometers from the laboratory were calibrated against this one). The hygrometer was not very accurate but readings reproducible within $\pm$ 2 RH units were obtained for repeated experiments with the same salt. Thus, the measured relative humidities form a self-consistent set, although the values obtained for the various salts were not always the ones listed by O'Brien (Ref. 10). The salts employed and the average relative humidities recorded at 21 - 23°C are listed below:

Salt	Nominal RH (O'Brien) %	Average RH obtained %
1. Dry nitrogen	--	33
2. Calcium chloride	33	53
3. Potasium carbonate	44	66
4. Sodium bromide	57	78
5. Sodium chlorate	75	85
6. Potasium chloride	86	91
7. Sodium tartrate	92	92
8. Potasium chlorate	98	94

Each experiment consisted in a series of measurements taken at progressively increasing relative humidities. The fibres were allowed to equilibrate for 1 - 2 hours at each humidity.

The fibre length (l) was measured between two vaterite crystals, as markers, conveniently selected on the edge of the fibre. The diameter of the fibre (d) and birefringence were also measured next to a marker.

The birefringence was measured in white light with a Zeiss

rotary compensator with a calcite plate; the fibre was oriented parallel to the slow axis of the compensator, for negative birefringences, and perpendicular to it for the rare case of positive birefringence. In order to distinguish the interference colours through the colour of a drug - DNA fibre the 60W microscope illuminator was run at its maximum voltage and the condenser aperture was fully open. An infra-red filter was placed below the condenser to protect the specimen from heating.

The angular position (θ) of the calcite plate at which the dark band of compensation appeared was recorded for every humidity. The accuracy of the measurement suffered due to the fact that the relative dispersion (i.e. wavelength dependence) of the birefringence of the fibre was not matched by that of the compensator. The manufacturers of the compensator reckoned that for tilt angles over 20^{o} the zero-order band would not be black, or if a near black band was seen it would not be of zero order; at intermediary pathdifferences the near black band would be replaced by two coloured bands (Ref. 11). The problem was overcome as suggested by Hartshorne and Stuart (Ref. 12). The band that was dark at the highest humidity, when the birefringence was lowest, was assumed to be of genuine zero order (θ min). This band was followed as the specimen was dried down. When the equilibration at the low humidity was reached, the distance (θ_c), in degrees, from this band (now coloured) to the dark band (θ_{max}, the false fringe of compensation) was determined. All the angles θ, between θ_{max} and θ_{min}, recorded for intermediary humidites were then corrected in a progressive fashion, according to the formula:

$$\theta \text{ (corrected)} = \theta - \theta_c(\theta - \theta_{min})/(\theta_{max} - \theta_{min}) \qquad (2.7)$$

The corrected angles of compensation were converted into path differences by interpolating in the table provided by the manufacturers of the compensator. The birefringence (Δn) was calculated as the

ratio of the pathdifference to the fibre diameter (eqn. 5.5, section 5.1.2).

As the relative humidity was increased, the volume of the fibre increased by a factor f, given by:

$$f = (d/d_o)^2(1/l_o) \qquad (2.8)$$

where d_o, l_o are the original, low humidity dimensions. As a consequence, the concentration of the birefringent material and the birefringence decreased by the same factor. The birefringence may be normalized to the low humidity condition with the formula:

$$\Delta n_n = f\,\Delta n \qquad (2.9)$$

In what follows, the birefringence values are quoted after having been normalized according to the equation (2.9).

2.5 Fibre X-ray diffraction

Fibre X-ray diffraction (XRD) photographs were taken with nickel filtered copper Kα radiation, on flat film, using a Searle camera with torroidal optics mounted on an Elliott rotating-anode generator, or in pinhole cameras mounted on Hilgers generators. The pinhole cameras were more suitable for cases when only a small region of the fibre was to be X-rayed.

The fibres were sprinkled with a polycrystalline powder of vaterite (precipitated calcium carbonate), known to produce a diffraction ring corresponding to a spacing of 3.4A, which was used for calibration.

The X-ray cameras were flushed at a moderate rate with helium humidified by the same procedure as described in the previous section. Inside the cameras a pot containing the appropriate saturated salt solution was placed. At least one hour was allowed for the humidity to equilibrate before each exposure. A hygrometer was placed inside the

Searle camera (or connected at the exit of the pinhole camera) and the relative humidity was recorded at the end of each run.

The coordinates of the diffraction spots in the XRD photographs were measured with a two-dimensional travelling microscope. A computer program was written to convert the film coordinates into reciprocal space parameters, according to the procedure outlined below.

In the first part, the radius (R) and the coordinates (Xo,Yo) of the centre of the calibration ring are obtained by an iterative least squares method (developed by Dr. W.J. Pigram). It involves the minimization of the function:

$$\phi = \sum_{j=1}^{m} (r_j - R)^2 \qquad (7.11)$$

with

$$r_j = (X_j - X_o)^2 - (Y_j - Y_o)^2 \quad ^{\frac{1}{2}} \qquad (7.12)$$

where X_j, Y_j are the coordinates of m points on the calibration ring. (For the first cycle, X_o, Y_o are taken as the average of all X_j, Y_j, and R as the average of all r_j). Next, the specimen to film distance (D) is determined using the basic formula (Ref. 13):

$$\frac{1}{d} = \frac{2}{\lambda} \sin\left(\tfrac{1}{2} \tan^{-1} \frac{E}{D}\right) \qquad (7.13)$$

where λ is the wavelength (1.54 A, for the Kα radiation), d is the calibration spacing, and the distance (E) from the centre of the pattern to the diffraction spot is substituted by R.

In the second part, the coordinates X, Y of the diffraction spots are converted into the reciprocal space coordinates , ζ, ξ, using the formulae:

$$\zeta = \frac{Y}{\lambda (D^2 + E^2)^{\frac{1}{2}}} \qquad (7.14)$$

$$\xi = (1/\lambda)\{2 - \lambda^2\zeta^2 - 2(1-\lambda^2\zeta^2)^{\frac{1}{2}}D/(D^2+X^2)^{\frac{1}{2}}\}^{\frac{1}{2}} \qquad (7.15)$$

2.6 Absorption spectra and dichroic ratios of fibres and fibre sections

The absorption spectra of the fibre specimens were recorded using a microspectrophotometer system based on a Zeiss Universal microscope. The construction of the microspectrophotometer is presented in Chapter 3. Because of their large absorbance, only fibres with P/D ratios greater than 20 could be measured directly. For other P/D ratios longitudinal sections, 2 - 4 μm thick, were cut from the fibres by standard electron microscope techniques. The fibres were embedded in Spur's resin (Ref. 14) and allowed to polymerize at 37°C for 2 - 3 days. The sections were cut with a dry glass knife using a Reichert ultramicrotome. Each section was pressed firmly in between two glass slides until the section adhered flat to one of the slides. This slide then became the bottom of the humidity cell already mentioned in section 2.4. The relative humidity was controlled in the manner already described.

The specimen (fibre or section) was placed on the rotating stage of the microspectrophotometer between crossed analyzer and polarizer and oriented for complete extinction. The analyzer was then removed. Visible absorption spectra were recorded for the polarizer orientations perpendicular and parallel to the fibre axis under various relative humidity conditons.

The dichroic ratio (D) is defined as the ratio of the absorbance recorded with the light polarized perpendicular to the fibre to the absorbance recorded with the light polarized parallel to the fibre (eqn.

7.1, section 7.1). The variation of the dichroic ratio was followed as a function of the relative humidity and interpreted quantitatively in terms of the orientation of the drug chromophore in the specimen (Chapter 7).

REFERENCES

1. R. LANGRIDGE, H.R. WILSON, C.W. HOOPER, M.H.F. WILKINS, L.D. HAMILTON; J. Mol. Biol. (1962) 2, 19.
2. W.J. PIGRAM; Thesis (1968), London University.
3. A.R. HODGSON; Thesis (1969), London University.
4. M.J. WARING; J. Mol. Biol. (1965) 13, 269.
5. F. ZUNINO, R. GAMBETA, A. DI MARCO, A. ZACCARA; Biochim. Biophys. Acta (1972) 277, 789-798.
6. A. TUSCONI; Biochim. Biophys. Acta (1966) 123, 627.
7. A.R. PEACOCKE, J.N.H. SKERRETT; Trans. Farad. Soc. (1956) 52, 261.
8. D.F. BRADLEY, G. FELSENFELD; Nature (1959) 184, 1920.
9. D.M. NEVILLE JR., D.R. DAVIES; J. Mol. Biol. (1966) 17, 57-74.
10. O'BRIEN; J. Scient. Instrum. (1948) 25, 73.
11. R.C. FAUST, H.J. MARRIMAN; Brit. J. Appl. Phys. (1955) 6, 351.
12. N.H. HARTSHORNE, A. STUART; Crystals and the Polarising Microscope, Edward Arnold, London, 1970 (4th edition).
13. M.J. BUERGER; X-Ray Crystallography; John Wiley and Sons, New York, 1945 (2nd edition).
14. A.R. SPUR; J. Ultrastructure Research (1969) 26, 31-43.

CHAPTER 3

THE CONSTRUCTION OF A MICROSPECTROPHOTOMETER

3.1 Introduction

The construction of a single beam microspectrophotometer system with polarized light facilities, operating in the visible range, will be described in this chapter.

As it was pointed out in Chapter 1, such a piece of equipment was needed for the study of the optical properties (particularly the dichroism) of drug-nucleic acid specimens in solid state, thus complementing the studies performed on the same kind of specimens using the X-ray diffraction technique. Besides their high cost, the commercially available systems were not particularly suitable for this type of work. The system described in this chapter combines favourably a high performance and flexibility with a low constructional cost. A list of the selected components (indicating their manufacturers) is given in an appendix at the end of the chapter.

The chapter begins with a presentation of the relevant background theory and continues with detailed description of the system. Finally, the performance of the apparatus will be assessed and practical aspects related to the work with fibre specimens (such as the cylindrical lens effect & light scattering) will be outlined.

A microspectrophotometer records transmission or absorption spectra of microscopic specimens. The transmittance at a wavelength λ is defined as:

$$T_\lambda = \frac{I}{I_0} \qquad (3.1)$$

where I is the intensity of light emerging from the specimen (the

"transmitted" intensity), and I_o is the intensity of the incident beam, which should be the same as the intensity of light reaching the detector in the absence of the specimen (called "background" intensity). A plot of T_λ against λ is a transmission spectrum.

The absorbance at a wavelength λ is defined by:

$$A_\lambda = - \log_{10} T_\lambda \qquad (3.2)$$

thus: $$A_\lambda = \log I_o - \log I \qquad (3.3)$$

In other words, the absorbance can be expressed as a difference of the logarithms of the two intensities.

A consequence of the relation (3.1) is that wavelength-dependent factors, such as the detector sensitivity, the output of the lamp, the reflectance of the diffraction grating, etc. have the same multiplying effect on both the numerator and denominator and, therefore, the ratio (the transmittance) remains a property of the specimen alone.

In a single beam spectrophotometer the background and transmitted intensities are recorded separately. The operations (3.1) or (3.3) would still yield the correct spectrum, provided the optical and electronic parameters of the spectrometer remained unaltered during the time taken to make the two recordings. From the above considerations it emerges that stability is an essential requirement for a single beam system.

3.2 The Basic Design

The microspectrophotometer has two basic parts. The first is the optical system, including a conventional microscope, an arrangement to illuminate the specimen with pulsed monochromatic light and an attachment to the microscope head to house the light detector, which is a photomultiplier. The second is the electronic system. It amplifies the photomultiplier signal by phase sensitive detection and displays the

light intensity (or its logarithm) as a function of wavelength.

The optical path can be followed in Fig. 3.1. The white light from the source (S) is focused onto the entrance slit of the monochromator (MC). The monochromator disperses it and focuses a selected wavelength at the exit slit. The widths of the two slits control the spectral bandwidth and the intensity of the light that will ultimately illuminate the specimen.

The emergent beam, periodically interrupted by a chopper (CH), illuminates a rectangular aperture (F). A 45^{o} mirror (MR) joins up the optical axis of the monochromator section with the optical axis of the microscope. The substage condenser (C) forms a reduced image of the aperture F in the plane of the specimen. F is equivalent to the field diaphragm (Fl) of the conventional microscope. The size of the aperture determines the area in the object plane that will be illuminated.

The Universal microscope has a beam splitter (not shown in the diagram), which directs the light either to the inclined binocular head (position normally employed for viewing the specimen), or into the vertical tube which carries the eyepiece (E), or both. The column of the photomultiplier is an extension of the vertical tube of the microscope, the photomultiplier being at the top end.

A part of the main beam branches off at the level of the triple mirror (T) enabling the observation of the specimen through the viewer (V). The object plane is imaged midway up the column in the plane of the measuring aperture (M). The role of M is to isolate from the image of the specimen only the area the transmittance of which is to be measured.

With the aid of a prism (P) light from a pilot lamp (PL) can be projected down through M. The triple mirror (T) directs it towards the viewer where the image of the measuring aperture becomes superimposed onto the field of view. The size of M is adjustable but it is always

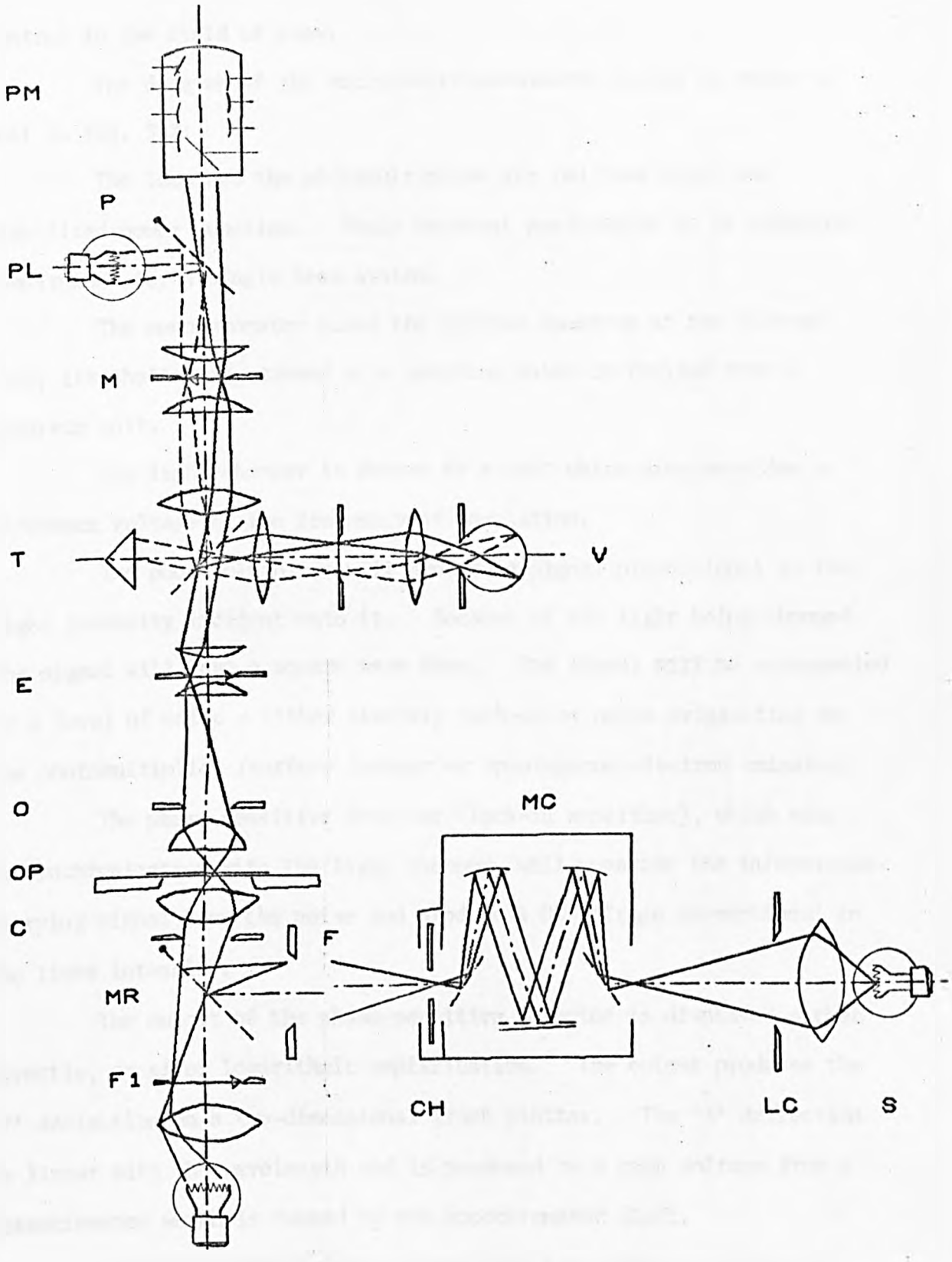

FIG. 3.1 OPTICAL DIAGRAM OF THE MICRO-SPECTRO-PHOTOMETER

(S-LIGHT SOURCE; LC-LAMP CONDENSER; MC-MONOCHROMATOR; CH-LIGHT CHOPPER; F, F1-FIELD APERTURES; MR-SWINGOUT MIRROR; C-SUB STAGE CONDENSER; OP-OBJECT PLANE (SPECIMEN STAGE); O-OBJECTIVE LENS; E-EYEPIECE; T-TRIPLE MIRROR; V-VIEWER; M-MEASURING APERTURE; P-SWING OUT PRISM; PL-PILOT LAMP; PM-PHOTOMULTIPLIER; SM-STEPPING MOTOR; R-RAMP GENERATOR).

central in the field of view.

The diagram of the microspectrophotometer system is shown in full in Fig. 3.2:

The lamp and the photomultiplier are fed from their own stabilized power supplies. Their constant performance is an essential requirement for a single beam system.

The monochromator scans the visible spectrum at the desired rate, its shaft being turned by a stepping motor controlled from a separate unit.

The light chopper is driven by a unit which also provides a reference voltage at the frequency of modulation.

The photomultiplier will produce a signal proportional to the light intensity incident onto it. Because of the light being chopped the signal will have a square wave form. The signal will be accompanied by a level of noise - either electric pick-up or noise originating in the photomultiplier (surface leakage or spontaneous electron emission).

The phase-sensitive detector (lock-in amplifier), which acts in synchronization with the light chopper, will separate the information-carrying signal from the noise and produce a DC voltage proportional to the light intensity.

The output of the phase-sensitive detector is displayed either directly, or after logarithmic amplification. The output produces the 'Y' deflection on a two-dimensional graph plotter. The 'X' deflection is linear with the wavelength and is produced by a ramp voltage from a potentiometer which is turned by the monochromator shaft.

The range control unit ensures that the spectra are always scanned between the same pre-selected wavelengths.

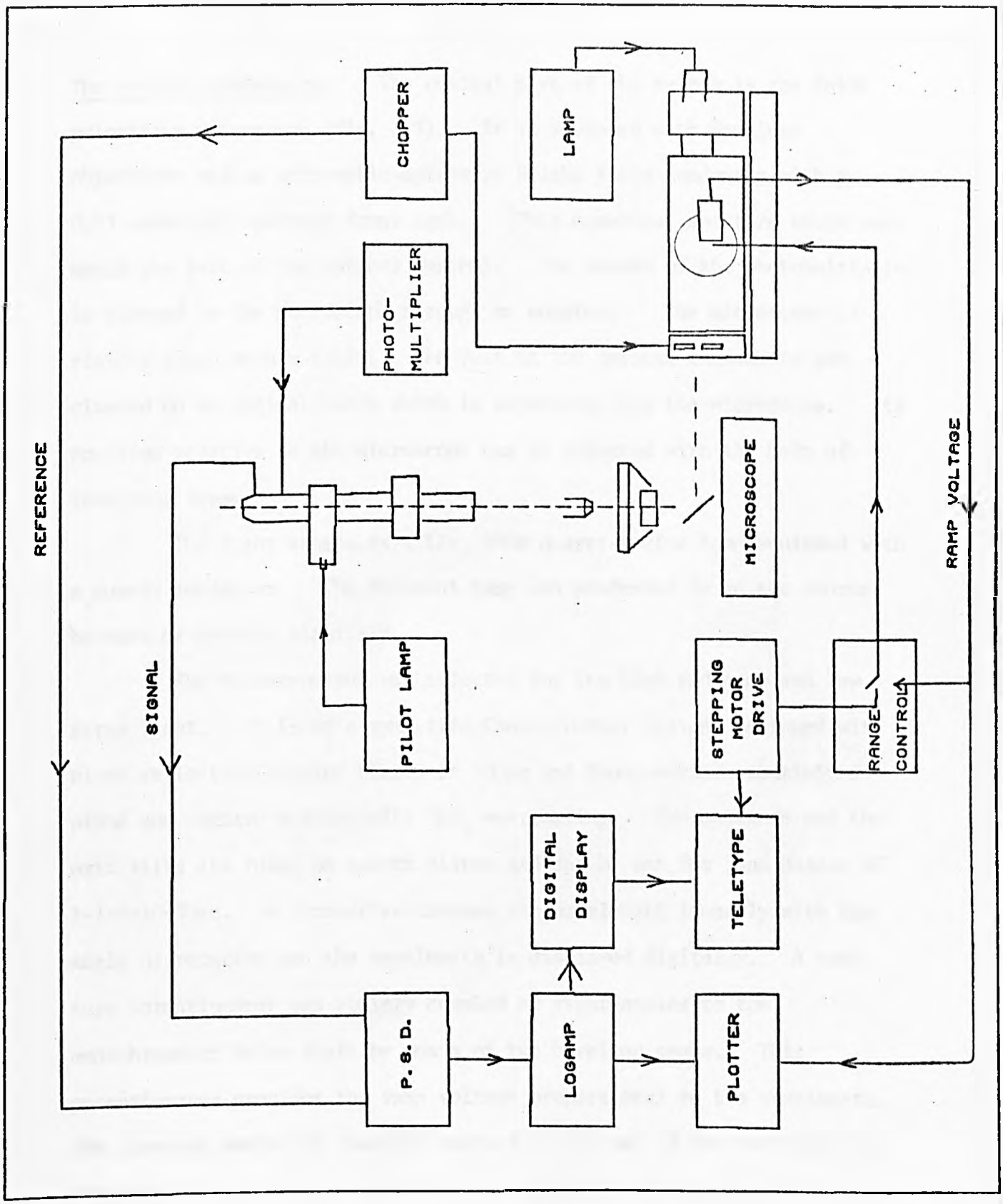

FIG. 3.2 THE FULL MICRO-SPECTRO-PHOTOMETER SYSTEM.

3.3 The construction of the microspectrophotometer

The optical components. The central part of the system is the Zeiss polarizing microscope (fig. 3.3). It is equipped with Neofluar objectives and an achromatic-aplanatic bright field condenser with a 0.63 numerical aperture front lens. (This numerical aperture would best match the rest of the optical system). The column of the photomultiplier is clamped to the microscope through an adaptor. The microscope is rigidly fixed onto a table. The rest of the optical components are clamped on an optical bench which is separated from the microscope. Its position relative to the microscope can be adjusted with the help of levelling screws.

The light source is a 12v, 100W quartz-iodine lamp equipped with a quartz condenser. The filament lamp was preferred to an arc source because of greater stability.

The monochromator was selected for its high radiance and low stray light. It is of a symmetric Czerny-Turner design, equipped with a plane reflection grating blazed at 500μm and front-surface aluminized plane and concave mirrors with MgF_2 overcoating. The entrance and the exit slits are ruled on quartz plates and can be set for band passes of 1-2-5-10-20nm. A sine-drive changes the wavelength linearly with the angle of rotation and the wavelength is displayed digitally. A ten-turn potentiometer was rigidly coupled at right angles to the monochromator drive shaft by means of two bevelled gears. This potentiometer provides the ramp voltage proportional to the wavelength. The stepping motor was flexibly coupled to the end of the shaft and the stepping motor control unit enables the scanning of the visible spectrum in both directions at a continuously adjustable speed. A revolution represents 100μm and the wavelength increments are of either 0.5 or 0.25nm per step.

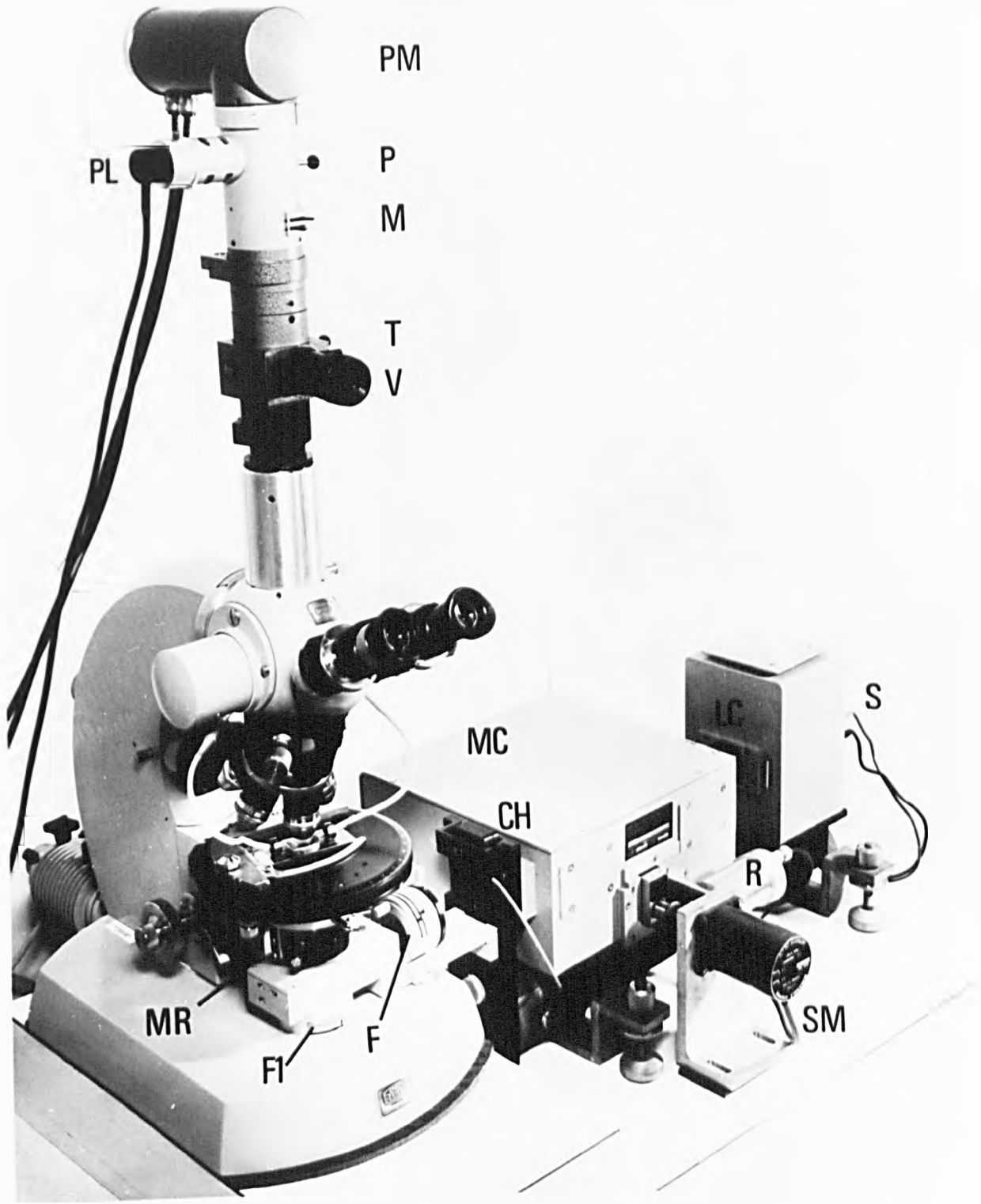

FIG. 3.3 THE MICROSPECTROPHOTOMETER

The light modulator is a compact vibrating-vane chopper operating at the frequency of 110Hz. A synchronous sine wave output is provided for driving the reference input of the phase sensitive-detector.

The field aperture is a four-leaf diaphragm of continuously adjustable size. Its centring mount is clamped on the holder of the 45^{o} mirror. The mirror holder is adjustable, firmly fixed on the optical bench, and does not rest on the microscope. The 45^{o} mirror is front surfaced. It can swing out when the microscope is to be used with its own light source.

The alignment of the optical components is essential for minimizing the stray light and is carried out in two stages. The first stage, in which the monochromator is removed from the bench, consists in achieving a unique optical axis for the lamp, its condenser lens, the 45^{o} mirror and the optical axis of the microscope, such that the image of the slit of the lamp condenser is in the centre of the field of view of the microscope. In the next stage the monochromator is set along the same optical axis. The chopper is then mounted and centered such that the square-wave photomultiplier signal, monitored on a cathode-ray screen, indicates equal intervals of light and dark.

The Detection System. The photomultiplier is a "side-on" RCA type 931A tube, operated at 1kV from its own stabilized power supply. The signal is developed across a load resistor of 56 Kohm. The quantum efficiency (or the response) of the photomultiplier as function of wavelength is shown in Fig. 3.4. Fig. 3.7 shows the characteristic spectrum (or the "background intensity") recorded in absence of any specimen. The bell-like shape of the intensity curve arises from the combined effect of the photomultiplier response (which is greater in the blue region of the spectrum), of the emissivity of the lamp (which is

FIG. 3.4 SPECTRAL RESPONSE OF THE PHOTOMULTIPLIER
(ARBITR. UNITS)
AND THE EMISSIVITY OF THE LAMP

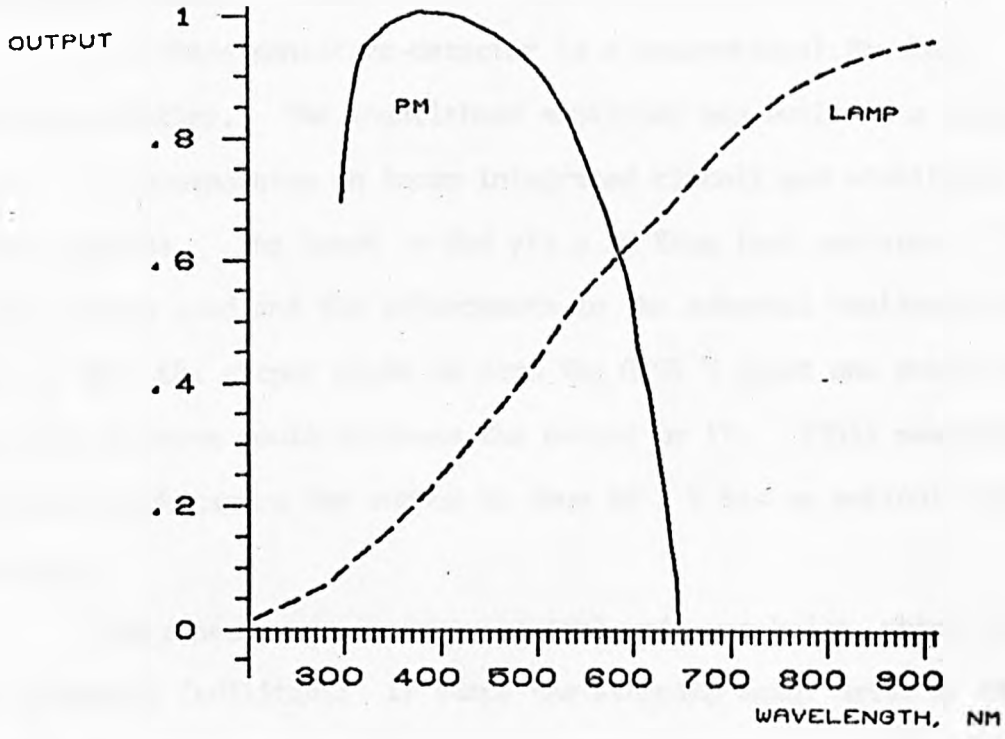

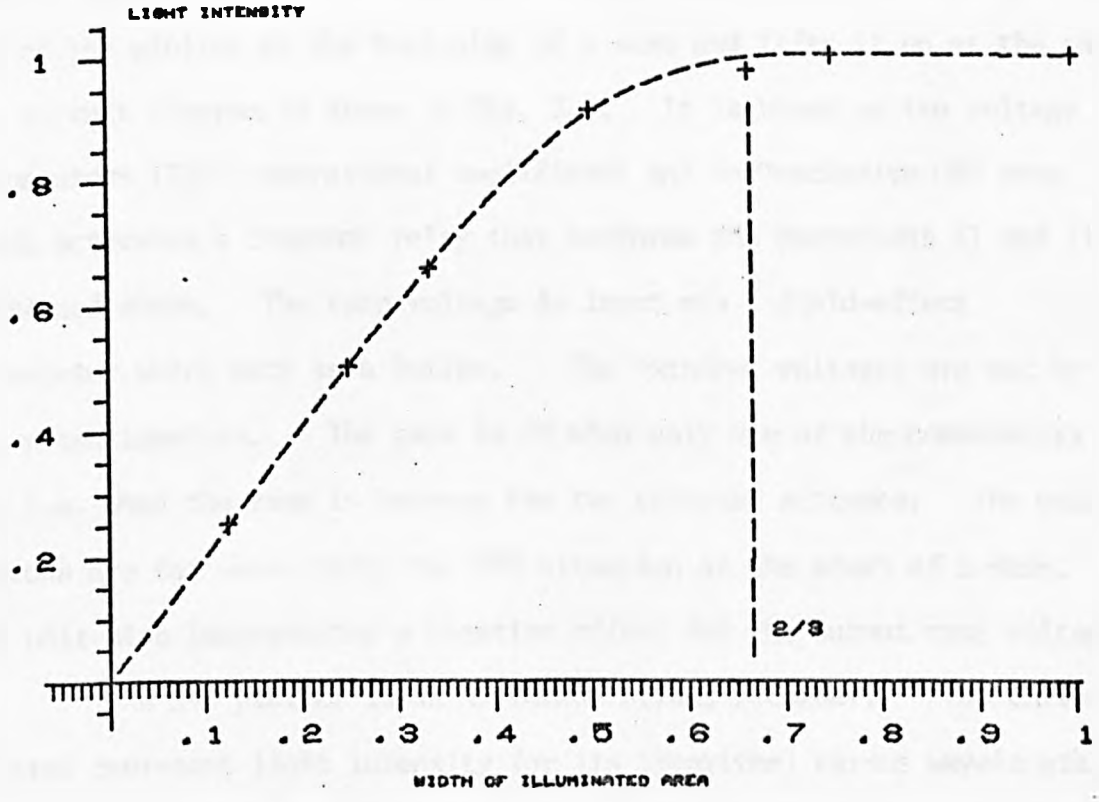

FIG. 3.5 INTENSITY OF LIGHT TRANSMITTED BY A CYLINDRICAL DNA FIBRE AS FUNCTION OF THE FRACTION OF THE FIBRE DIAMETER ILLUMINATED. THE MEASURING APERTURE HAD THE SAME WIDTH AS THE FIBRE. (FIBRE DIAMETER 0.1 MM, WAVELENGTH 525 NM, RELATIVE HUMIDITY 75 %)

greater towards the infra-red end of the spectrum, as shown in Fig. 3.4) and of the blazing of the diffraction grating (which has a maximum reflectance around 500nm).

The phase sensitive-detector is a conventional Brookdeal lock-in amplifier. The logarithmic amplifier was built as a separate unit. It incorporates an Ancom integrated circuit and stabilized power supplies. The input is fed via a 10 Kohm load resistor. The choice of the load and the adjustments to the external resistors were made so that the output would be zero for 0.01 V input and every ten-fold increase in input would increase the output by 1V. (This means that a specimen which causes the output to drop by 1 V has an optical density of unity.)

For convenience, a range-control unit was built, which provides the following facilities: i) stops the stepping motor drive at the two extreme values of a pre-selected wavelength range; ii) depresses the pen of the plotter at the beginning of a scan and lifts it up at the end. The circuit diagram is shown in Fig. 3.6. It is based on two voltage comparators (710 - operational amplifiers) and an "exclusive-OR" gate which activates a compound relay that performs the operations i) and ii) mentioned above. The ramp voltage is input via a field-effect transistor which acts as a buffer. The "window" voltages are set by two potentiometers. The gate is ON when only one of the comparators is ON, i.e. when the ramp is between the two selected extremes. The push-buttons are for over-riding the OFF situation at the start of a scan. The unit also incorporates a negative offset for the output ramp voltage.

The X-Y plotter is an A3 format Bryans recorder. The curves plotted represent light intensity (or its logarithm) versus wavelength. In order to obtain the absorption spectrum of a specimen two consecutive scans are required, as explained in section 3.1: the first one, giving

ELECTRONIC WINDOW OR HIGH AND LOW VOLTAGE COMPARATOR

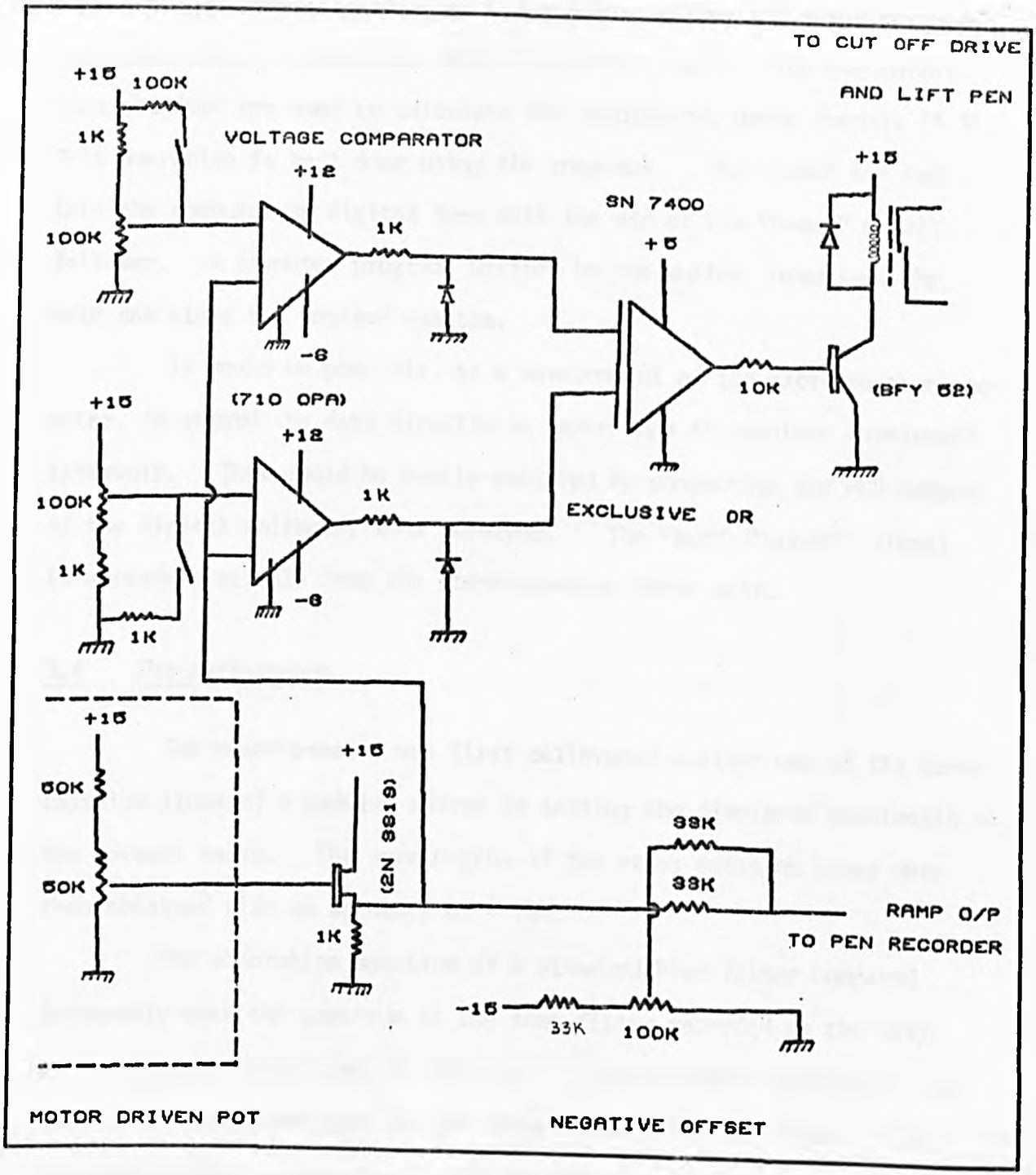

FIG. 3.6 THE CIRCUIT DIAGRAM FOR THE RANGE CONTROL UNIT OF THE MICRO-SPECTRO-PHOTOMETER.

the "transmitted" intensity, and the second one, for the "background" intensity (see Fig. 3.7). All the settings, i.e. the position of the polarizer, the magnification and the openings of the field and measuring apertures have to remain the same for the two scans. The two curves thus obtained are used to calculate the absorbance, using formula (3.3). This operation is best done using the computer. The curves are fed into the computer in digital form with the aid of the "D-mac" pencil follower. A computer program, written by the author, processes the data and plots the desired spectra.

It would be possible, as a development of the microspectrophotometer, to record the data directly on paper tape at constant wavelength intervals. This could be easily achieved by connecting the BCD output of the digital voltmeter to a teletype. The "act" ("punch") signal is already available from the stepping-motor drive unit.

3.4 The performance

The monochromator was first calibrated against one of the known emission lines of a cadmium source by setting the displayed wavelength to the correct value. The wavelengths of the other emission lines were then obtained with an accuracy of $\pm$ 1nm.

The absorption spectrum of a standard blue filter compared favourably with the spectrum of the same filter recorded on the Cary spectrophotometer as shown in Fig. 3.8. The agreement between the two spectra is remarkably good in the range between 410 and 610nm. The accuracy of the reproduction breaks down for wavelengths greater than 610nm, which is, in fact, the region where the intensity of the recorded signals becomes very low. Correct absorbance values were also obtained for calibrated neutral density filters, for any orientation of the polarizer and irrespective of the magnification employed, provided

FIG. 3.7

BLUE FILTER. TRANSMISSION SPECTRUM.

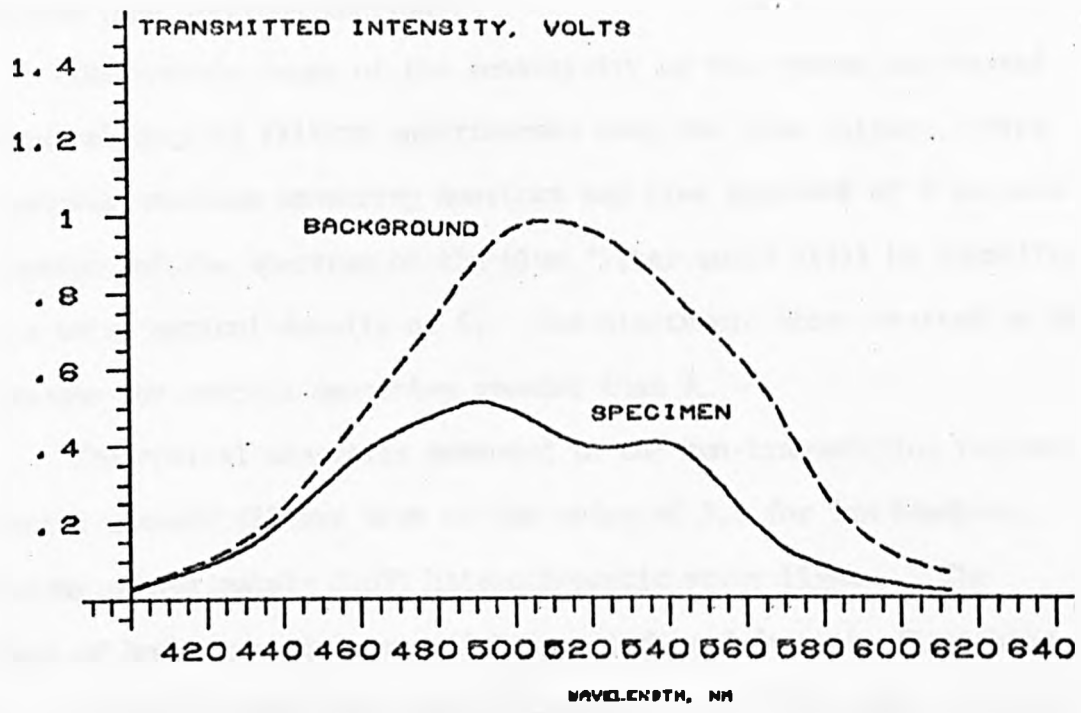

FIG. 3.8

ABSORPTION SPECTRA OF A BLUE FILTER

FULL LINE: RECORDED WITH THE MICROSPECTROPHOTOMETER

DASHED LINE: RECORDED WITH THE CARY SPECTROPHOTOMETER

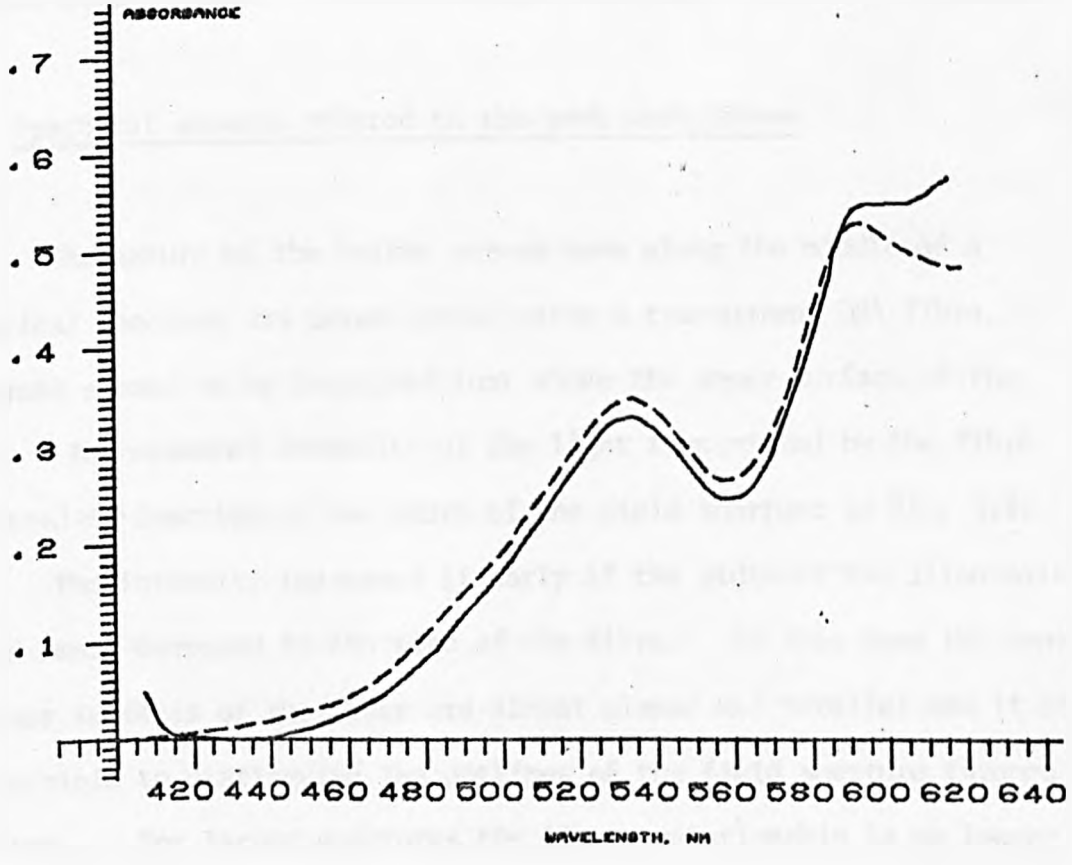

the transmitted and background intensities were recorded in the same conditions (see previous section).

The dynamic range of the sensitivity of the system was tested with neutral density filters superimposed over the blue filter. With 1nm bandpass, maximum measuring aperture and time constant of 3 seconds the features of the spectrum of the blue filter could still be identified up to a total optical density of 5. The electronic noise started to be troublesome for optical densities greater than 4.

The optical densities measured in the non-transmitting regions of several cut-off filters were of the order of 3.5 for 2nm bandpass, indicating approximately 0.03% heterochromatic stray light. The presence of homochromatic stray light was inferred from the flattening of the absorbance peaks for optical densities over 3, but this was very much dependent on the specimen used.

The thermal, mechanic and electronic stability of the system was found satisfactory. The wavelength was stable within 1 nanometre.

3.5 Practical aspects related to the work with fibres

The nature of the bright streak seen along the middle of a cylindrical specimen was investigated using a transparent DNA fibre. The streak seemed to be localized just above the upper surface of the fibre. The measured intensity of the light transmitted by the fibre is plotted as a function of the width of the field aperture in Fig. 3.5.

The intensity increases linearly if the width of the illuminated area is small compared to the size of the fibre. In this case the upper and lower surfaces of the fibre are almost planar and parallel and it is even possible to distinguish the outlines of the field aperture through the fibre. For larger apertures the linear relationship is no longer

obeyed and when the width of the image of the field aperture approaches that of the fibre the recorded intensity is practically constant. This is because of the cylindrical lens effect of the fibre which makes the outer rays be deflected by an angle larger than the angle corresponding to the numerical aperture of the objective. In addition, the outer rays, incident at near tangential angles, have an increased probability of suffering reflections both at the surface of the fibre and internally, (Ref. 1). Because of a smaller amount of light reaching the detector the absorbance of the specimen will appear greater.

In the subsequent work the field aperture was normally set as to illuminate 2/3rds of the width of the fibre, as a compromise between minimizing the effect just mentioned and having the largest amount of light. Under these conditions it was found that the amount of light recorded did not depend critically on the level at which the specimen was focused.

Fig. 7.3b shows the spectrum recorded from a DNA fibre, for two different orientations of the polarizer relative to the fibre axis. The DNA has no absorption band in the visible region. However, one recorded an absorbance of the order of 0.3 O.D. units (about 15% larger at 450μm than at 600μm), which is the combined result of the cylindrical lens effect mentioned above and of the light scattering by the specimen (particularly by salt crystallites and impurities present in the fibre).

One should be aware of the fact that these effects are also present in the absorption spectra of the drug-DNA fibres and allowance should be made for them in order to obtain absolute absorbance values. Typical 'parallel' and 'perpendicular' absorption spectra obtained from an adriamycin-DNA fibre are shown in Fig. 7.3a. A correction for the vertical displacement of the baseline may be performed by reference to

a wavelength where the drug does not absorb (see section 7.2.1).

The effect of the convergence of the illuminating rays, encountered in the optical systems of large numerical apertures was shown by Seeds (Ref. 2) to be negligible. For example, there would be an increase of the absorbance of about 1% when a specimen of unit optical density was measured through an objective of 0.3 numerical aperture.

The effect of the fluorescence of the specimen was also investigated. If the specimen fluoresces, the light intensity (I) normally reaching the detector is increased by the quantity

$$I_F = Q.I_o \ , \qquad (3.4)$$

where Q takes into account the fluorescence quantum yield of the specimen, the sensitivity of the detector to the fluoresced wavelength and the numerical aperture of the objective. Using the equations (4.1) and (4.4), the recorded transmittance is given by:

$$T \text{ recorded} = \frac{I + I_F}{I_o} = T \text{ true} + Q \ , \qquad (3.5)$$

which shows that the disturbing effect of the fluorescence is negligible as long as the true transmittance of the specimen is much larger than Q.

APPENDIX

Manufacturers of the basic components of the Microspectrophotometer system

1. Carl Zeiss Oberkochen, West Germany: Universal Research Microscope.
2. Leitz Wetzler, West Germany:
   "MPV basic unit with beam splitter, triple mirror, eyepiece and bulb for projection of diaphragm outlines".
   "Swing-out mirror and centring diaphragm holder".
3. Applied Photophysics Limited, London, England:
   Quartz-Iodine lamp with stabilized power supply.
   M500 High radiance monochromator.
   Stepping motor with control unit.
   Photomultiplier power supply.
4. Brookdeal Electronics Limited, Berks., England:
   9501 Lock-in amplifier.
   9478 Vibrating vane light chopper and drive unit.
5. Ancom Limited, Cheltenham, England:
   15 LN-1 logarithmic DC amplifier.
6. Bryans Southern Instruments Limited, Surrey, England:
   9200 X Y/t Plotter.

REFERENCES

1. D. Keilin, E.F. Hartree; Nature (1950) 165, 504.
2. W.E. Seeds; thesis (1951), London University.

CHAPTER 4

SPECTROSCOPIC STUDY OF DRUGS AND DRUG-POLYNUCLEOTIDE COMPLEXES IN SOLUTION

4.1 Experimental Results

4.1.1 Absorption spectra of Ethidium Bromide and Ethidium-DNA complexes in solution

The absorption spectrum of a dilute aqueous solution of EB has a visible band at 480nm and a UV band at 285 nm (Figs. 4.1 and 4.4). The absorbance at 480nm obeys Beer's law up to concentrations around 1mM (Ref. 1), above which departures occur due to the aggregation of the drug molecules (Ref. 2 and Ref. 3). The spectra of EB solutions of increasing concentrations are hypochromic and red shifted and pass through an isobestic point (Fig. 4.1/a, Ref. 3).

An effect similar to that caused by increasing the drug concentration was observed on increasing the ionic strength of the solution. The magnitude of this effect was dependent on the size of the anion present in solution (Fig. 4.2). Indeed, the effect became more pronounced as one moved down the sodium halide series (NaCl, NaBr, NaI), the most effective in causing hypochromism and red shift being the Sodium Iodide. With EB at 1mM concentration and NaI at 2 M, the drug precipitated in the form of a violet crystalline deposit. The precipitation did not occur for NaI concentrations below 3mM, but even in this case the red shift and hypochromism were greater than with the other halides at 2 M concentration. The effect of Na_2HPO_4 solutions was also investigated, as it was thought that this might be comparable to the interaction between the drug and the phosphate backbone of the polynucleotides. As it can be seen in Fig. 4.2, the Sodium phosphate

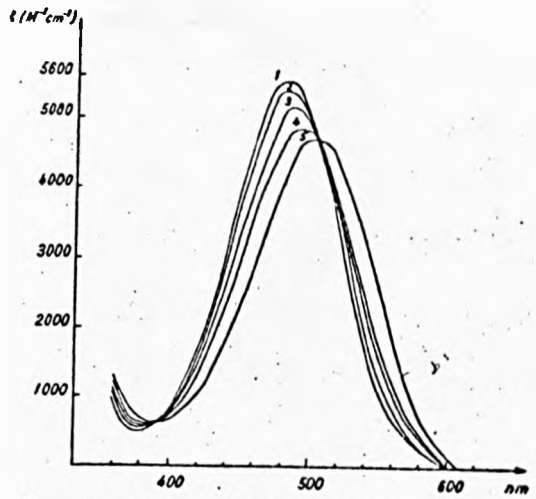

A . Absorption spectra of various EB concentrations in aqueous solution 1) 10^{-3} M; 2) 2×10^{-3} M; 3) 5×10^{-3} M; 4) 10^{-2} M; 5) 10^{-1} M. The quartz cuvettes were of 0.5 mm optical length except for 5 where it was of 10 μm.

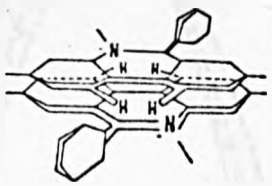

B . Proposed structure for the stacked complex between two EB molecules.

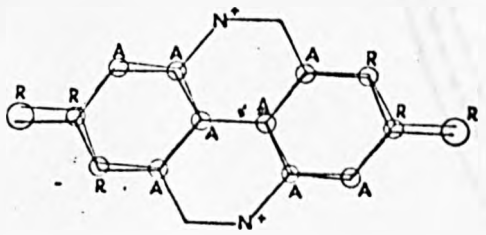

C. Electrostatic attraction (A) and repulsion (R) sites

FIG. 4.1. THE AGGREGATION OF ETHIDIUM BROMIDE AT HIGH CONCENTRATIONS: A. SPECTRAL EFFECT (REF. 9). B. PROPOSED DIMER MODEL (REF. 9). C. ELECTROSTATIC ATTRACTION AND REPULSION SITES IN THE DIMER MODEL (REF. 12).

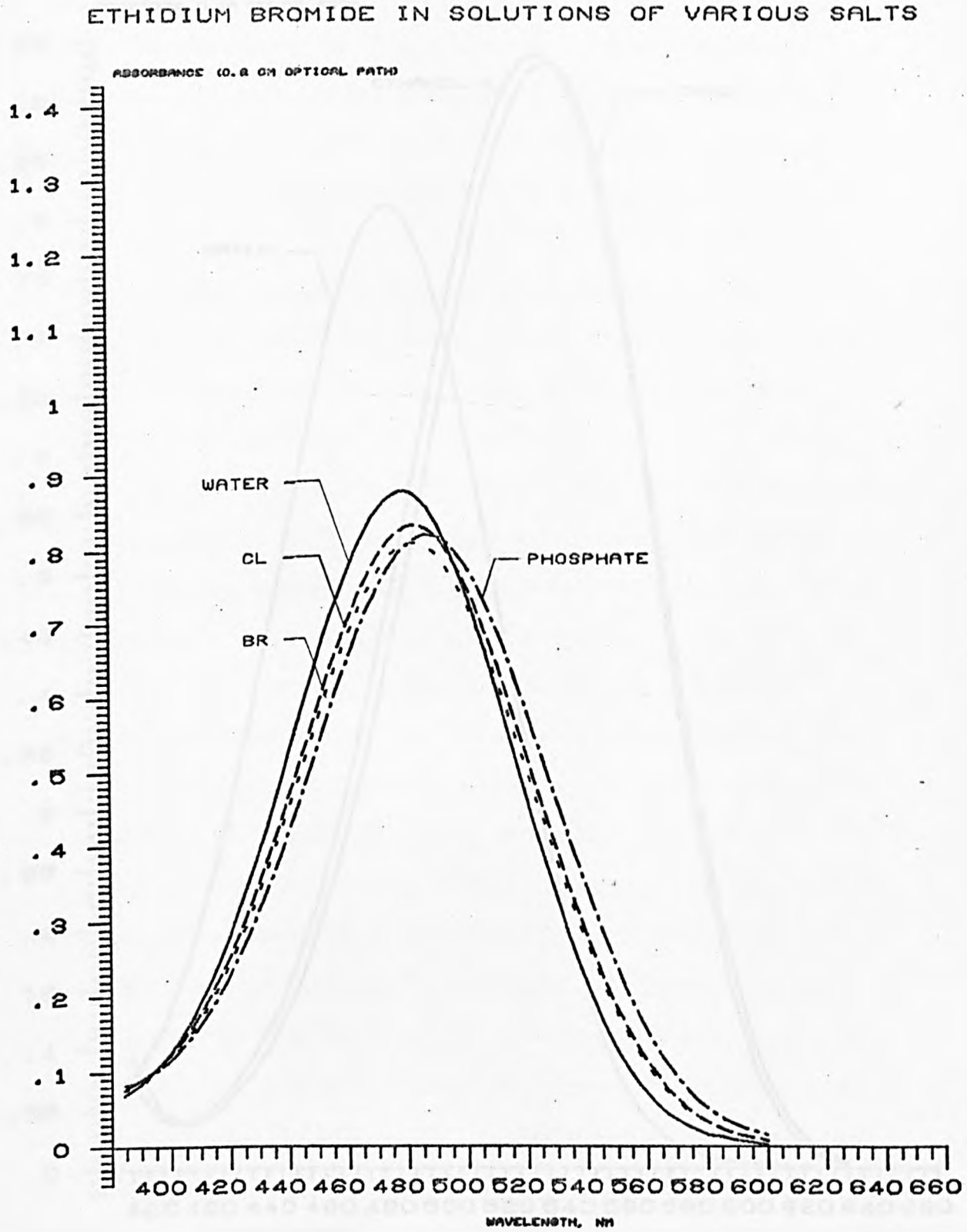

FIG. 4.2. VISIBLE ABSORPTION SPECTRA OF AQUEOUS ETHIDIUM BROMIDE (0.001 M CONCENTRATION) IN THE PRESENCE OF SODIUM SALTS AT 2.0 M CONCENTRATION .

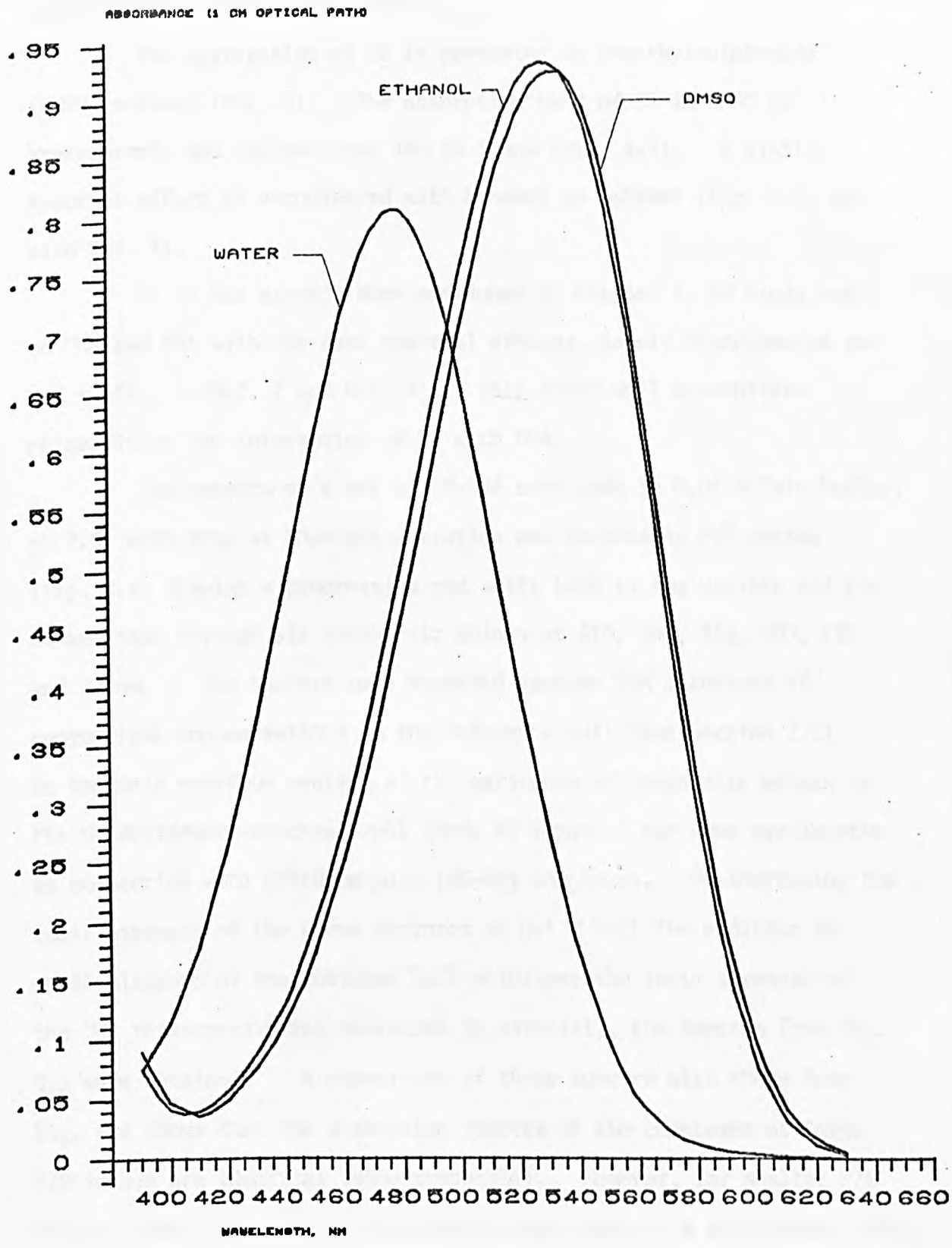

FIG. 4.3. VISIBLE ABSORPTION SPECTRA OF ETHIDIUM BROMIDE IN WATER, 95 % ETHANOL AND 100 % DMSO; EB CONCENTRATION 145 MICROMOLAR

caused an even greater red shift.

The aggregation of EB is prevented in Dimethylsulphoxide (DMSO) solvent (Ref. 3). The absorption band of EB in DMSO is hyperchromic and shifted from 480 to 535nm (Fig. 4.3). A similar spectral effect is encountered with Ethanol as solvent (Fig. 4.3, see also Ref. 4).

As it has already been mentioned in Chapter 1, EB binds both to DNA and RNA with the same spectral effects, namely hypochromism and red shift. (Ref. 1 and Ref. 5). This study will concentrate primarily on the interaction of EB with DNA.

The spectra of a set of EB-DNA complexes in 0.04 M Tris buffer, pH 7.9, with drug at 20μM concentration and increasing P/D ratios (Fig. 4.4) display a progressive red shift both in the visible and the UV and pass through six isosbestic points at 510, 390, 318, 300, 232 and 225nm. The spectra were recorded against DNA solutions of appropriate concentrations in the reference cell (see Section 2.1). In the only previous mention of the existence of isosbestic points in the UV difference-spectra, Pohl (Ref. 6) reported the same wavelengths in connection with Ethidium-poly (dG-dC) complexes. By increasing the ionic strength of the above mixtures to 0.1 M NaCl (by addition of small aliquots of concentrated NaCl solution; the ionic strength of the DNA references being increased in parallel), the spectra from Fig. 4.5 were obtained. A comparison of these spectra with those from Fig. 4.4 shows that the absorption spectra of the complexes of large P/D ratios are identical (superimposable). However, for smaller P/D ratios (lower than 10) the absorption bands suffered a significant shift towards blue and an increase of their intensity.

A part of each of these mixtures was spun in the ultracentrifuge in order to separate the free drug from the drug bound onto the DNA. In

LOW IONIC STRENGTH EB-DNA COMPLEXES

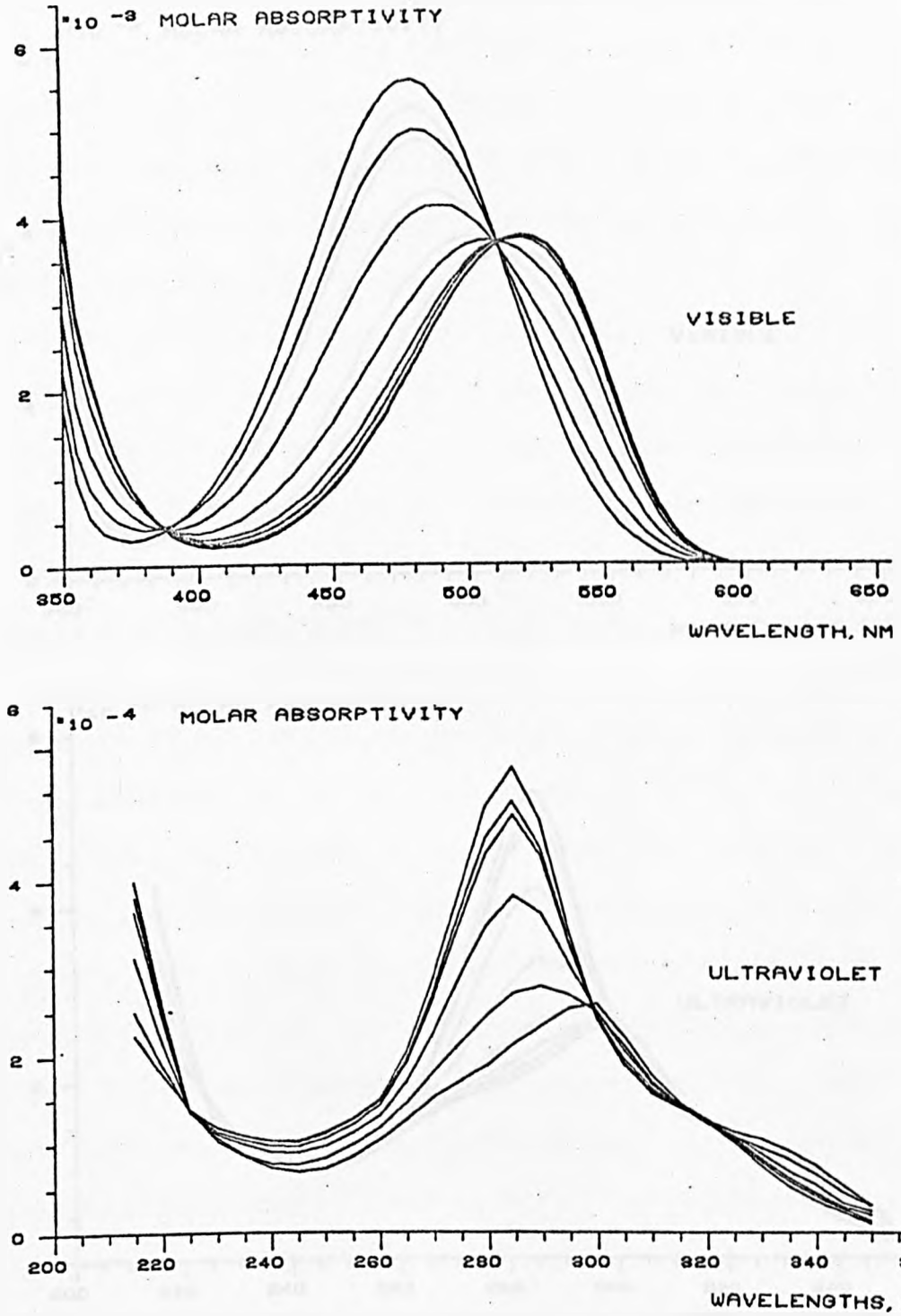

FIG. 4.4. VISIBLE AND UV DIFFERENCE SPECTRA OF EFHIDIUM-DNA COMPLEXES IN 0.04 M TRIS; EB CONCENTRATION = 20 MICROMOLAR. VISIBLE RANGE : P/D RATIOS IN ORDER = 0, 0.7, 2, 4, 7, 10, 15, 20; UV RANGE: P/D = 0, 0.3, 0.7, 2, 4, 7. (P/D=0 IS MARKED) .

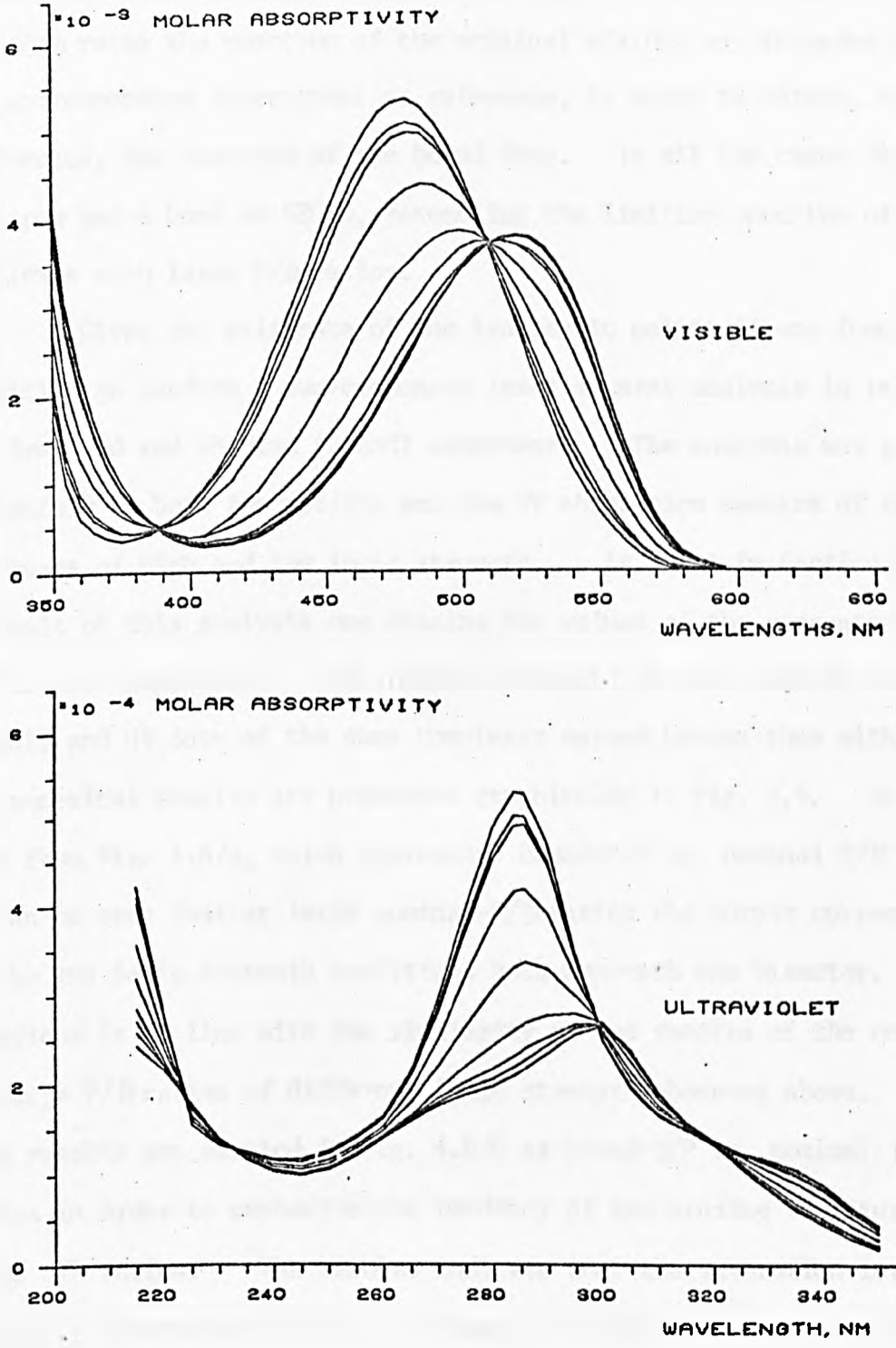

FIG. 4.5. VISIBLE AND UV DIFFERENCE SPECTRA OF ETHIDIUM-DNA COMPLEXES IN 0.1 M NACL, 0.04 M TRIS; EB CONCENTRATION = 19.5 MICROMOLAR; P/D RATIOS, IN ORDER : 0, 0.3, 0.7, 2, 4, 7 , 10, 20, 30 ; (P/D=0 IS MARKED). THESE COMPLEXES WERE OBTAINED BY THE ADDITION OF 0.1 ML 4M NACL SOLUTION TO 4 ML OF THE COMPLEXES FROM FIG. 4.4 .

doing so it was implicitly assumed that all the molecules which were bound to the DNA in solution sedimented together with the DNA. For each P/D ratio the spectrum of the original mixture was recorded against its corresponding supernatant as reference, in order to obtain, by difference, the spectrum of the bound drug. In all the cases this spectrum had a band at 520nm, resembling the limiting spectrum of the complexes with large P/D ratios.

Given the existence of the isosbestic points it was found justified to perform a two-component least squares analysis in terms of the free and red shifted (bound) components. The analysis was performed separately on both the visible and the UV absorption spectra of the complexes of high and low ionic strength. As shown in Section 2.2, as a result of this analysis one obtains the values of the concentrations of the two components. The results obtained on the basis of the visible and UV data of the same complexes agreed better than within 3%. The numerical results are presented graphically in Fig. 4.6. In the plot from Fig. 4.6/a, which represents bound-P/D vs. nominal P/D ratios, it can be seen that at large nominal-P/D ratios the curves corresponding to the two ionic strength conditions both approach the bisector. This behaviour is in line with the similarity of the spectra of the complexes of large P/D ratios of different ionic strength observed above. The same results are plotted in Fig. 4.6/b as bound-D/P vs. nominal-D/P ratios in order to emphasize the tendency of the binding to saturate at large D/P ratios. The results indicate that the saturation level is inversely related to the ionic strength, varying from about bound-D/P = 0.25 at low ionic strength* to bound D/P = 0.20 at 0.1 M NaCl (see also Ref. 1), but in neither case a perfectly horizontal plateau is achieved.

---

* In the low ionic strength complex (0.04 M Tris buffer), no NaCl was added but the solution contained the Sodium ions which were brought by the Sodium-DNA (P.J. Blackeley, personal communication).

EB-DNA COMPLEXES
UNDER HIGH AND LOW IONIC STRENGTH CONDITIONS

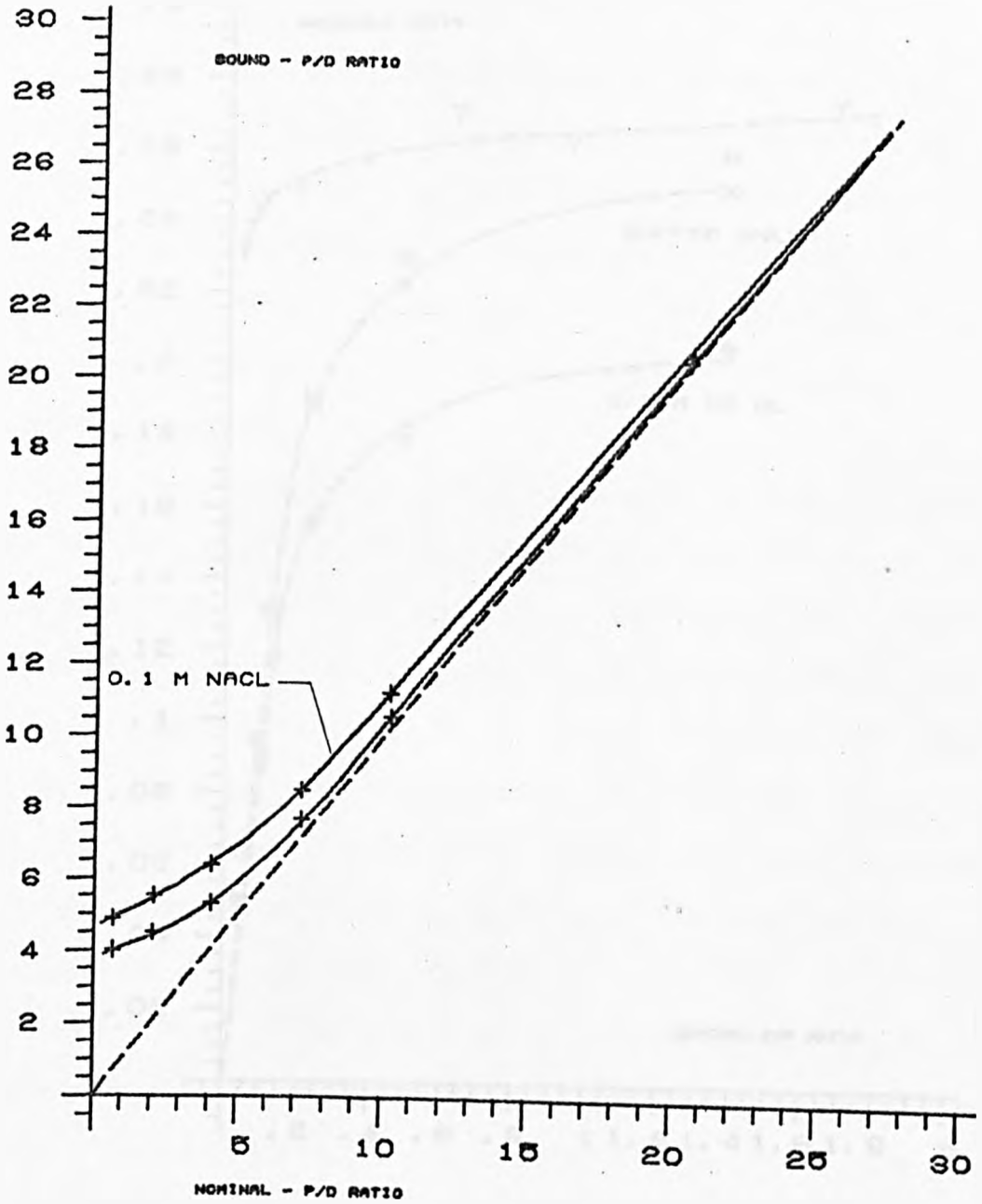

FIG. 4.6/A BOUND-P/D VS. NOMINAL P/D RATIOS, AS OBTAINED BY TWO COMPONENT ANALYSIS OF THE VISIBLE SPECTRA FROM FIGS. 4.4 & 4.5; IONIC STRENGTH: UPPER CURVE-0.1 M, LOWER CURVE- TRIS BUFFER ONLY .

EB-DNA COMPLEXES

UNDER HIGH AND LOW IONIC STRENGTH CONDITIONS

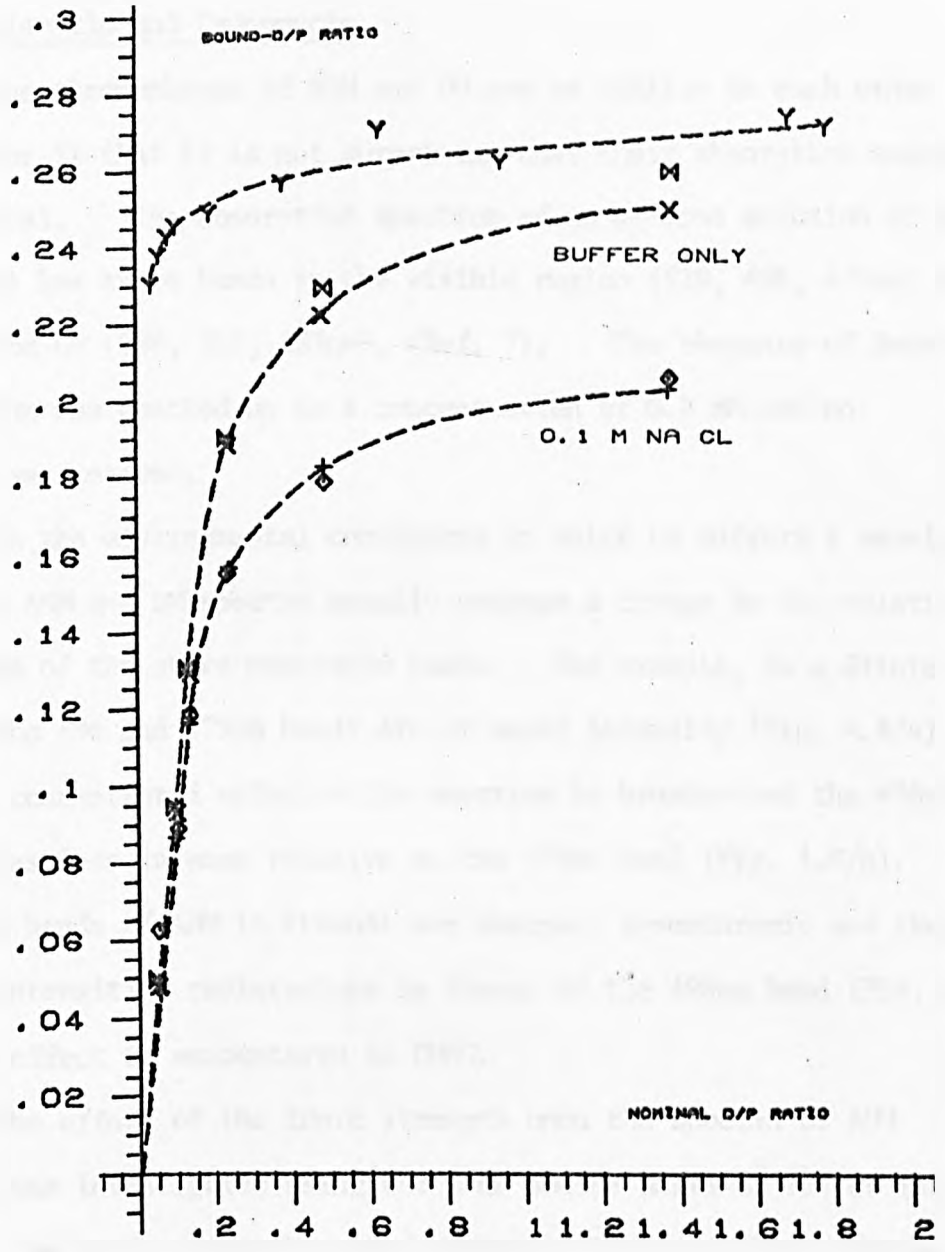

FIG. 4.6/B BOUND-D/P VS. NOMINAL-D/P RATIOS AS OBTAINED BY TWO COMPONENT ANALYSIS. THE POINTS MARKED +, X, Y DERIVE FROM VISIBLE SPECTRA, THEOTHER POINTS DERIVE FROM UV SPECTRA. THE DATA FROM THE UPPER CURVE BELONG TO A SET OF COMPLEXES OF LOW P/D RATIOS PREPARED BY STEPWISE ADDITION OF DNA TO AN 80 MICROMOLAR EB SOLUTION (HORIZONTAL SCALE CONTRACTED TEN-FOLD)
THEOTHER CURVES, SAME COMPLEXES AS IN FIG. 4.6/A.

The significance of the results presented above will be discussed in Section 4.2.

4.1.2 Adriamycin and Daunomycin

The chromophores of ADM and DM are so similar to each other (see Chapter 1) that it is not surprising that their absorption spectra are identical. The absorption spectrum of an aqueous solution of ADM (Fig 4.7/a) has three bands in the visible region (529, 496, 479nm) and three in the UV (288, 252, 233nm), (Ref. 7). The obeyance of Beer's law at 479nm was checked up to a concentration of 0.8 mM and no departure was noticed.

In the environmental conditions in which EB suffers a wavelength shift, the ADM and DM spectra usually undergo a change in the relative intensities of the above mentioned peaks. For example, in a dilute solution the 496 and 479nm bands are of equal intensity (Fig. 4.8/a). In a more concentrated solution the spectrum is broader and the 496nm band becomes less intense relative to the 479nm band (Fig. 4.8/b). The absorption bands of ADM in Ethanol are sharper, hyperchromic and their relative intensities redistribute in favour of the 496nm band (Fig. 4.8). A similar effect is encountered in DMSO.

The effect of the ionic strength upon the spectra of ADM solutions was investigated using the same sodium salts as for EB (section 4.1.1). The ionic strength caused similar effects to those brought about by increasing the drug concentration, namely, band broadening and the predominance of the peak at 479nm (Fig. 4.9). Down the Sodium halide series the magnitude of these effects increased up to Sodium iodide. The effect of the phosphate ion was even greater. The ADM solutions containing NaI and Na_2HPO_4 had a colloidal aspect and sedimented in time as a dark red crystalline deposit, which could be

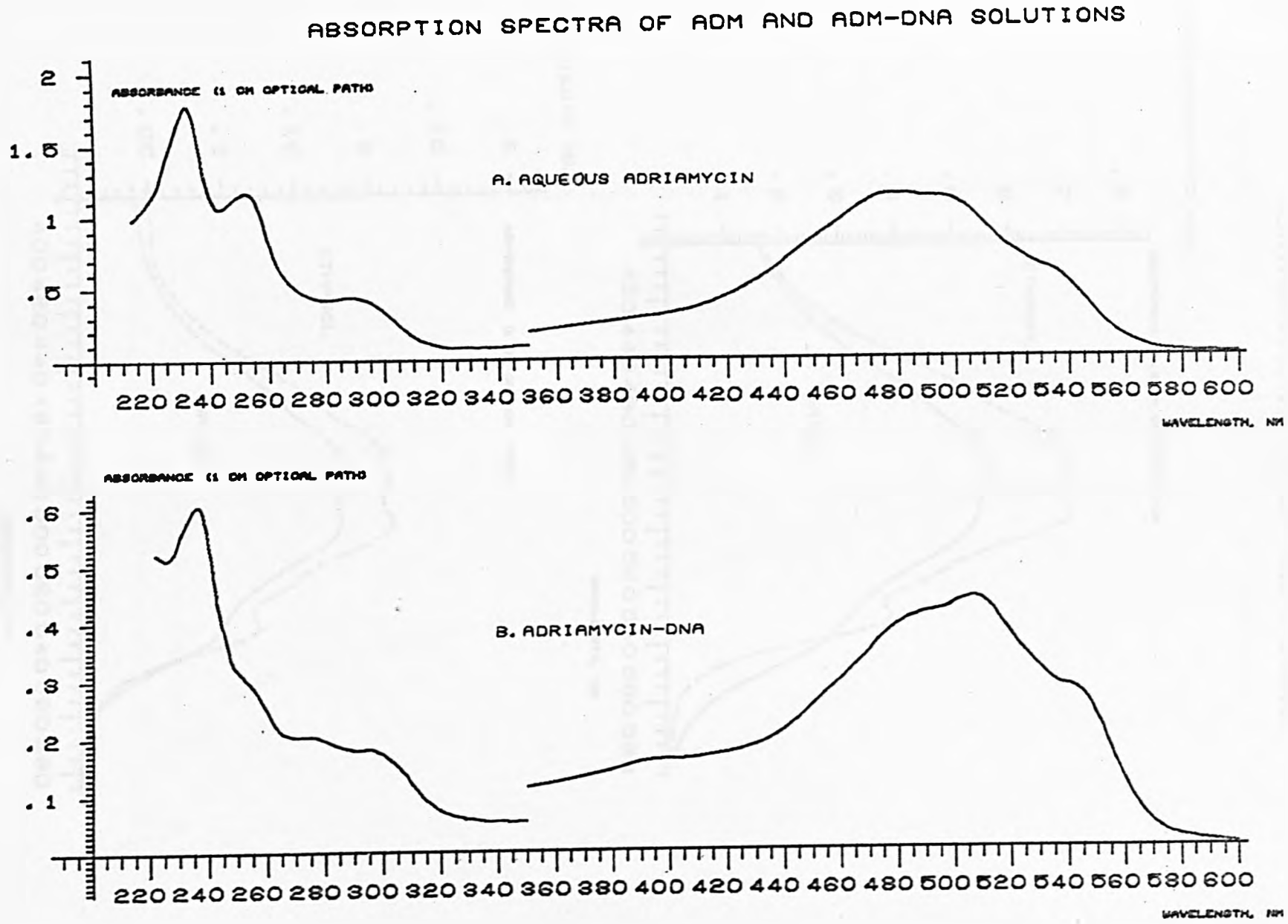

FIG. 4.7. VISIBLE AND UV DIFFERENCE SPECTRA OF ADRIAMYCIN: AE. AQUEOUS ADM, 58 MICROMOLAR CONCENTRATION; B). ADM-DNA COMPLEX P/D=30, 0.01 M NACL, ADM CONCENTRATION 35 MICROMOLAR .

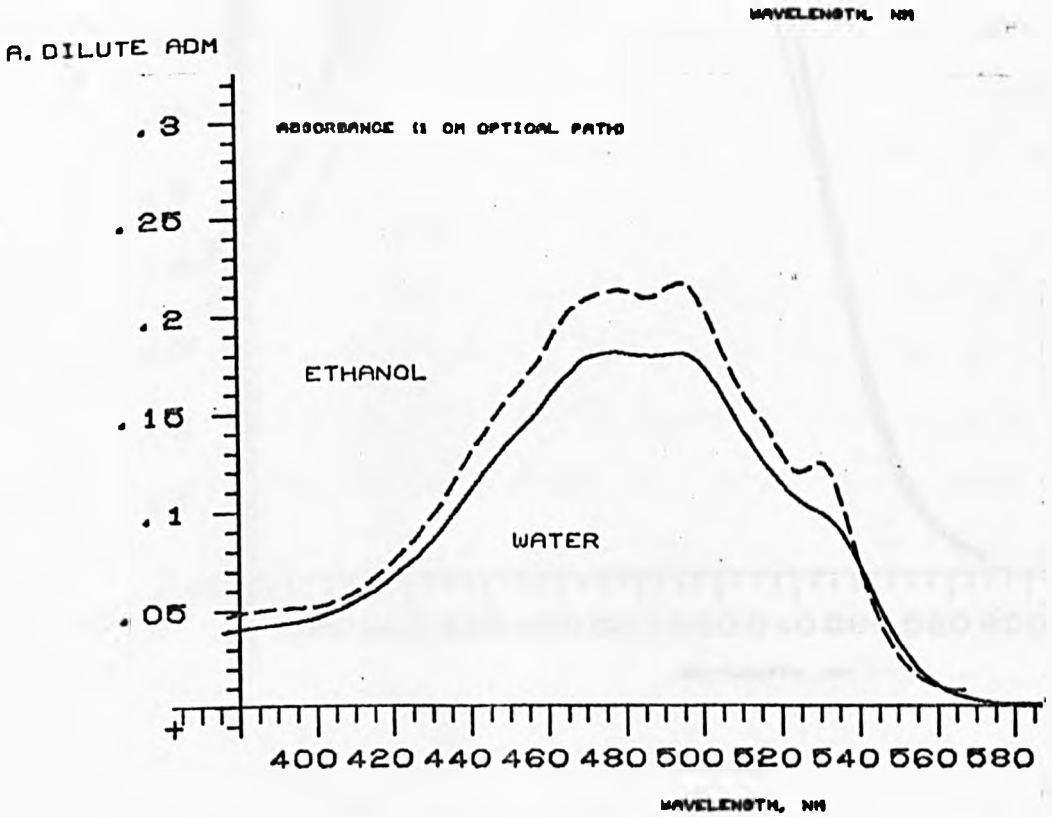

FIG. 4.8. VISIBLE ABSORPTION SPECTRA OF ADRIAMYCIN IN WATER AND 95% ETHANOL.

ADRIAMYCIN IN WATER AND ETHANOL

B. CONCENTRATED ADM

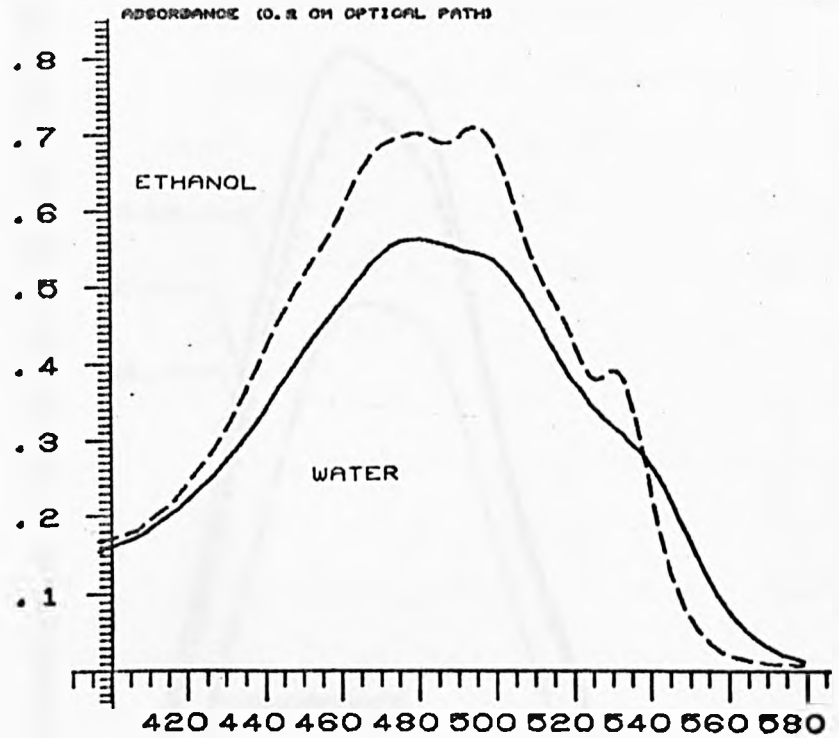

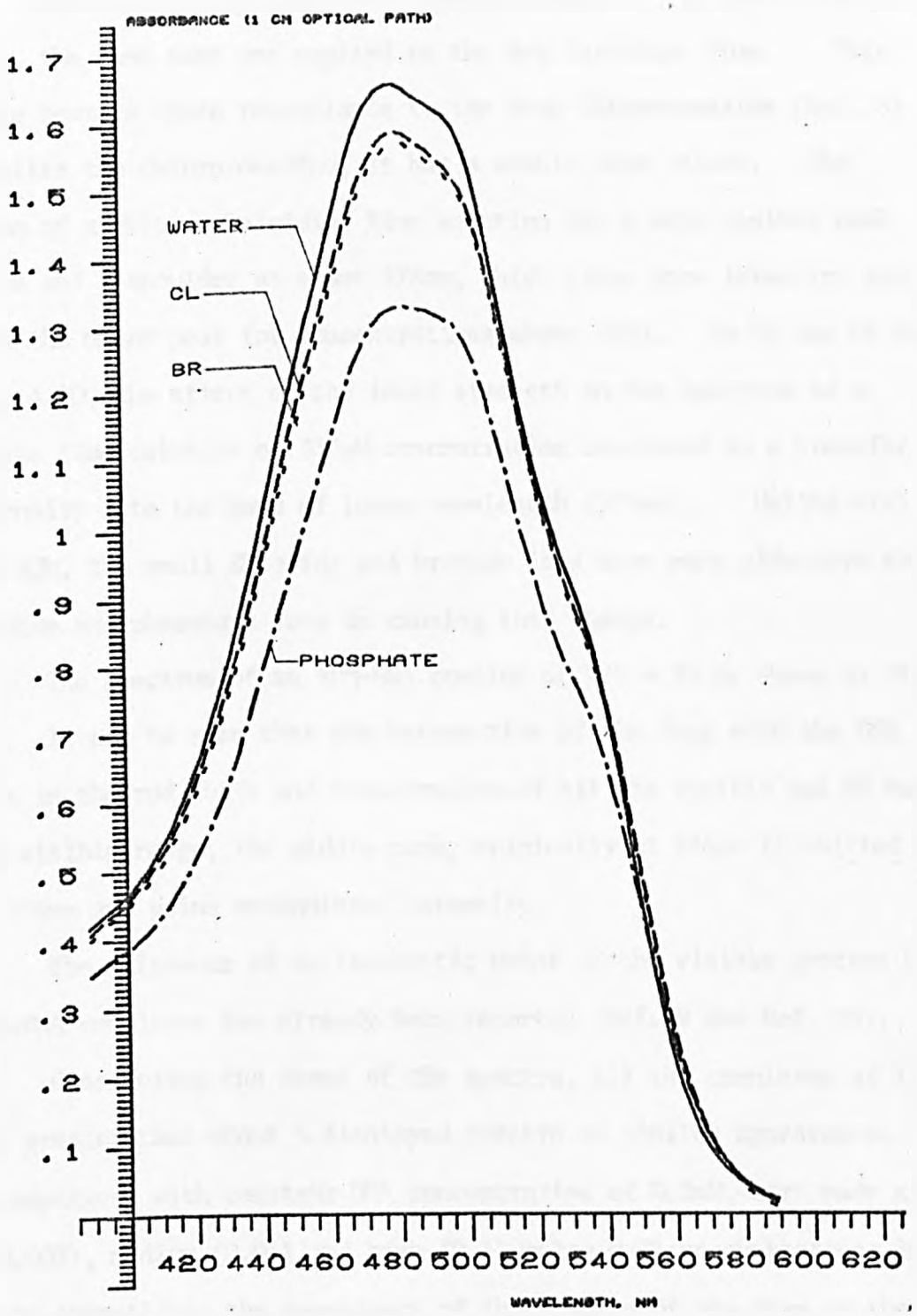

FIG. 4.9. VISIBLE ABSORPTION SPECTRA OF ADRIAMYCIN (150 MICROMOLAR) IN THE PRESENCE OF VARIOUS SODIUM SALTS; SALT CONCENTRATIONS : 1 M (CL , BR) , 0.003 M (PHOSPHATE) .

re-dissolved by stirring.

With the aim to extend the understanding of the ionic strength effects, the same test was applied to the dye Toluidine Blue. This molecule bears a close resemblance to the drug Chlorpromazine (Ref. 8) but, unlike the Chlorpromazine, it has a stable blue colour. The spectrum of a dilute Toluidine Blue solution has a main visible peak at 627nm and a shoulder at about 578nm, which gains more intensity and becomes the major peak for concentrations above 50μM. As it can be seen in Fig. 4.10, the effect of the ionic strength on the spectrum of a Toluidine Blue solution of 330μM concentration consisted in a transfer of intensity into the band of lower wavelength (578nm). Unlike with EB and ADM, the small Chloride and bromide ions were more effective than the iodide and phosphate ions in causing this change.

The spectrum of an ADM-DNA complex of P/D = 30 is shown in Fig. 4.7/b. It can be seen that the interaction of the drug with the DNA results in the red shift and hypochromism of all the visible and UV bands. In the visible range, the middle peak, originally at 496nm is shifted to about 505nm and gains predominant intensity.

The existence of an isosbestic point in the visible spectra of the DM-DNA complexes has already been reported (Ref. 9 and Ref. 10).

Considering the shape of the spectra, all the complexes of P/D ratios greater than about 5 displayed spectra of similar appearance. Such complexes, with constant DNA concentration of 0.3mM, were made at low (0.003), medium (0.01) and high (0.1) molar NaCl concentrations in order to investigate the dependence of the binding of the drug on the ionic strength, but the comparison of their spectra did not reveal any significant difference. The supernatants of these large P/D complexes, obtained by ultracentrifugation, contained no detectable amounts of free drug.

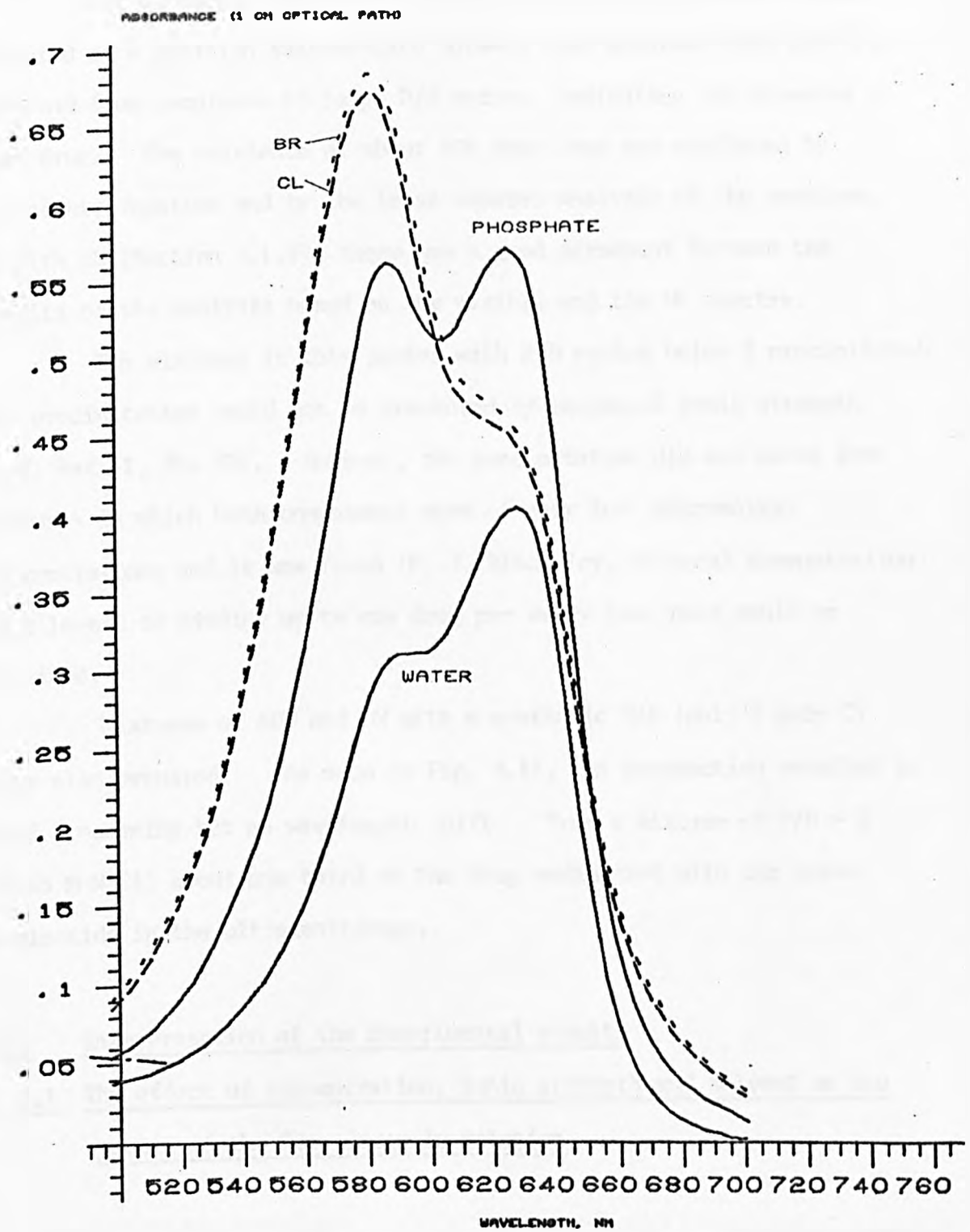

FIG. 4.10. VISIBLE ABSORPTION SPECTRA OF AQUEOUS TOLUIDINE BLUE (330 MICROMOLAR) IN THE PRESENCE OF VARIOUS SODIUM SALTS OF 2 M CONCENTRATION. THE EFFECT OF LIGHT SCATTERING IS OBSERVABLE .

For a mixture with P/D = 4 (0.01 M NaCl) the absorbance peak appeared at a position intermediate between that obtained from the free drug and from complexes of large P/D ratios, indicating the presence of free drug. The existence of about 10% free drug was confirmed by ultracentrifugation and by the least squares analysis of the spectrum. As with EB (Section 4.1.1), there was a good agreement between the results of the analysis based on the visible and the UV spectra.

The mixtures in this series with P/D ratios below 3 precipitated. The precipitation could not be prevented by increased ionic strength (c.f. Ref. 1, for EB). However, the precipitation did not occur from mixtures in which both components were of very low (micromolar) concentrations and it was found (P. J. Blackeley, personal communication) that levels of binding up to one drug per every base pair could be obtained.

Mixtures of ADM and DM with a synthetic RNA (poly I poly C) were also prepared. As seen in Fig. 4.11, the interaction resulted in band broadening but no wavelength shift. From a mixture of P/D = 5 (0.05 M NaCl) about one third of the drug sedimented with the polynucleotide in the ultracentrifuge.

4.2 Interpretation of the Experimental results

4.2.1 The effect of concentration, ionic strength and solvent on the spectra of the free drugs in solution

The effect of the concentration - the tendency of aqueous EB to aggregate at large concentrations has been established on the basis of proton magnetic resonance evidence (Ref. 3). As a result of that study it was proposed that EB aggregated in the form of antisymmetric dimers (Fig. 4.1/b). The dimer model was also substantiated by the

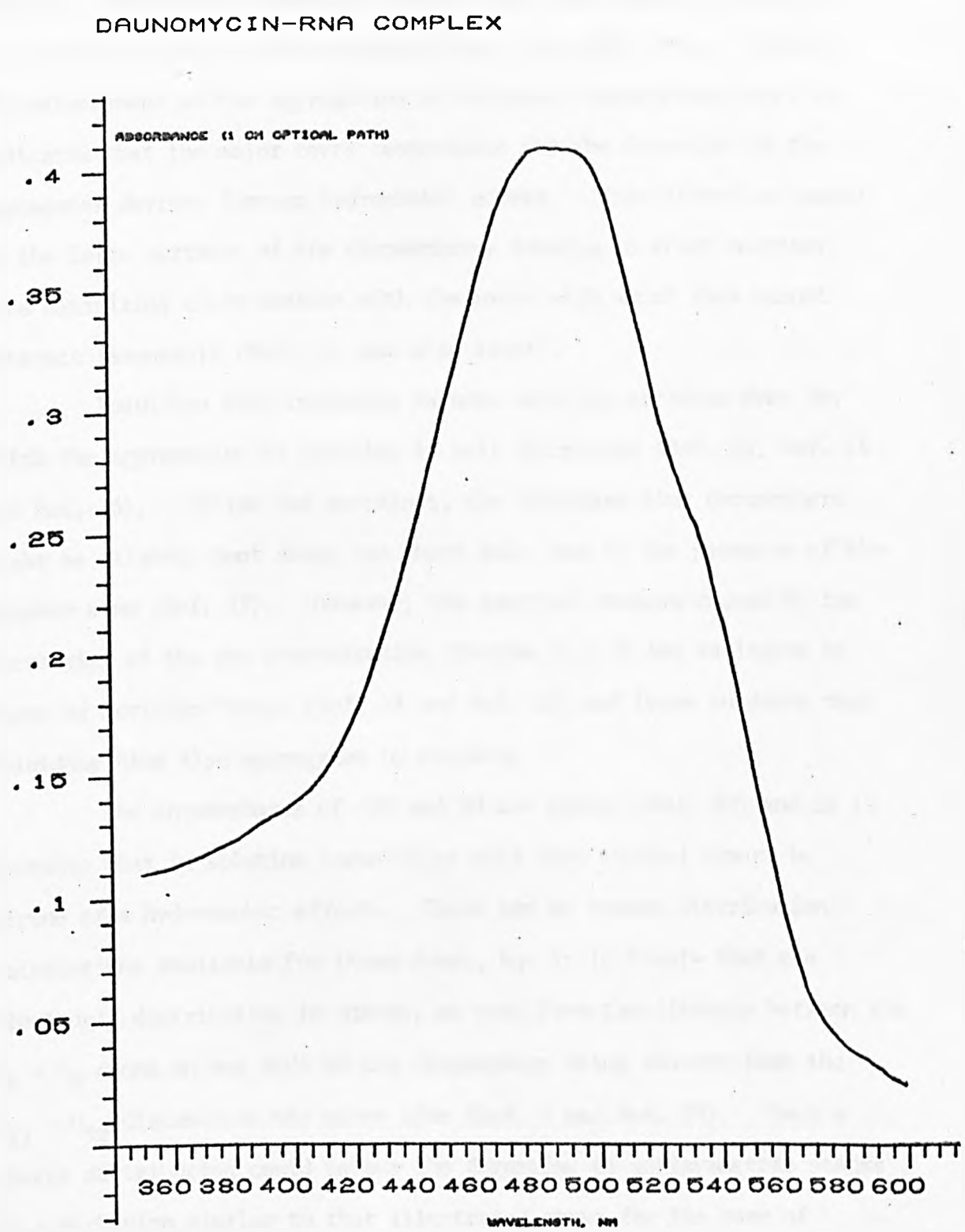

FIG. 4.11. VISIBLE SPECTRUM OF A COMPLEX OF DAUNOMYCIN WITH THE SYNTHETIC RNA POLY I-POLY C , P/D=5, 0.05 M NACL .

planarity of the drug chromophore, as deduced from the crystal structure (Ref. 11) and by the distribution of the electronic charge leading to attractive forces, as illustrated in Fig. 4.1/c (Ref. 12). However, the enhancement of the aggregation by increased temperature (Ref. 2) indicates that the major force responsible for the formation of the aggregates derives from an hydrophobic effect. This effect is caused by the large surfaces of the chromophores tending to stack together, thus minimizing their contact with the water with which they cannot interact favourably (Ref. 13; see also later).

Toluidine Blue resembles in many ways the acridine dyes for which the aggregation by stacking is well documented (Ref. 14, Ref. 15 and Ref. 16). Unlike the acridines, the Toluidine Blue chromophore might be slightly bent along its short axis, due to the presence of the sulphur atom (Ref. 17). However, the spectral changes caused by the increasing of the dye concentration (Section 2.1.2) are analogous to those of Acridine Orange (Ref. 18 and Ref. 19) and leave no doubt that Toluidine Blue also aggregates by stacking.

The chromophores of ADM and DM are planar (Ref. 20) and it is possible that in solution these drugs will form stacked dimers by virtue of a hydrophobic effect. There are no charge distribution calculations available for these drugs, but it is likely that the electronic distribution is uneven, as seen from the distance between the $O_5 - O_6$ atoms on one side of the chromophore being shorter than the $O_{11} - O_{12}$ distance on the other side (Ref. 9 and Ref. 20). Such a charge distribution could favour the formation of antisymmetric stacks by a mechanism similar to that illustrated above for the case of ethidium.

There are two theories that can be invoked for explaining the spectral changes that take place upon aggregation (Ref. 19).

The first theory is due to Zanker (Ref. 21) who introduced it in order to account for the blue shift displayed by the acridines in concentrated solutions. The theory is based on the assumption that both the original and the shifted bands belong to the same electronic transition but involve different vibrational levels. The aggregation of the chromophores results in a differential shift of the potential energy curves of the ground and excited states (Ref. 22) as a result of which the probabilities of the transitions change, thus accounting for the observed redistribution of band intensities. The authors were led to this assumption by the observation that the monomer spectrum presented a shoulder in the region where the 'dimer' peak would develop. According to their interpretation, this shoulder belongs to the resolved vibrational structure of the band and corresponds to a transition (to a vibrational level) of low probability in the monomeric chromophore, but which gains intensity in the dimer. Thus, for Acridine Orange, it is the 0→0 transition appearing in the monomer and the 0→1 transition (blue shifted) appearing in the dimer spectrum.

The same model could be applied to Toluidine Blue, because of the similarity of the spectra of the two molecules.

Unfortunately, no information is available on the nature of the bands in the absorption spectra of ADM and DM. However, it might be possible that the three visible bands of ADM (see Section 4.1.2) represent a resolved vibrational structure of a single transition and that the (slight) intensity redistribution taking place upon aggregation is the result of a change in the vibrational pattern of the chromophore.

The second of the two explanations is in terms of the exciton interaction theory (Ref. 23, Ref. 24, Ref. 25, Ref. 26 and Ref. 27).

The theory is based on the assumption that the electronic transitions in the neighbouring chromophores are coupled by Coulombic

interactions. If one further assumes that the electric transition dipoles can be approximated to point dipoles (Ref. 26) one can express the energy of interaction of the two transitions in a dimer by the formula:

$$V = \frac{\underline{\mu a}.\underline{\mu b}}{R^3} - \frac{3(\underline{\mu a}.\underline{R})\ (\underline{\mu b}.\underline{R})}{R^5} \quad , \qquad (4.1)$$

where $\underline{\mu a}$ and $\underline{\mu b}$ are the transition dipoles in the chromophores a and b, and $\underline{R}$ is the vector joining their origins.

It can be shown that as a result of this interaction the positions of the absorption bands will be shifted from the original energies Ea, Eb to new positions, given by the formula:

$$E\pm = \frac{E_a + E_b}{2} \pm \{V^2 + \frac{(E_a - E_b)^2}{2}\}^{\frac{1}{2}} \qquad (4.2)$$

From this formula it is apparent that the new transitions will always diverge from the original positions, i.e., the low energy transition is always shifted to the red and the high energy transition goes to even lower wavelengths.

The wavelength shift is followed by a redistribution of the oscillator strength which often involves transfer of intensity from one transition which is thus 'hypochromic', to the other, which is 'hyperchromic'. For a complete treatment, see Philpott (Ref. 27).

In the case of identical chromophores, the transition, originally of energy E is symmetrically split up into two transitions, of energies $E\pm$, given by:

$$E\pm = E \pm V \qquad (4.3)$$

The intensity of the bands is proportional to the square of the corresponding transition dipoles, $\mu\pm$, given by:

$$\mu\pm = 2^{-\frac{1}{2}}\ (\underline{\mu a} \pm \underline{\mu b}) \qquad (4.4)$$

For the geometry of a stacked aggregate the equations (4.1) and (4.3) predict that the energy of interaction and therefore the splitting of the original transition are largest when the transition dipoles are parallel or antiparallel and become zero when the dipoles are at right angles. The equation (4.4) predicts transfer of intensity from the lower energy transition to the higher energy transition ('blue shift'). On the other hand, a head-to-tail arrangement of the chromophores would result in red shift.

This theory is indeed successful in predicting the blue shift displayed by the absorption spectra of Toluidine blue upon aggregation.

Considering the case of ethidium, it will be remembered that this drug red-shifts upon stacking, contrary to the blue shift expected on the basis of the exciton interaction theory. However, it is known that the calculated transition dipole of the visible band of ethidium (Ref. 12) makes an angle of 34 degrees with the line joining the amino extremities of the molecule and, therefore, in the antisymmetric dimer of EB (Fig. 4.1/c) the dipoles would be nearly perpendicular to each other and thus the energy of their interaction would be very small (see above). Hence it is concluded that the exciton splitting cannot be a major effect in the case of EB and the observed red shift should reflect the simultaneous occurrence of another phenomenon.

It could be the case that the Bromine counterion, freely dissociated in a solution of manomeric ethidium, is offerred the possibility to attach specifically to a site on the ethidium dimer created as a result of aggregation. The presence of a negative ion in the close proximity of the chromophore, as, in general, the presence of any substituent with electron-donating powers ('auxochrome') is equivalent to enlarging the territory available to the pi-electron system with the consequence that the wavelength of the electronic

transition is red shifted (Ref. 28, Ref. 29 and Ref. 30). Thus, in order to account for the red shift displayed by the concentrated EB solutions, it is suggested that the Bromine ion acts as an auxochrome substituent to the aggregated (but not the monomeric) ethidium chromophores. The dependance of this effect on the size of the counterion, to be mentioned later, will substantiate this hypothesis.

Referring to Fig. 4.1/b, it seems likely that the Bromine ion would attach onto the main ring, in the positively charged area of the N_5^+ and C_6 atoms (Ref. 12), sheltered by the phenyl and ethyl substituents of one chromophore and the concavity of the phenantridinium rings of the other chromophore. This protected site is only provided by the dimers, but not the monomer drug molecules. The attachment of the Bromine ion to the amino side groups of EB (as observed in the crystal form, Ref. 11) might produce the same effect, but it is thought that in solution the binding to this exposed site would be too loose for an efficient charge donation to occur.

The lack of a blue shift in the case of ADM and DM might be explained by the perpendicularity of the transition dipoles, as in the case of EB, since it has already been suggested that the ADM dimer might be antisymmetric (see above). The absence of exciton splitting as a result of this geometry enables the observation (only as a secondary effect) of the suggested redistribution of the band intensities caused by the alteration of the vibrational pattern of the chromophore upon aggregation (see above).

The present discussion could be ended with the conclusion that the most general phenomenon which is expected to take place upon the stacking of the drug chromophores is the exciton interaction. However, in cases when for geometrical reasons the exciton splitting is minimum, other phenomena, probably specific to particular chromophores may become apparent.

The exciton interaction theory has also been used successfully to account for the hypochromism of the nucleic acid bases upon the formation of the helices (Ref. 23 and Ref. 24) and has been extended to describe the drug-polynucleotide interactions (Ref. 27; see section 4.2.2).

The effect of the ionic strength. Considering the effect of the ionic strength on the drug spectra, the experimental results presented in the previous sections (Figs. 4.2, 4.9 and 4.10) suggest that in all the cases the increased ionic strength facilitates the drug aggregation. Evidence for this conclusion comes from the similarity between the spectral changes obtained upon increasing the ionic strength and those caused by increasing the drug concentration and the observed tendency of the drugs (eg. EB and ADM in NaI and Na_2HPO_4 solutions) to precipitate in higher ionic strength conditions.

As the drugs contain basic groups which are expected to be ionized at the neutral pH, it can be inferred that the mechanism by which the presence of the salts facilitates the stacking of the chromophores consists primarily in the screening of the positive charges by the anions of the salts, thus annihilating the electrostatic repulsion unfavourable to the aggregation.

In the case of Toluidine Blue (Fig. 4.10) the chloride and bromide appear to be more effective than the iodide and the phosphate, indicating that the small ions are probably better in creating a non-specific electrostatic shielding.

However, the situation is reversed in the case of EB and ADM, where spectral effects increase with increased ion size.

In so far as EB is concerned (Fig. 4.2), the magnitude of the spectral effects suggests that the large Iodine and phosphate ions not only cause non-specific screening which may promote aggregation up to the point of precipitation, but are also able to replace the Bromine

from its suggested site (see above) and act as more powerful electron donors with the consequence of a larger spectral red shift.

The mechanism by which the large ions (especially the phosphate) enhance the aggregation of ADM remains unclear. It is possible that the phosphate ion might be involved in intramolecular (or intermolecular) Hydrogen-bonding.

The effect of the solvent. It has already been mentioned that the hydrophobic drive towards aggregation arises because the interaction of the water with the drug chromophore is less favourable than the interaction of the water molecules among themselves. Therefore it is expected that the hydrophobic drive will vanish in an apolar solvent such as DMSO or Ethanol, in which the solvent molecules do not interact considerably. Indeed, it has been confirmed by P.M.R. studies (Ref. 3) that EB is monomeric in DMSO solvent. However, the absorption spectra of the drugs in DMSO or Ethanol (Figs. 4.3 and 4.8) are different than those obtained from aqueous solutions of monomeric drugs, indicating that in addition to de-aggregation the apolar solvents caused other changes (see below). (In all the cases, the DMSO and Ethanol produced similar effects).

Following Ingraham's argument for Proflavine (Ref. 18), the red shift displayed by EB in Ethanol (Fig. 4.3) can be explained in terms of a different degree of solvation of the ground states of the drug in water and Ethanol media, the energy of the ground state in water being lower because of a stronger solvation. Thus the electronic transition appears red shifted in Ethanol because the energy gap between the ground and excited states is narrower than in water.

The drugs ADM and DM do not seem to conform to this mechanism, since there is no red shift upon transfering them into Ethanol,

although the sharpening of their absorption bands (Fig. 4.8) clearly indicates a reduced degree of solvation: it is known that if there is considerable interaction between dissolved molecules and solvent, the vibrational bands are generally broadened (Ref. 29); the observed broad appearance of the bands of aqueous DM and the increased resolution of the bands in ethanol is indeed consistent with the less polar nature of the second environment.

The reasons for the different behaviour in apolar solvents of EB on one hand and the anthracyclines on the other hand is not clear.

The analogy between the red shift displayed by EB in Ethanol and the red shift caused by the binding of EB to DNA (Ref. 4 and Ref. 1) has often been invoked as indicating the apolar nature of the DNA intercalation site. It is significant in this respect that the anthracyclines, although they red shift upon intercalation (see next section), they do not do so in any alcohol. This throws doubts upon the validity of the analogy between the effects of the intercalation and of the apolar solvents and suggests that the mechanisms operating in the two situations are different.

4.2.2 The interpretation of the absorption spectra of the drugs bound to nucleic acids in solution

The six isosbestic points in the visible and UV spectra of the EB complexes (Figs. 4.4 and 4.5) and the finding (Section 4.1) that the difference-spectra of the 'bound' drug were alike (i.e. red shifted) over the entire range of P/D ratios could give the impression that the 'bound' component was a unique species at all P/D ratios. However, the experimental results (Fig. 4.6) revealed a significant difference between the nature of the binding at large and low P/D ratios. The

ability to form complexes at P/D ratios greater than about 10 was independent of the ionic strength (Fig. 4.6/a), whereas at low P/D ratios the higher ionic strengths resulted in lower levels of binding (Fig. 4.6/b). Taking as an example the complexes with P/D = 1, at low ionic strength the fraction of drug bound represented a quarter of the total amount of drug present, whereas at high ionic strength (0.1 M NaCl) it represented one fifth, i.e. a 25% decrease in the level of binding caused by raising the ionic strength. Similar observations, related to both Ethidium and the acridines have previously been reported (Ref. 1, Ref. 31 and Ref. 32).

The results just mentioned are consistent with the existence of two modes of binding of EB to DNA (see Chapter 1). The basically hydrophobic nature of the intercalation process, which is the mode of binding that predominates at large P/D ratios, is consistent with the observed insensitivity of these complexes to the ionic strength. On the other hand, the ionic strength dependence of the binding at low P/D ratios indicates that the second mode of binding is primarily electrostatic. By analogy with the acridines (Ref. 14), it can be assumed that at low P/D ratios EB binds to the negatively charged phosphate backbone of the DNA by virtue of the cationic nature of its chromophore. The question which remains to be answered is why the absorption spectra of both the intercalated and the outside-bound species display the same characteristics.

Considering the intercalated drug, the red shift and hypochromism of its visible band may be explained in terms of the coupling of the transitions in the DNA and the drug chromophore (Ref. 27). By assuming an interaction between two transition dipoles, one corresponding to the visible band of the drug and the other associated with the UV band of a DNA base, the same results as those of the extensive treatment

of Philpott (Ref. 27) can be obtained, qualitatively, with the simple theory presented in Section 4.2.1. According to this theory (equation 4.2), the transition energies will diverge (in particular the visible band of the drug will be red shifted) and it is easy to show that for the geometry of intercalation the red shift will also be accompanied by hypochromism.

The red shifted spectrum of the outside-bound drug may be explained if one makes an analogy with the red shift displayed by the spectra of aqueous EB on increasing the ionic strength (Section 4.1.1, Fig. 4.2). It was suggested that the negatively charged ions were bound to the aggregated drug molecules where they acted as charge donors with the consequence of the observed red shift (see Section 4.2.1). In the case of the outside-bound drug, it is possible that the attachment of the chromophore to the phosphate backbone of the DNA meets the condition under which an efficient charge donation can occur from the phosphate group to the Ethidium chromophore, resulting in a similar red shift*.

In conclusion, both the intercalated and outside-bound species display red shifted spectra, although the mechanisms responsible for these spectral effects are different in the two cases.

By analogy with EB, the same mechanisms are also expected to operate in the case of the drugs ADM and DM. This analogy involves the observation that the drugs red-shift upon binding to the DNA (Fig. 4.7) and, as in the case of EB (see Chapter 1), the Scatchard plots (Ref. 36) display two regions of different affinities towards the DNA: a high affinity region, at large P/D ratios, which is insensitive to the ionic strength (see Section 4.1.2) and a low affinity region, at low P/D ratios, which is dominated by the electrostatic interaction

---

* The red shift resulting upon the binding of EB and other dyes to single stranded polynucleotides (Ref. 33) or polyelectrolytes (Ref. 34 and Ref. 35) may be explained in the same way.

between the drugs and the DNA, as deduced from the precipitation of the complexes of P/D ratios below 3 (see section 4.1.2). It is thus suggested that, as in the case of EB, the two regions are associated with the intercalated and the outside-bound species respectively.

It was mentioned in Chapter 1 that the binding of EB to RNA produced the same spectral effects as those observed on its binding to DNA. Although the mixing of DM with RNA (Fig. 4.11) did not cause the same spectral shift as with the DNA (the spectrum being broader, but otherwise similar to that of the free drug), the formation of a complex between the drug and RNA could be deduced from the tendency of the drug to sediment with the RNA in the ultracentrifuge (section 4.1.2). The nature of this complex cannot be inferred from the available spectral data alone.

The significance of the least squares two component analysis of the absorption spectra of the drug-polynucleotide complexes. The analysis consisted in determining the concentrations of the two spectroscopically distinguishable components, 'free' and 'bound' drug from both visible and UV spectra of the EB-DNA and ADM-DNA complexes. The analysis in terms of only one bound species, instead of two (intercalated and outside bound drug), was justified by the existence of the isosbestic points, consistent with the similarity of the spectra of the 2 bound components (see section 4.2.2).

The remarkable agreement between the results obtained on the basis of the visible and UV spectra for both EB and ADM indicates that the UV difference-spectra are the potential carriers of the same information on the proportion of free and bound drug as the spectra from the visible region.

The fact that the simple subtraction of the absorbance of a DNA

reference (section 4.1.1) made the UV difference-spectrum a two component system similar to the visible one implies that the binding of the drug did not alter the absorption spectrum of the DNA in the complex to any considerable extent. Under these circumstances, it appears that the method presented above could also be used for quantitative analysis on systems containing DNA and other small molecules, such as amino acids, the spectra of which are confined only to the UV region.

REFERENCES

1. M. J. WARING; J. Mol. Biol. (1965) 13, 269.
2. J. L. BRESLOFF; Thesis (1973), Yale University.
3. G. THOMAS, B. ROQUES; FEBS Letters (1972) 26, 169-175.
4. J. B. LE PECQ, C. PAOLETTI; J. Mol. Biol. (1967) 27, 87-106.
5. BITTMAN; J. Mol. Biol. (1969) 46, 251-268.
6. F. M. POHL, T. M. JOUIN, W. BACHR, T. J. HOLBROOK; Proc. Nat. Acad. Sci. U.S.A. (1972) 69, 3805-3809.
7. A. DI MARCO, M. GAETANI, B. SCARPINATO; Cancer Chemotherapy Reports (1969) 53, 33-37.
8. T. PORUMB; Thesis (1976), Keele University.
9. A. DI MARCO, F. ARCAMONE; Drug Research (1975) 25, 368-375.
10. W. J. PIGRAM; Thesis (1968), London University.
11. SUBRAMANIAN, FROTTER, BUGG; J. Cryst. Mol. Stud. (1971) 1, 3.
12. P. U. GIACOMONI, M. LE BRET; FEBS Letters (1973) 29, 227-230.
13. V. A. BLOOMFIELD, D. M. CROTHERS, I. TINOCO JR.; Physical Chemistry of Nucleic Acids (1974), Harper and Row, New York.
14. A. R. PEACOCKE, J. N. H. SKERRETT; Trans. Farad. Soc. (1956) 52, 261.
15. A. L. STONE, D. F. BRADLEY; J. Amer. Chem. Soc. (1961) 83, 3627-3637.
16. D. F. BRADLEY, M. K. WOLF; Proc. Nat. Acad. Sci. U.S. (1959) 45, 944.
17. S. HOSOYA; Acta Cryst. (1963) 16, 310-312.
18. L. I. INGRAHAM, H. JOHANSEN; Archives of Biochemistry and Biophysics (1969) 132, 205-209.

19. M. E. LAMM, D. M. NEVILLE JR.; J. Phys. Chem (1965) 69, 3872-7.

20. R. ANGUILI, I. ArCAMONE, E. FORESTI, N.W. ISACCS, O. KENNARD, W. O. S. MOTHERWELL, L. RIVA DI SANSEVERINO, D. L. WAMPLER; Nature New Biol. (1971) 234, 78-80.

21. V. ZANKER, M. HELD, H. RAMMENSEE; Z. Naturforsch (1959) 146, 789.

22. J. N. MURELL; The Theory of the Electronic Spectra of Organic Molecules (1963), John Wiley and Sons, New York.

23. I. TINOCO JR.; J. Amer. Chem. Soc. (1960) 82, 4785; (1961) 83, 5047.

24. I. TINOCO JR., R. W. WOODY, D. F. BRADLEY; J. Chem. Phys. (1963) 38, 1317.

25. H. DE VOE; J. Chem. Phys. (1964) 41, 393.

26. G. S. LEVINSON, W. T. SIMPSON, W. CURTIS; J. Amer. Chem. Soc. (1957) 79, 4314-20.

27. M. R. PHILPOTT; J. Chem. Phys. (1970) 53, 968.

28. H. H. PERKAMPUS; (in): UV Atlas of Organic Compounds, Vol. 5; (1971), Butterworths, Verlag Chemie.

29. F. DÖRR; (in): UV Atlas of Organic Compounds, Vol. 5; (1971), Butterworth, Verlag Chemie.

30. A. STREITWIESER JR.; Molecular Orbital Theory for Organic Chemists; (1961), Wiley, New York.

31. D. S. DRUMMOND, V. F. W. SIMPSON-GILDEMEISTER, A. R. PEACOCKE; Biopolymers (1965) 3, 135-153.

32. D. S. DRUMMOND, N. J. PRITCHARD, U. F. W. SIMPSON-GILDEMEISTER, A. R. PEACOCKE; Biopolymers (1966) 4, 971-987.

33. M. J. WARING; Biochim. Biophys. Acta (1966) 114, 234.

34. V. VITAGLIANO, L. COSTANTINO; J. Phys. Chem. (1970) 74, 197-202.

35. G. WEILL, M. CALVIN; Biopolymers (1963) 1, 401-417.

36. F. ZUNINO, R. GAMBETTA, A. DI MARCO, A. ZACCARA; Biochim. Biophys. Acta (1972) 277, 489-498.

CHAPTER 5

THE BIREFRINGENCE OF THE POLYNUCLEOTIDE FIBRES

5.1. Introduction

5.1.1 The Physical basis of the birefringence

The birefringence is the property of some materials of having different refractive indices for different polarizations of the light traversing them. Many materials in which the molecules assume a preferential orientation, such as crystals, sheets, fibres or macromolecular solutions under streaming conditions usually are birefringent.

According to the physical optics theory, the velocity of light and the refractive index of the medium through which the light propagates are inter-related. The usual reduction of the velocity of the light in a medium, compared to vacuum, is due to the atoms acting as radiators of secondary waves after they have been polarized by the incident light. The retardation of the light is larger if the polarization effect is larger. The possibility of polarizing the electronic atmosphere of an atom is determined by the polarizability (α), which is defined as the proportionality constant relating the electric field (E) and the induced dipole ($q.\bar{s}$):

$$q \cdot s = \alpha E \qquad (5.1)$$

($\overset{+}{-}$ q are charges, separated by the distance s; (Ref. 1).

It can be shown that if the atoms are not independent, but linked by bonds, the polarizability will depend on the orientation of the electric field relative to the bond, usually being greater along the bond, (Ref. 1). If the molecules are arranged in a regular fashion about particular directions to form crystals or long fibres, the polarizabilities will suffer an averaging process about these particular

directions. As a result, these directions (eg. the fibre axis) will usually have the maximum (or minimum) polarizabilities of the specimen.

The refractive index for light polarized in a particular direction is related to the polarizability of the specimen along that direction by the Lorentz-Lorentz formula:

$$\frac{n^2 - 1}{n^2 + 2} \cdot \frac{M}{D} = \frac{4}{3} \pi N_o \alpha , \qquad (5.2)$$

where n is the refractive index, M is the molecular weight, D is the density and N_o is Avogadro's number. If we note that $(n^2 - 1)/(n^2 + 2)$ is approximately constant (Ref. 2), the equation (5.2) can be expressed in the form:

$$(n - 1) \tilde{} \text{ const. } \alpha, \qquad (5.3)$$

which shows the nearly-linear relationship between n and α. The concentration dependence of the 'constant' should be noted. Following from the relationship (5.3), the extreme values of the refractive index of an oriented specimen will occur along the same directions as those of the polarizability. The directions of the maximum and minimum refractive indices (also referred to as the slow and fast axes respectively) are normally at right angles to each other. In the case of a fibre they correspond to the directions along and across the fibre axis. The birefringence of a fibre, Δn, is defined as the difference between the values of the refractive indices for light polarized parallel and perpendicular to the fibre axis:

$$\Delta n = n_{11} - n_1 \qquad (5.4)$$

5.1.2 The measurement of the birefringence

A birefringent specimen placed between the crossed polarizer and analyser of a microscope is extinct at four orientations, at 90 degree intervals. Light, usually coloured, emerges from the specimen

for other orientation.

This behaviour can be understood if it is assumed that the incident polarized light is split into two beams polarized along the slow and fast axes of the specimen respectively, which travel through the specimen independently (Ref. 3). It is easy to see that if the orientation of the specimen is so that its slow or fast axis is collinear with that of the polarizer there will be no component along the axis of the analyser and this will lead to extinction.

Normally, the fibre is set at 45^{o} to the polarizer, as in Fig. 5.1. When reaching the fibre, the electric vector E is resolved into E_1 and E_{11}. The two components travel through the specimen at different speeds, dictated by the different refractive indices, so, they will emerge out of phase. Along the axis of the analyser they will project as E'_1 and E'_{11}. If their phase difference is zero or an integer number of wavelengths they will cancel out and extinction will result. With white light only the zero-order condition is met by all the wavelengths at the same time. For the higher path-differences only one wavelength at a time will be cancelled and the others will be passed by the analyser. They will combine together to give what are known as Newton's colours.

The retardation of one component relative to the other, in wavelength units, divided by the length travelled through the specimen,

$$\Delta n = \text{retardation/pathlength}, \qquad (5.5)$$

is another definition of the birefringence, equivalent to (5.4). The fact that it is expressed in terms of the retardation of the light of a particular wavelength is to be noted. The principle of measuring the birefringence is to produce a known retardation of opposite sign, so that the condition for complete zero-order extinction is restored. This is achieved with a calibrated compensator. The procedure of using the

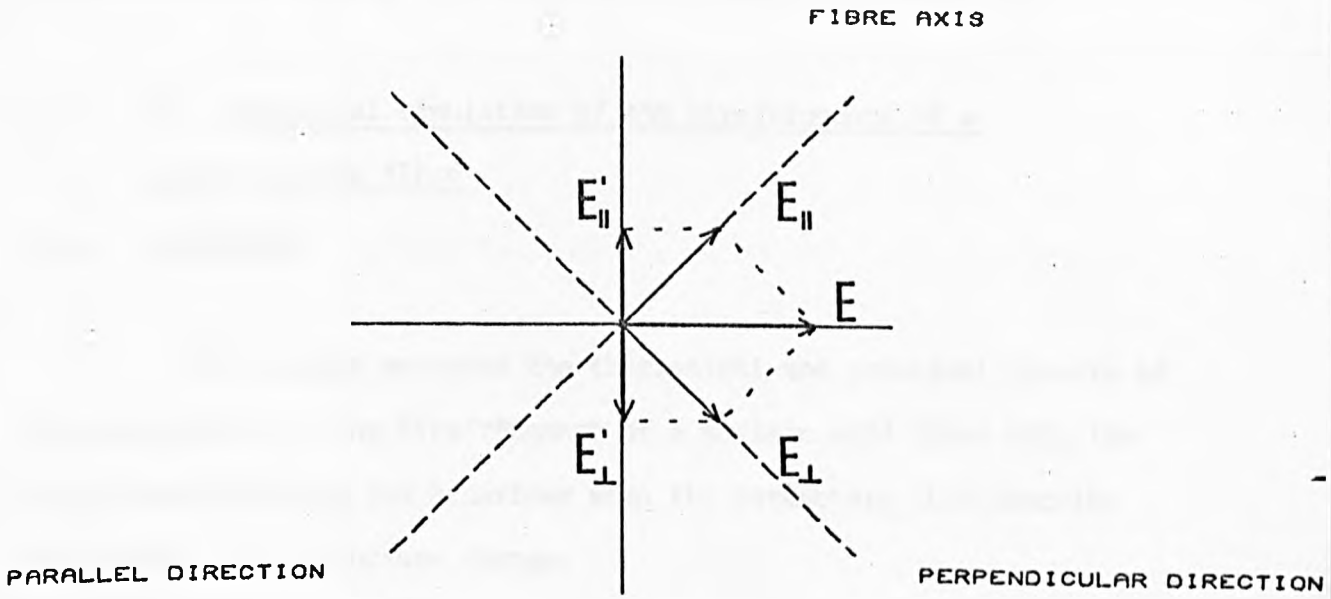

FIG. 5.1. A BIREFRINGENT FIBRE BETWEEN CROSSED ANALYZER & POLARIZER

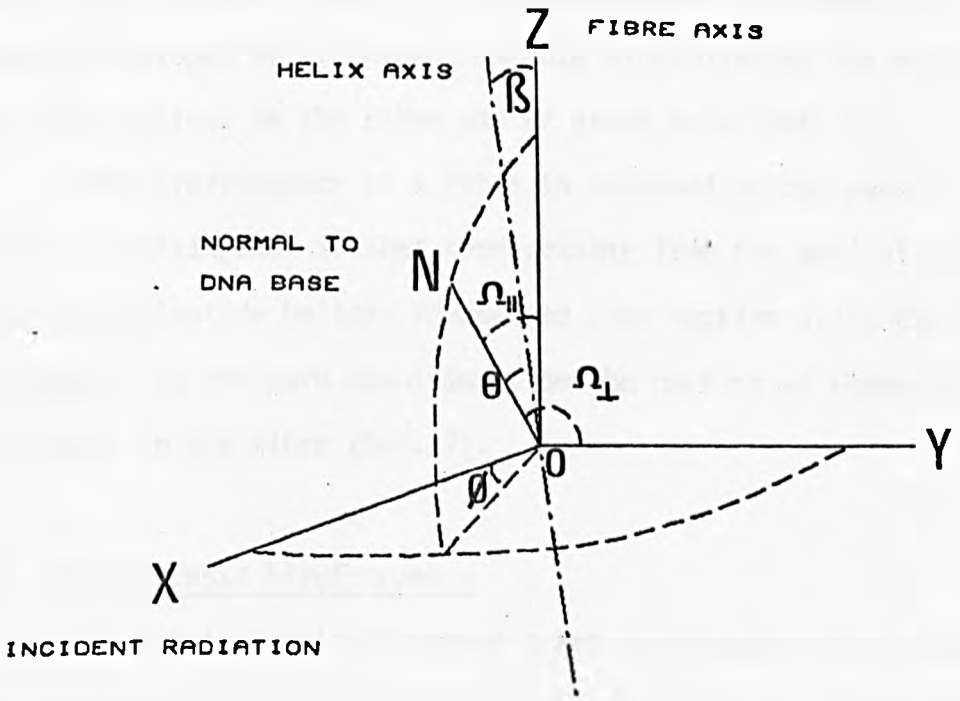

FIG. 5.2. A TRIGONOMETRIC SYSTEM ATTACHED TO A DNA FIBRE

compensator has already been described in detail in Section 2.4.

5.2 The theoretical simulation of the birefringence of a polynucleotide fibre

5.2.1 Background

This section presents the theoretical and practical aspects of the calculation of the birefringence of a nucleic acid fibre with the aim of understanding its behaviour when the parameters that describe the nucleic acid structure change.

The attempts to relate the flow birefringence of the nucleic acid solutions to the polarizability of the building units of the helix - the nucleotides - Ref. 4 and Ref. 5), and the geometrical considerations of Seeds (Ref. 2) about the birefringence of films and fibres served as models to this piece of work. The availability of a computer programme developed by T. Porumb, capable of simulating the missalignment of the helices in the fibre was of great help (Ref. 6).

The birefringence of a fibre is composed of two parts: the intrinsic birefringence is that term arising from the optical anisotropy of the polynucleotide helices themselves (see Section 5.1); the form birefringence is the term resulting from the packing of these helices side-by-side in the fibre (Ref. 7).

5.2.2 The intrinsic birefringence

The intrinsic birefringence takes into account the anisotropy of the polarizability of all the bonds in the system. According to Hartshorne (Ref. 1), the contribution of a bond to the polarizability in a particular direction is given by:

$$\alpha = \alpha_L \cos^2 \Omega + \alpha_T \sin^2 \Omega \,, \qquad (5.6)$$

where Ω is the angle of the bond with the given direction and α_L and α_T are the polarizabilities along and perpendicular to the bond (see Section 5.1). The amplitude of the problem is reduced by Tsvetkov's demonstration that the bases of the nucleic acids are highly anisotropic, whereas the sugars and the phosphate groups are practically isotropic, thus contributing very little to the birefringence (Ref. 4).

The estimates of the polarizabilities of the DNA bases vary (Ref. 4, Ref. 5 and Ref. 8), but their common feature is that the polarizability perpendicular to the heterocyclic system of the base is much smaller than within the plane of the base. It is reasonable to assume that the polarizability in the plane of the base is isotropic. In this way the entire electronic system of a base can be treated as a 'bond' orientated along the normal to the plane of the base, with large transversal polarizability (α_T) and small longitudinal polarizability (α_L).

Let us assume that the bases are tilted by an angle θ with respect to the plane perpendicular to the helix axis. Let us choose OZ in the trigonometric system from Fig. 5.2 to represent the fibre axis. The angle between the fibre axis and the axis of a particular helix is β. The angles between the normal (ON) to the plane of a base and the directions OZ (parallel) and OY (perpendicular to the fibre axis) are Ω_{11} and Ω_1. According to (5.6), the polarizability of the base along the direction OZ is given by:

$$\alpha_{11} = \alpha_L \cos^2 \Omega_{11} + \alpha_T \sin^2 \Omega_{11} \qquad (5.7)$$

and the polarizability along OY is given by:

$$\alpha_1 = \alpha_L \cos^2 \Omega_1 + \alpha_T \sin^2 \Omega_1 \qquad (5.8)$$

It is very easy to obtain an analytic expression for the birefringence of a fibre in which the helices are perfectly aligned

with the fibre axis. In this case the normals ON describe a cone of semi-angle θ about OZ and α_{11} becomes:

$$\alpha_{11} = \alpha_L \cos^2\theta + \alpha_T \sin^2\theta , \qquad (5.7^1)$$

The angle Ω_1 depends on the angular orientation (ϕ) of the base about the helix axis (Fig. 5.2). By expressing the projection of ON onto OY in two ways, one obtains the relationship:

$$\sin\Omega_1 = \sin\theta \cdot \sin\phi , \qquad (5.9)$$

Hence, α_1 becomes:

$$\alpha_1 = \alpha_L (1 - \sin^2\theta \sin^2\phi) + \alpha_T(\sin^2\theta \sin^2\phi) \qquad (5.8^1)$$

By subtracting (5.8^1) from (5.7^1) and cylindrically averaging for all values of ϕ one obtains the difference between the parallel and perpendicular polarizabilities of the fibre:

$$\Delta\alpha = (\alpha_L - \alpha_T).\ (1 - 1.5 \sin^2\theta) , \qquad (5.10)$$

In view of what was said earlier, the quantity $(\alpha_L - \alpha_T)$ is negative. Using the relationship (5.3) together with the definition (6.4) one obtains:

$$\Delta n = K (1 - 1.5 \sin^2\theta) , \ (K = \text{negative constant}), \qquad (5.11)$$

which is the expression for the intrinsic birefringence of a perfectly orientated polynucleotide fibre in terms of the tilt angle of the bases to the helix axis. It is represented by the curve (0) in Fig. 5.3 . It can be seen that when the tilt is nil the intrinsic birefringence has its maximum negative value. It becomes zero for an angle $\theta = 54^\circ 44'$ after which it changes sign. In the range $0 - 5^\circ$ the birefringence is practically constant and for a change of tilt from 0 to 20°, as encountered during the B to A transition in DNA, the birefringence changes by 18%.

The birefringence of a fibre in which there is a certain degree of misorientation was calculated numerically, by an extension of the computer programme originally developed by T. Porumb for the simulation of the fibre ESR spectra (Ref. 6, Ref. 9 and Ref. 10). The misorientation was assumed to take the form of a gaussian spread of the axes of the helices about the fibre axis, the probability of a polynucleotide helix lying along the generator of a cone of semi-angle β being proportional to:

$$\exp\ (-\ \beta^2/2\ \Delta^2), \qquad (5.12)$$

where Δ is the half width of the distribution.

The computer programme operated a cylindrical averaging routine at the level of both the fibre and the nucleic acid helix, in which the individual contribution of each base to the polarizabilities parallel and perpendicular to the fibre axis, given by the equations (5.7) and (5.8), were accumulated separately, account being taken of the weight of each orientation, (ref. 6). The two quantities were then subtracted as above.

The calculations showed that the results were dependent only on the difference of the in-plane and normal-to-the-plane polarizabilities and not on the actual values of α_L and α_T assumed. These results, normalized for an extreme birefringence of - 0.1 are presented in Fig. 5.3. It is interesting to note that the zero birefringence is obtained at the same tilt angle regardless of the degree of misalignment in the fibre.

5.2.3 The form birefringence

A solution of non-spherical molecules under streaming conditions or a body consisting of aligned elongated particles are often positively birefringent even if the component particles are isotropic, (Ref. 1 and

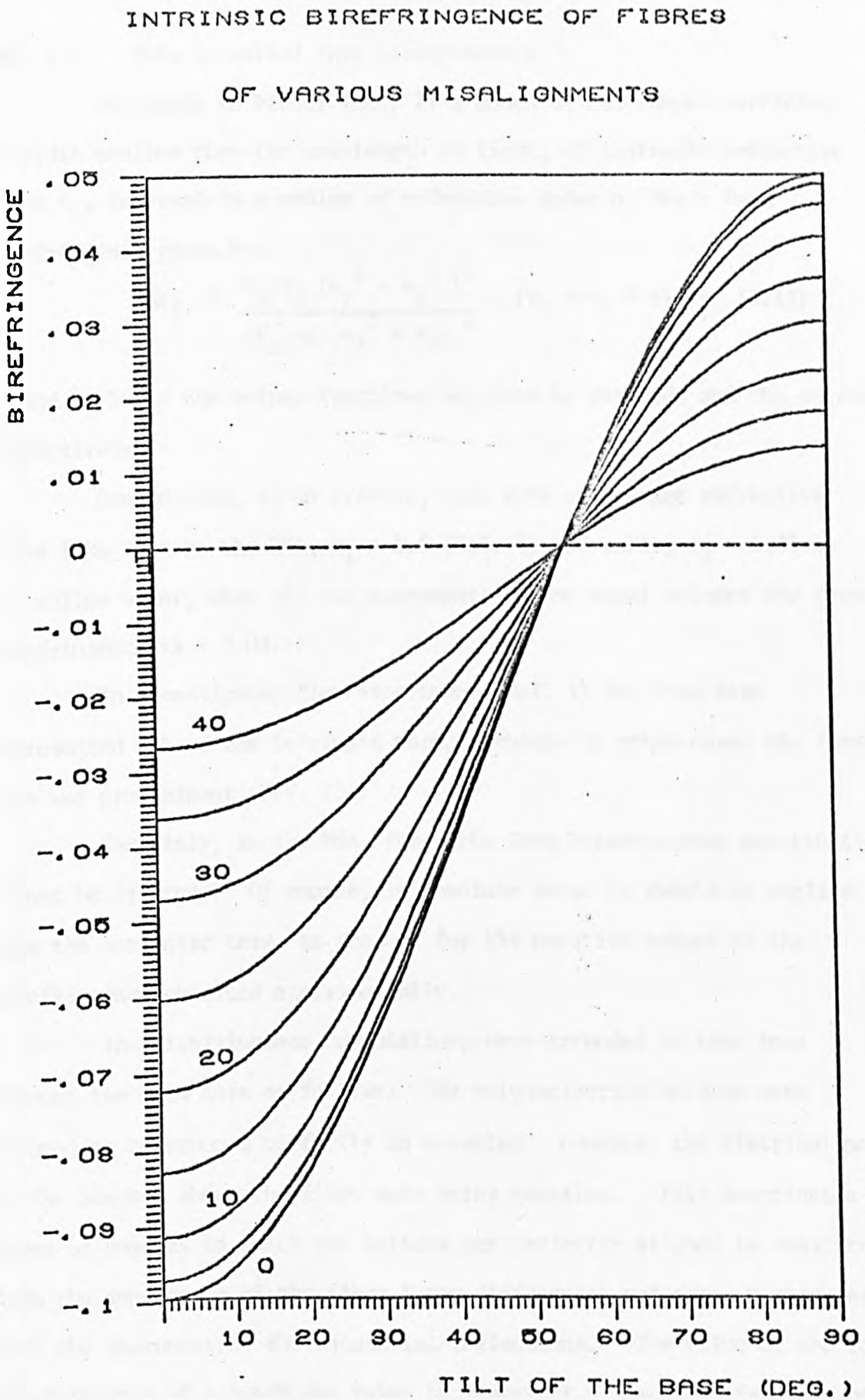

FIG. 5.3. COMPUTER SIMULATION OF THE INTRINSIC BIREFRINGENCE OF A POLYNUCLEOTIDE FIBRE. THE GAUSSIAN PARAMETER OF MISALIGNMENT IS INDICATED ON EACH CURVE .

Ref. 11). This is called form birefringence.

According to Wiener (Ref. 7) a bunch of rod-shaped particles, of width smaller than the wavelength of light, of isotropic refractive index n_1, immersed in a medium of refractive index n_2 has a form birefringence given by:

$$\Delta n_f = \frac{V_1 V_2 (n_1^2 - n_2^2)^2}{(V_1 + 1) n_2^2 + V_2 n_1^2}, \quad (V_1 + V_2 = 1), \qquad (5.13)$$

V_1 and V_2 being the volume fractions occupied by the rods and the solvent respectively.

Considering, as an example, rods with an average refractive index like that of the DNA, $n_1 = 1.6$ (Ref. 4) and taking $n_2 = 1.33$ as for saline water, when the two components occupy equal volumes the form birefringence is + 0.04.

In a particular flow experiment (Ref. 4) the form term represented 58% of the intrinsic term, although in other cases the form term was predominant (Ref. 12).

Certainly, in the DNA fibres the form birefringence contribution cannot be ignored. Of course, in absolute value it should be smaller than the intrinsic term, to account for the negative values of the birefringence obtained experimentally.

The birefringence computations were extended to take into account the form term as follows: The polynucleotide helices were assumed to be grouped perfectly in oriented bunches, the distribution of the bunches about the fibre axis being gaussian. This description in terms of bunches in which the helices are perfectly aligned is consistent with the appearance of the fibre X-ray diffraction patterns, particularly with the sharpness of the equatorial reflections. The value of the form birefringence of a bunch was taken to represent a specified fraction of the intrinsic birefringence of a perfectly aligned fibre with zero base

tilt. A bunch is analogous to a 'bond' oriented along its length, because the polarizability (refractive index) is maximum along the axis of the bunch. Based on this analogy, the calculation of the form birefringence becomes equivalent to that of the intrinsic birefringence and the formulae (5.7) and (5.8) are applicable. Using the same averaging routines as before the values of the form birefringence of fibres with specified degrees of misalignment were obtained and then subtracted from the corresponding values of the intrinsic birefringence.

The result is shown in Fig. 5.4 for the case in which the form term was chosen to represent 58% of the maximum intrinsic term and the maximum birefringence was arbitrarily set to the value of -0.1.

By comparison with Fig. 5.3 it can be noted that, as a consequence of the subtraction of a positive quantity from the intrinsic term, the birefringence varies faster with the angle of tilt and changes sign at a smaller angle. The crossover still takes place at a unique angle of tilt for all the degrees of misalignment (for the particular numeric application considered in Fig. 5.4 this angle is 32^{o}).

The contribution of the flat drugs to the birefringence of the fibre was not considered explicitly in this simulation. It is reckoned that, by analogy with the bases, they have a large polarizability in the planes of their chromophores, which would enhance the negative birefringence of the polynucleotide fibres if they had a similar orientation to that of the bases.

5.3 Experimental Results

5.3.1 The fibre dimensions

When the polynucleotide fibres are transferred from the room atmosphere (approx. 50% relative humidity) to an atmosphere of high

FIBRE BIREFRINGENCE

INCLUDING A FORM BIREFRINGENCE TERM

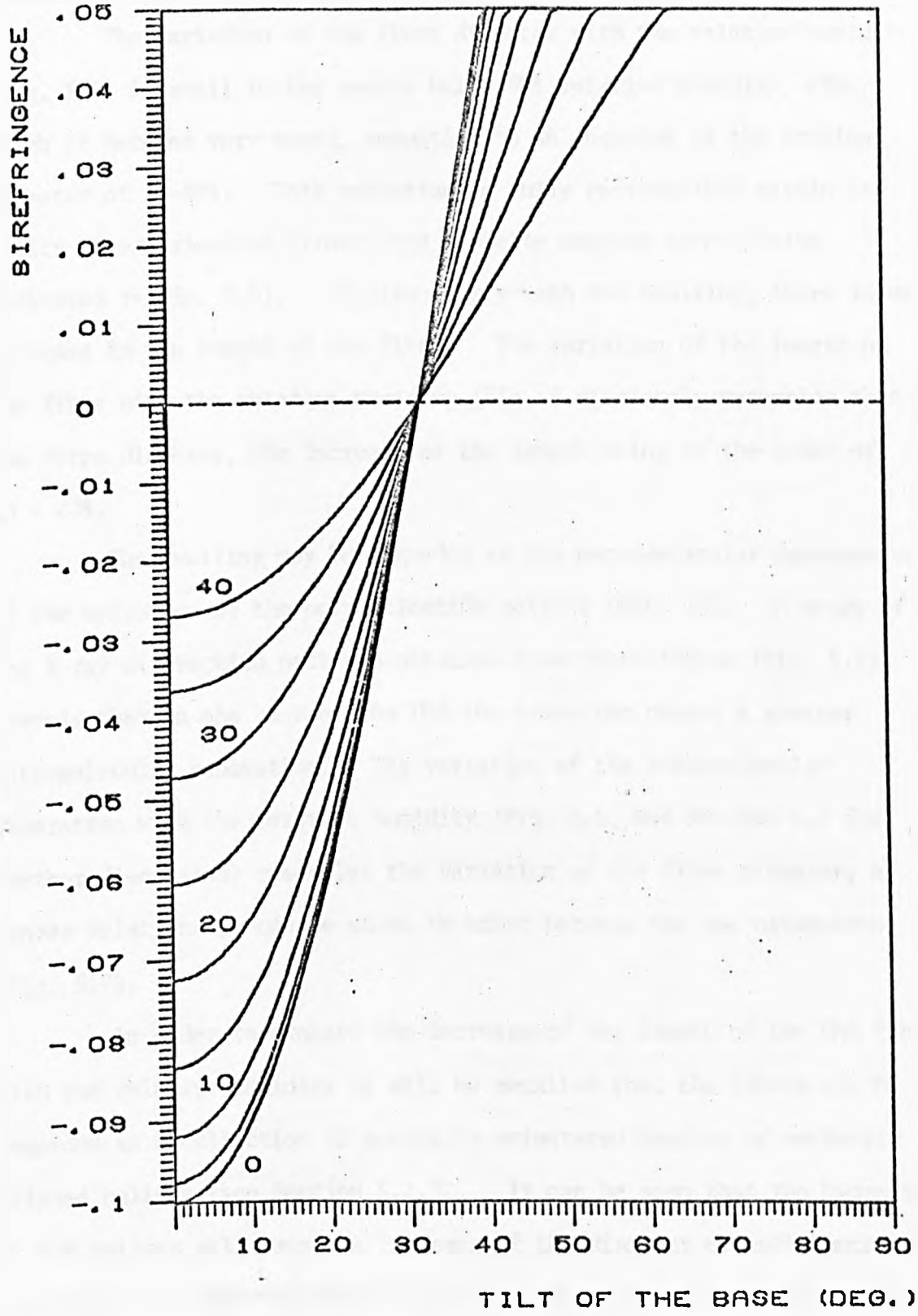

FIG. 5.4. THE TOTAL BIREFRINGENCE OF A FIBRE IN WHICH THE FORM TERM REPRESENTS 58% OF THE MAXIMUM INTRINSIC TERM .

relative humidity, they suffer an increase of both their diameter and length. This effect occurs irrespective of the nature of the polynucleotide or of the presence of drugs in the fibres.

The variation of the fibre diameter with the relative humidity (Fig. 5.5) is small in the region below 80% relative humidity, after which it becomes very rapid, amounting to an increase of the original diameter of 30-60%. This variation is fully reproducible within the limits of experimental errors (the probable maximum errors being indicated in Fig. 5.5). Simultaneously with the swelling, there is an increase in the length of the fibre. The variation of the length of the fibre with the relative humidity (Fig. 5.6) closely resembles that of the fibre diameter, the increase of the length being of the order of 10 - 20%.

The swelling may be regarded as the macromolecular consequence of the hydration of the polynucleotide helices (Ref. 13). A study of the X-ray diffraction patterns obtained from these fibres (Fig. 6.1), reveals that in the case of the DNA the hydration causes a greater intermolecular separation. The variation of the intermolecular separation with the relative humidity (Fig. 6.5, see Section 6.2 for further discussion) resembles the variation of the fibre diameter; a linear relationship can be shown to exist between the two parameters (Fig. 5.7).

In order to explain the increase of the length of the DNA fibres with the relative humidity it will be recalled that the fibres can be regarded as a collection of partially orientated bunches of perfectly aligned helices (see Section 5.2.3). It can be seen that the hydration of the helices will cause an increase of the diameter of each bunch, thus resulting in a swelling which will have components both across the fibre axis (responsible for the increase in the fibre diameter) and along the

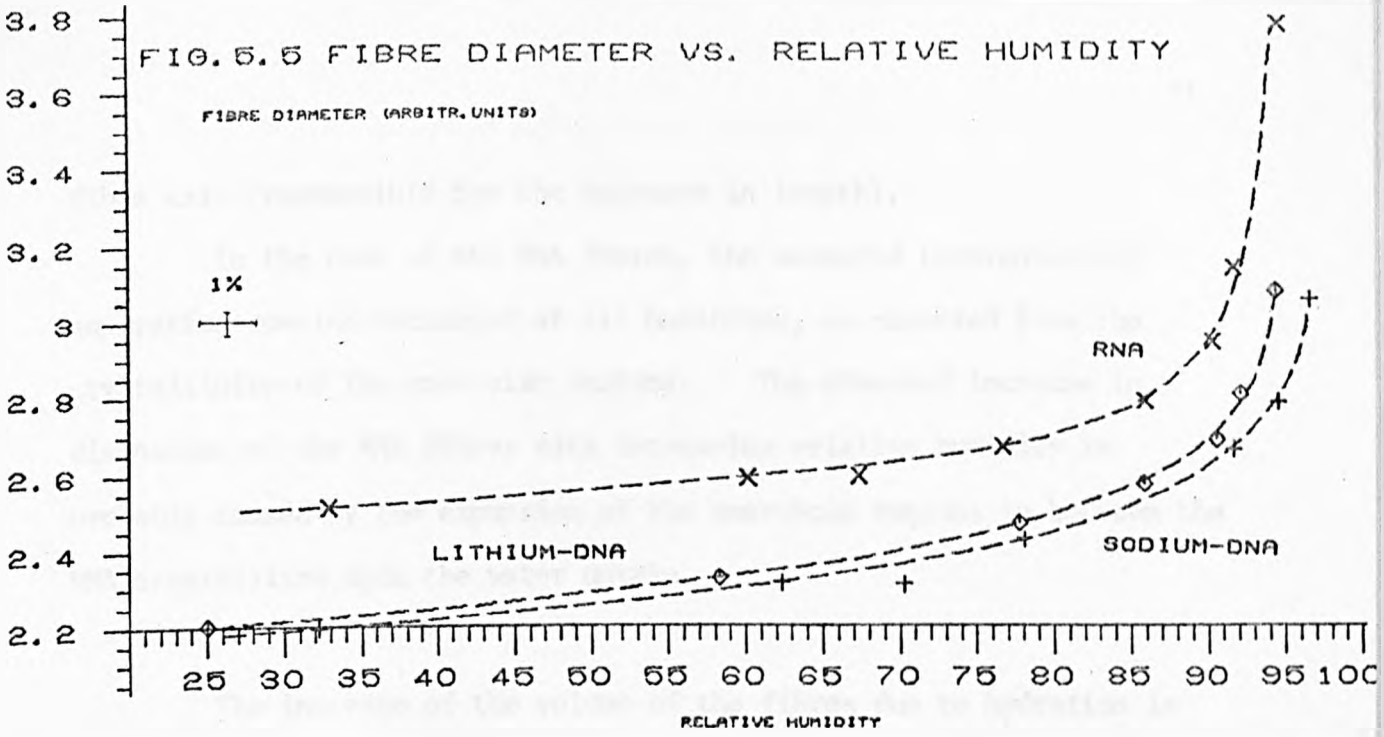
FIG. 5.5 FIBRE DIAMETER VS. RELATIVE HUMIDITY
FIBRE DIAMETER (ARBITR. UNITS)
3.8
3.6
3.4
3.2
3
2.8
2.6
2.4
2.2
1%
RNA
LITHIUM-DNA
SODIUM-DNA
25 30 35 40 45 50 55 60 65 70 75 80 85 90 95 100
RELATIVE HUMIDITY

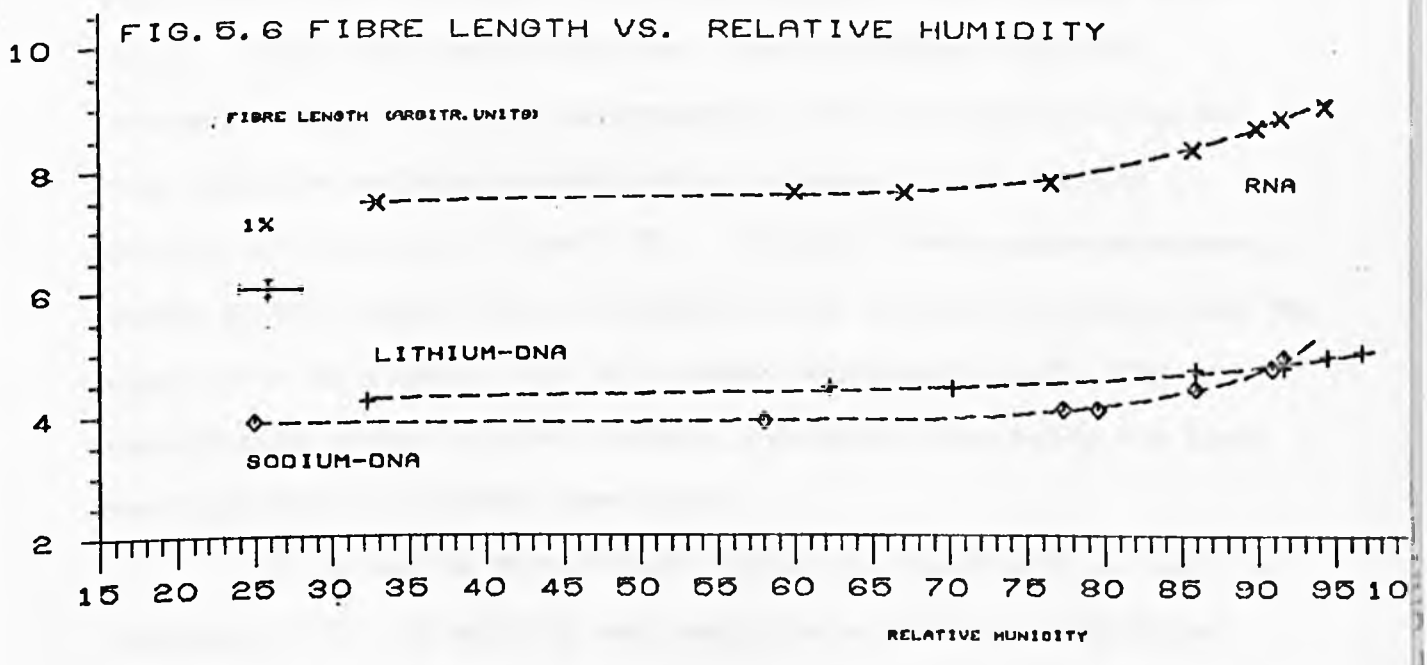
FIG. 5.6 FIBRE LENGTH VS. RELATIVE HUMIDITY
FIBRE LENGTH (ARBITR. UNITS)
10
8
6
4
2
1%
RNA
LITHIUM-DNA
SODIUM-DNA
15 20 25 30 35 40 45 50 55 60 65 70 75 80 85 90 95 10
RELATIVE HUMIDITY

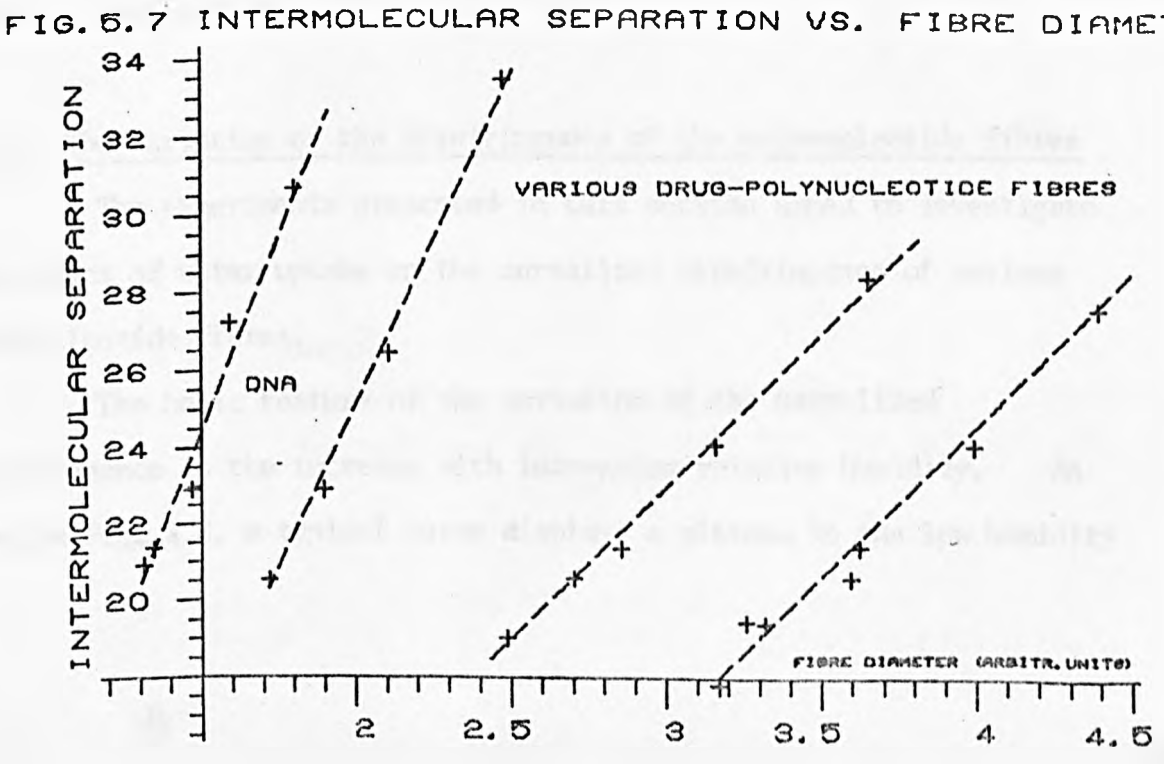
FIG. 5.7 INTERMOLECULAR SEPARATION VS. FIBRE DIAMETER
INTERMOLECULAR SEPARATION
34
32
30
28
26
24
22
20
VARIOUS DRUG-POLYNUCLEOTIDE FIBRES
DNA
FIBRE DIAMETER (ARBITR. UNITS)
2
2.5
3
3.5
4
4.5

fibre axis (responsible for the increase in length).

In the case of the RNA fibres, the measured intermolecular separation remains unchanged at all humidites, as expected from the crystallinity of the molecular packing. The observed increase in dimensions of the RNA fibres with increasing relative humidity is probably caused by the expansion of the amorphous regions in between the RNA crystallites upon the water uptake.

The increase of the volume of the fibres due to hydration is expected to cause a dilution of the polarizable material present in the fibre. Since both the intrinsic and form birefringence will be reduced by dilution in the same proportion, it is possible to allow for this affect by applying a normalization procedure as described in Section 2.4 (equations 2.8 and 2.9). All the birefringence measurements quoted in this chapter were normalized for the effect of swelling. Apart from placing the experimental data on a common concentration scale, the normalization permitted other features, previously obscured by the large swelling effect, to become conspicuous.

The normalized birefringence values are quoted with an estimated accuracy of $\pm$ 5% (of which 2% represents the uncertainty in the value before normalization).

5.3.2 The variation of the birefringence of the polynucleotide fibres

The experiments presented in this section aimed to investigate the effect of water uptake on the normalized birefringence of various polynucleotide fibres.

The basic feature of the variation of the normalized birefringence is the increase with increasing relative humidity. As seen in Fig. 5.8, a typical curve displays a plateau in the low humidity

FIG. 5.8 NORMALIZED BIREFRINGENCE VS. RELATIVE HUMIDITY

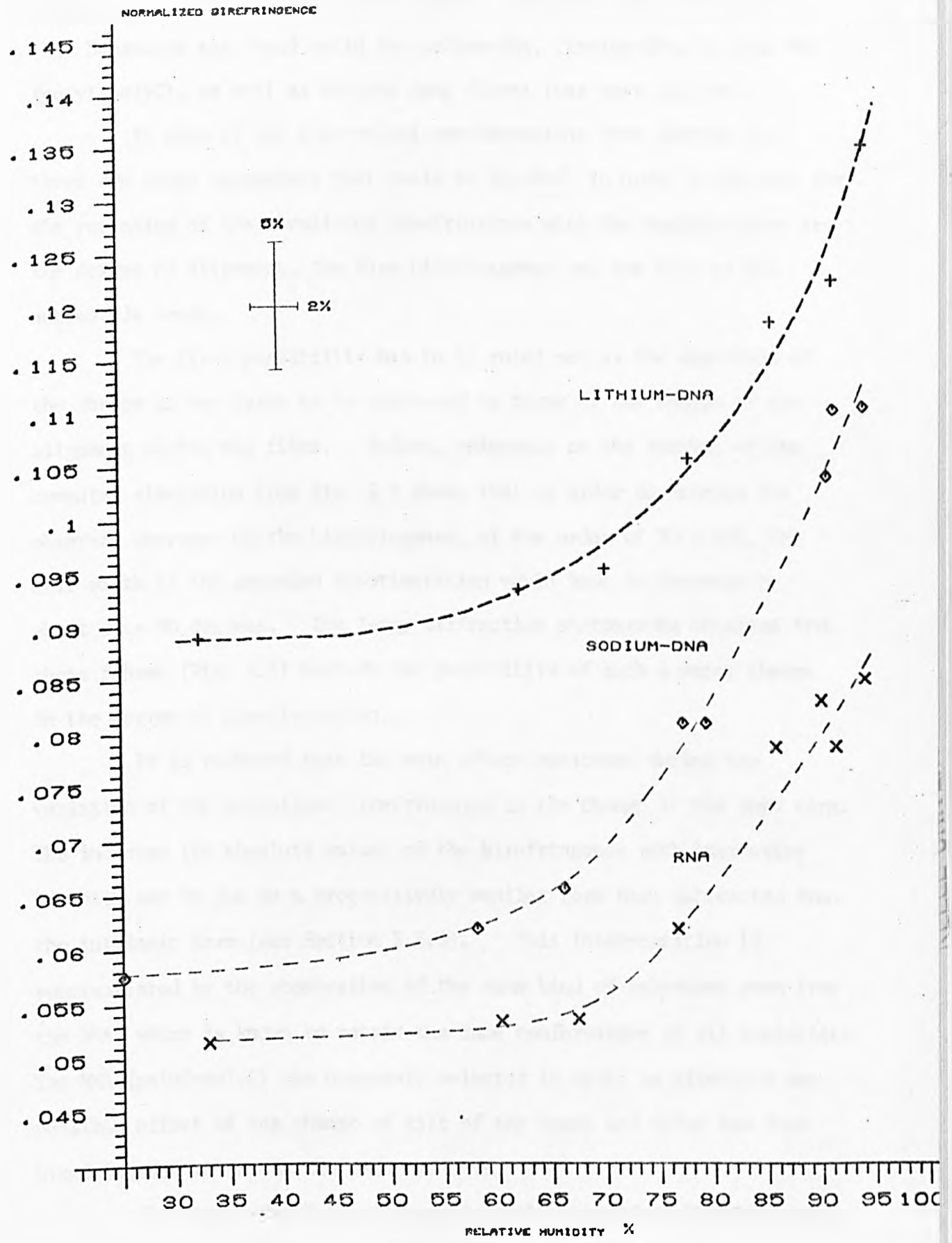

FIG. 5.8. POLYNUCLEOTIDE FIBRES: LITHIUM-DNA (0.05 M LICL)
SODIUM-DNA (0.01 M NACL); 12-FOLD RNA POLY I.POLY C (0.05 M NACL)

region and a rapid increase in the region around 80% relative humidity. This behaviour was found valid for sodium-DNA, lithium-DNA, 12-fold RNA (polyI-polyC), as well as for the drug fibres (see next section).

In view of the theoretical considerations from Section 5.2 there are three parameters that could be invoked in order to account for the variation of the normalized birefringence with the humidity;they are the degree of alignment, the form birefringence and the tilt of the nucleotide bases.

The first possibility has to be ruled out as the magnitude of the change is too large to be explained in terms of the change of the alignment within the fibre. Indeed, reference to the results of the computer simulation from Fig. 5.3 shows that in order to produce the observed decrease of the birefringence, of the order of 30 - 50%, the half width of the gaussian misorientation would have to increase by about 20 - 30 degrees. The X-ray diffraction photographs obtained from these fibres (Fig. 6.1) exclude the possibility of such a major change in the degree of misorientation.

It is reckoned that the main effect monitored during the variation of the normalized birefringence is the change in the form term. The increase (in absolute value) of the birefringence with increasing humidity may be due to a progressively smaller form term subtracted from the intrinsic term (see Section 5.2.3). This interpretation is substantiated by the observation of the same kind of behaviour even from the RNA, which is known to retain the same conformation at all humidities. The RNA (polyI-polyC) was purposely selected in order to eliminate any possible effect of the change of tilt of the bases and allow the form birefringence to act as the main variable.

The magnitude of the 'step-up' of the normalized birefringence of the RNA fibre upon increasing the relative humidity, of about 60%,

is smaller than the approx. 90% increase in the case of the DNA fibre which has undergone an A to B transition (see the X-ray diffraction photographs, Fig. 6.1). Indeed, in the case of the DNA fibre, in addition to the change in the form term, one also detected the increase of the intrinsic birefringence due to the change of the tilt of the bases (see Section 5.2.2). As it appears from the above percentages, the change of tilt is only of second order importance compared to the role played by the form term. The exact mechanism of the variation of the form term is not known.

It is possible that the larger birefringence of the lithium-DNA fibre compared to that of the sodium-DNA (Fig. 5.8) is to a great extent due to a better orientation, noticeable at high humidity, when both of them are in the same B conformation (compare the X-ray diffraction patterns, Fig. 6.1). In the low humidity range, one has the additional effects of the slightly different tilt angles and modes of molecular packing.

A more quantitative comparison of the birefringence value of the polynucleotide fibres of different types is difficult because of the combined effect of the different tilt angles of the bases, molecular packings and degrees of alignment. However, as a general rule, it was found that at room humidity the polyI-polyC fibres had a smaller birefringence (-0.05 or lower, in absolute value) than that of the sodium-DNA fibres, which ranged between -0.06 and -0.07; the birefringence of the lithium-DNA fibres was slightly higher, up to -0.09; the thin fibres often had a larger birefringence than the thick ones, possibly reflecting a better orientation; at the same time, it was found that the fibres with larger salt content were less birefringent, maybe due to the presence of sodium chloride microcrystals.

5.3.3 The birefringence of the drug-DNA fibres

The main observation resulting from the study of the drug-DNA fibres is that their birefringence is greater than that of the control fibres without drug, the birefringence being larger for increasing amounts of drug present. Nevertheless, the normalized birefringence varies with the humidity in a similar fashion to that of the polynucleotide fibres mentioned in Section 5.3.2.

The variation with the relative humidity of the normalized birefringence of fibres of different P/D ratios is shown in Figs. 5.9 and 5.10 for two sets of daunomycin-DNA and adriamycin-DNA complexes. The maximum and mimimum values of the birefringence are plotted as function of the nominal D/P ratio of each fibre in Fig. 5.11. Except for the P/D = 4, (see also Section 6.2.2), the relationship is linear both for the high and low humidity values of the birefringence and the two lines are slightly divergent.

The birefringence of several freshly-cut fibre sections of different drug content was measured at the room humidity both before and after they were subjected to a wet atmosphere. Two sets of birefringence values were obtained, which are plotted against the D/P ratio in Fig. 5.12. Within the experimental errors, the points lie on two straight lines of different slopes. The slope corresponding to the sections measured before the wet treatment represents about 40% of the value of the slope corresponding to the sections measured after the treatment.

The proportional increase of the birefringence with the D/P ratio could be accounted for if the drug was intercalated or else, oriented nearly perpendicular to the helix axis, so that the anisotropy of the drug chromophore would add to the anisotropy of the DNA

NORMALIZED BIREFRINGENCE VS. RELATIVE HUMIDITY

ANTHRACYCLINE FIBRES

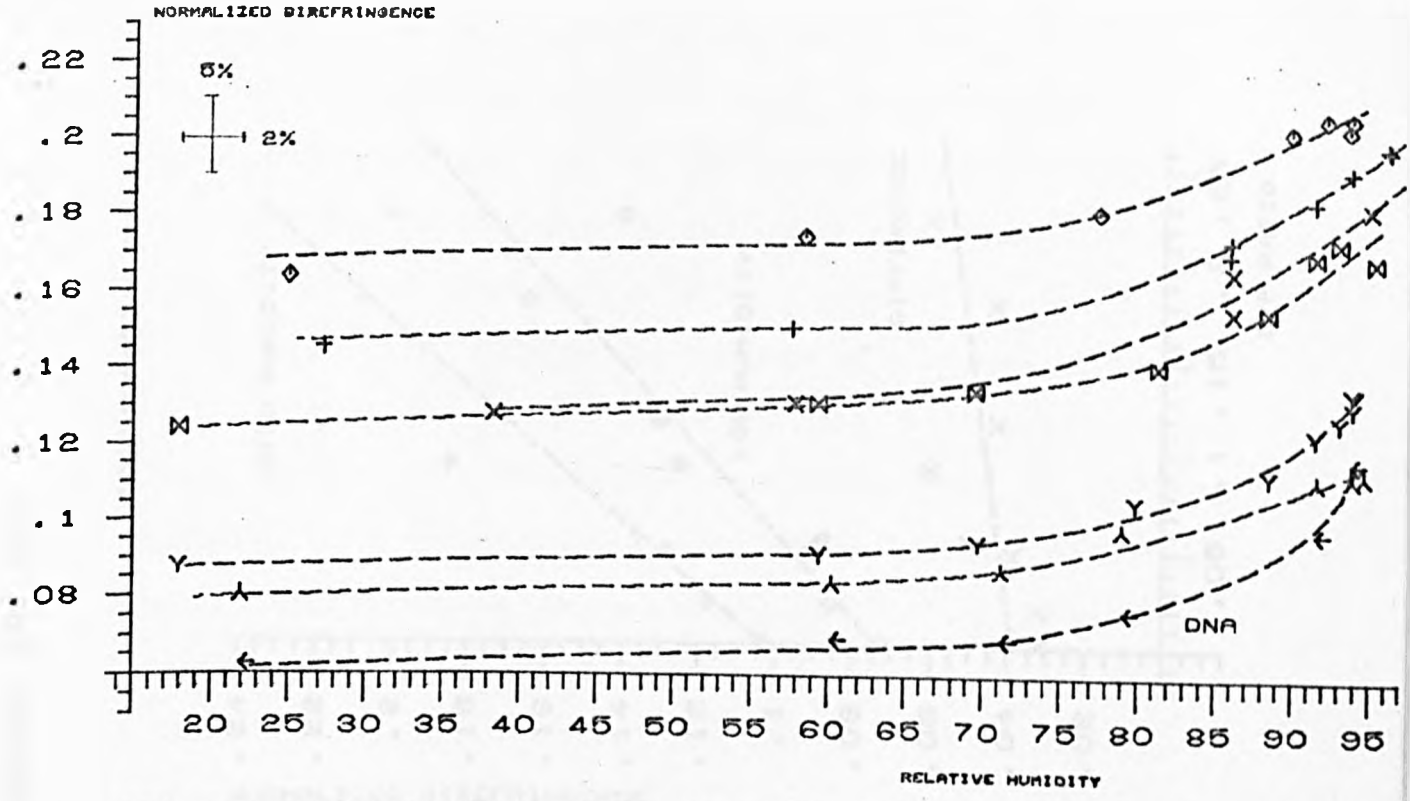

FIG. 5.9. DAUNOMYCIN-DNA, P/D = 4.1, 5.1, 7.8, 10.1, 15.4, 20.0, 50.0;

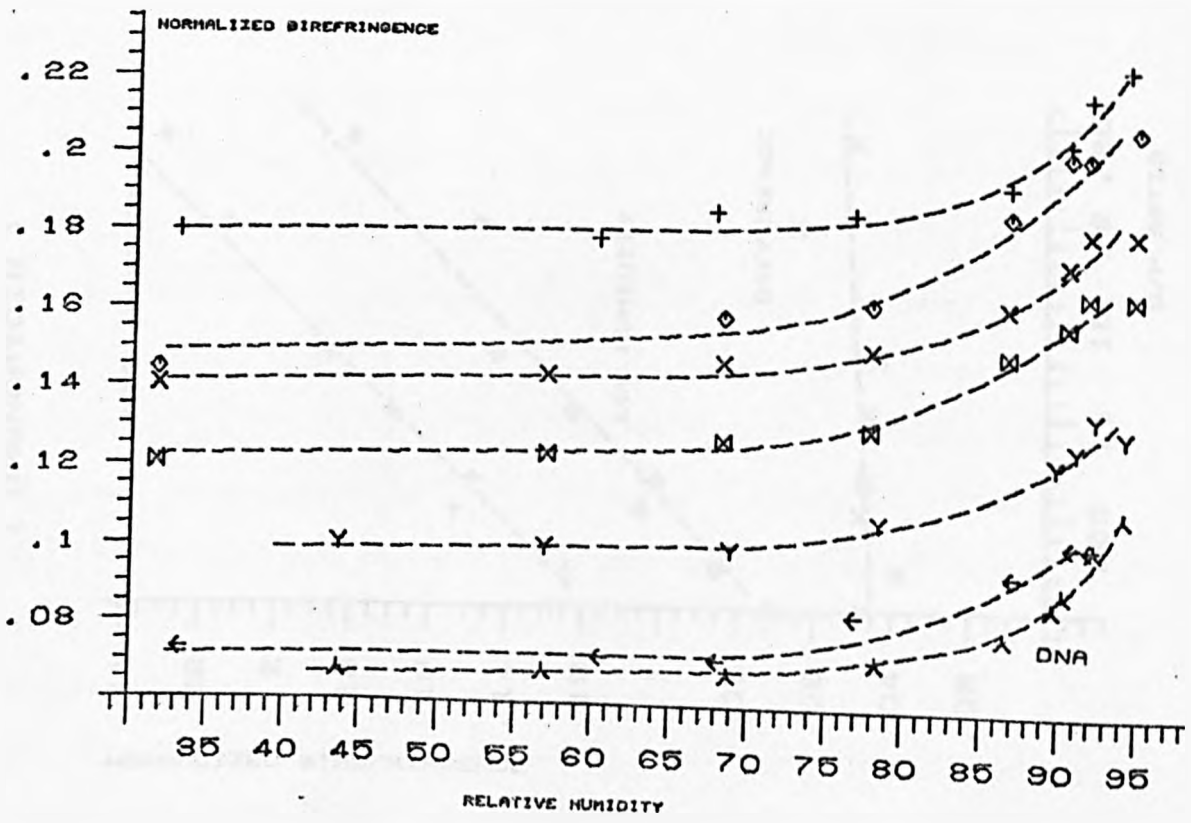

FIG. 5.10. ADRIAMYCIN-DNA, P/D= 4.5, 5.6, 8.6, 10.9, 18.8, 20.4, 50.0;

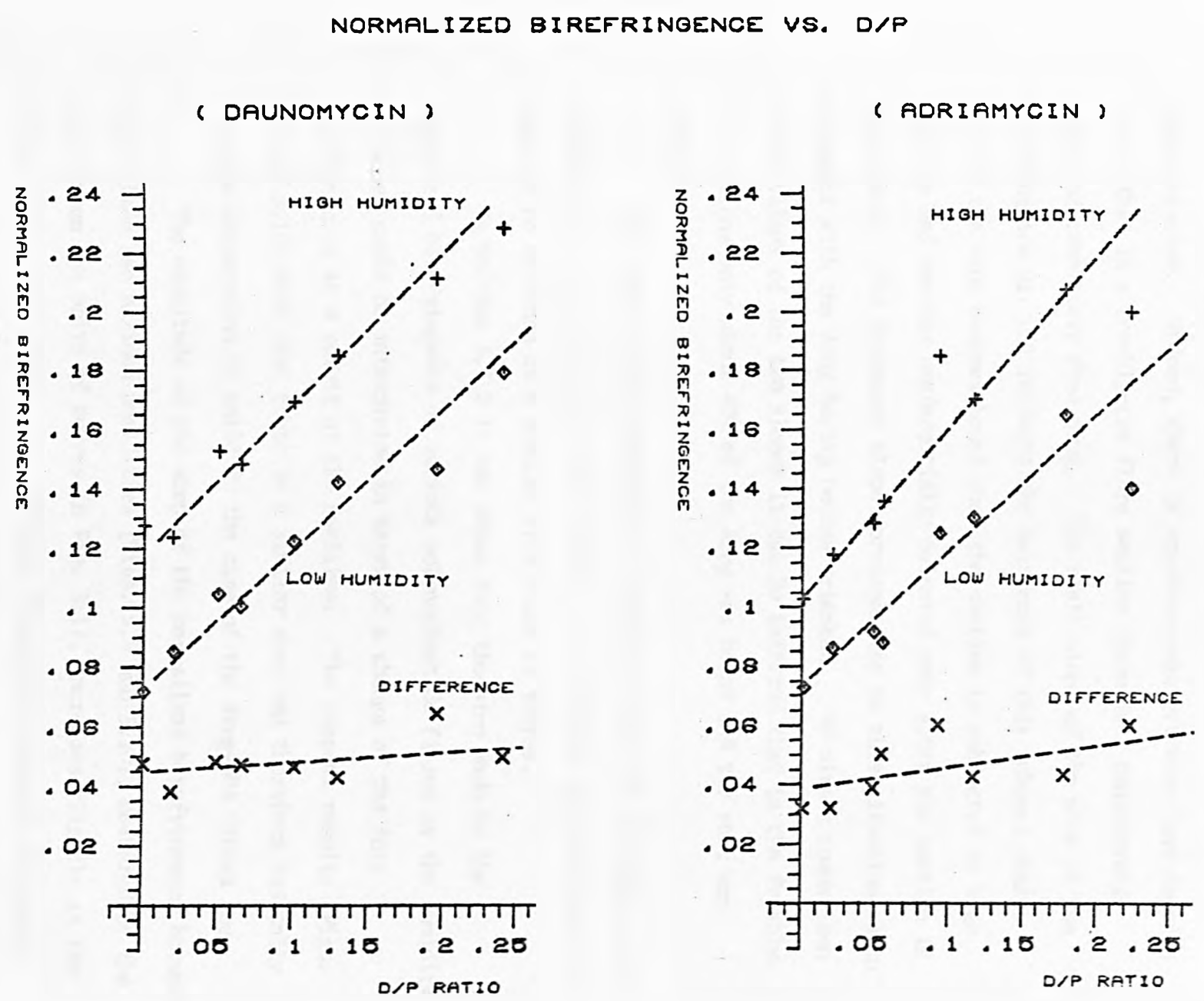

FIG. 5.11. MAXIMUM AND MINIMUM VALUES OF THE NORMALIZED BIREFRINGENCE

(see also Section 5.2). The free drug, when randomly distributed, would not contribute to the birefringence of the fibre.

The results presented in Fig. 5.12 substantiate this interpretation. Indeed, there is spectroscopic evidence (see Section 7.2.1) that in a freshly-cut fibre section there is a considerable amount of completely free drug. The small slope of the plot of the birefringence vs. D/P reflects the existence of this unbound phase. Most of the drug becomes bound when the section is subjected to high humidity and remains preferentially oriented even after the section is dried back. The increased slope corresponding to this situation is in agreement with the drug having become oriented. By direct comparison of the values of the two slopes it can be inferred that in the freshly-cut sections only about 40% of the drug was bound and the rest was unbound.

The effect just mentioned is encountered only in sections and is probably related to the treatment during the embedding (see Section 2.5). There is no evidence of a similar free phase in fibres.

In Section 5.3.2 it was shown that the step made by the normalized birefringence of various polynucleotide fibres as the humidity increased could be interpreted in terms of a change of the form birefringence as a result of the swelling. The present results (Figs. 5.9 and 5.10) show that there is a similar step and therefore basically the same explanation is valid in the case of the drug-DNA fibres too.

The magnitude of the step of the normalized birefringence between the minimum and maximum humidities (Figs. 5.9 and 5.10), measured by the gap between the pairs of curves in Fig. 5.11, increases slightly as the D/P ratio becomes larger, i.e., the two lines have slightly different slopes. Extending the argument presented in connection with Fig. 5.12, the divergence of the two lines ought to indicate some redistribution of the drug taking place during the transition from the dry to the wet state

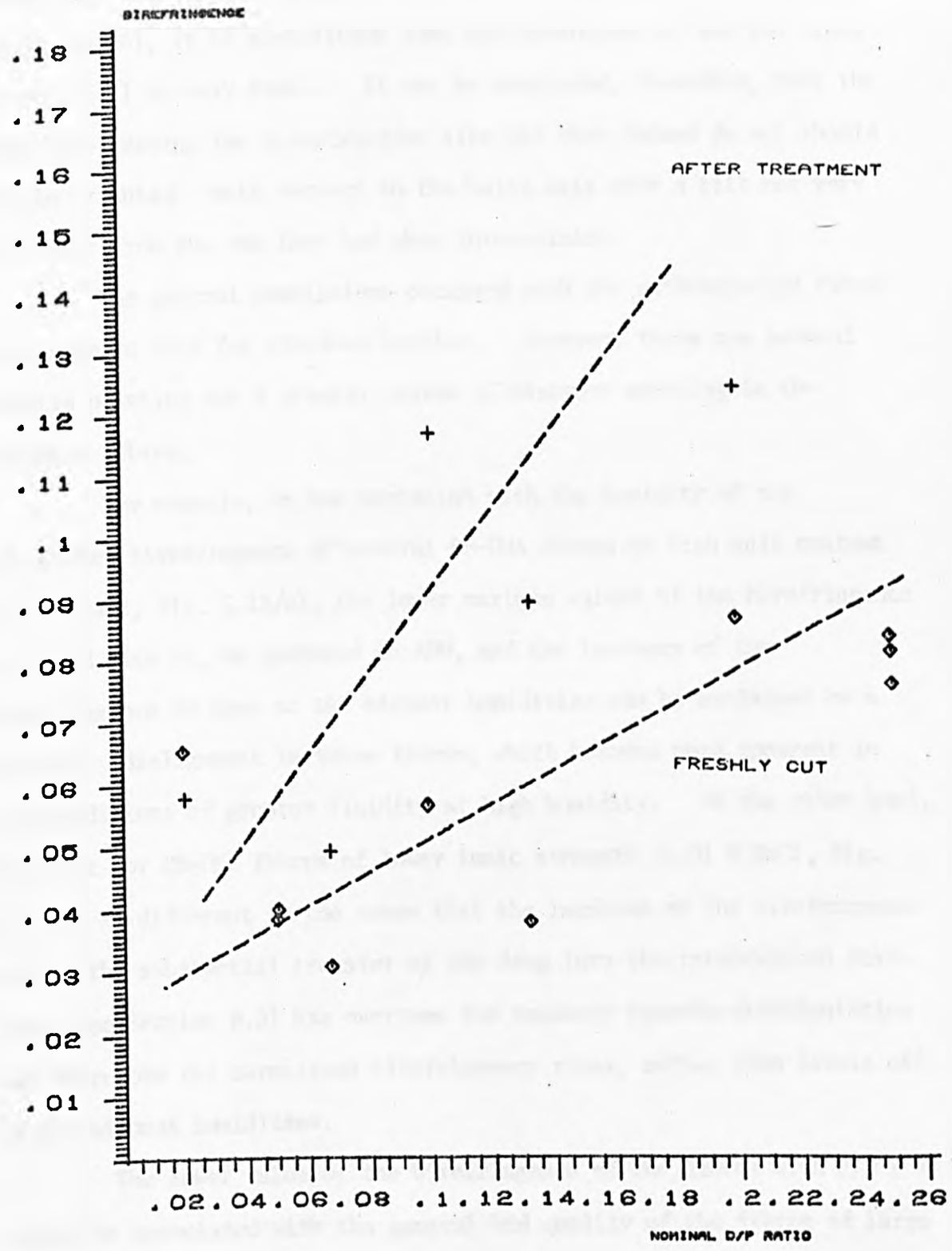

FIG. 6.12. BIREFRINGENCE OF FIBRE SECTIONS (AT ROOM HUMIDITY) BEFORE AND AFTER TREATMENT AT HIGH HUMIDITY .

of the fibre. However, in relation to the general belief that a considerable proportion of the drug molecules leave the intercalated state upon lowering the humidity (Ref. 14 ; see also the X-ray evidence in Chapter 6), it is significant that the divergence of the two lines in Fig. 5.11 is very small. It can be concluded, therefore, that the molecules leaving the intercalation site (if they indeed do so) should remain oriented with respect to the helix axis with a tilt not very different from the one they had when intercalated.

The general conclusions obtained with the anthracycline fibres also seem to hold for ethidium bromide. However, there are several details pointing out a greater degree of disorder existing in the ethidium fibres.

For example, in the variation with the humidity of the normalized birefringence of several EB-DNA fibres of high salt content (0.1 M NaCl, Fig. 5.13/a), the lower maximum values of the birefringence obtained with EB, as compared to ADM, and the tendency of the birefringence to drop at the highest humidities can be explained by a greater misalignment in these fibres, which becomes more apparent in the conditions of greater fluidity at high humidity. On the other hand, the plot for EB-DNA fibres of lower ionic strength (0.01 M NaCl, Fig. 5.13/b) is different in the sense that the increase of the birefringence due to the substantial transfer of the drug into the intercalated state (see also Section 6.3) has overcome the tendency towards misorientation and therefore the normalized birefringence rises, rather than levels off at the highest humidities.

The lower value of the birefringence of the fibres with P/D = 7 should be associated with the general bad quality of the fibres of large EB content (see Section 6.3).

FIG. 5.13 NORMALIZED BIREFRINGENCE VS. RELATIVE HUMIDITY,

EB-DNA FIBRES

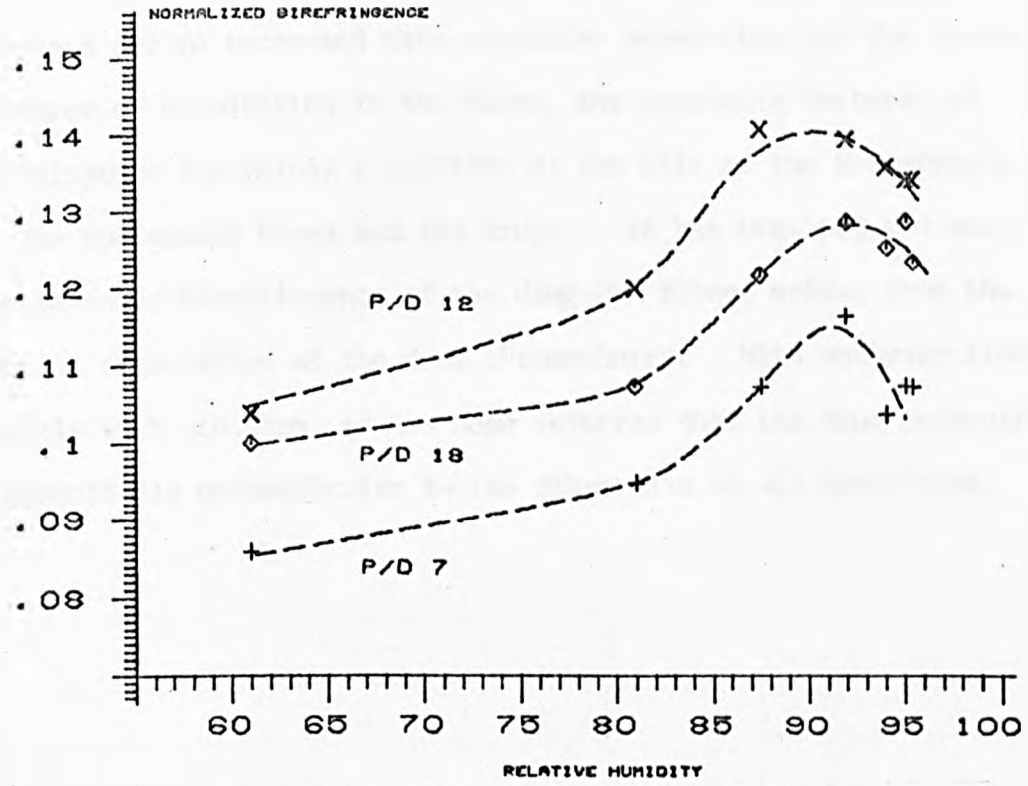

A. HIGH IONIC STRENGTH 0.1 M NACL

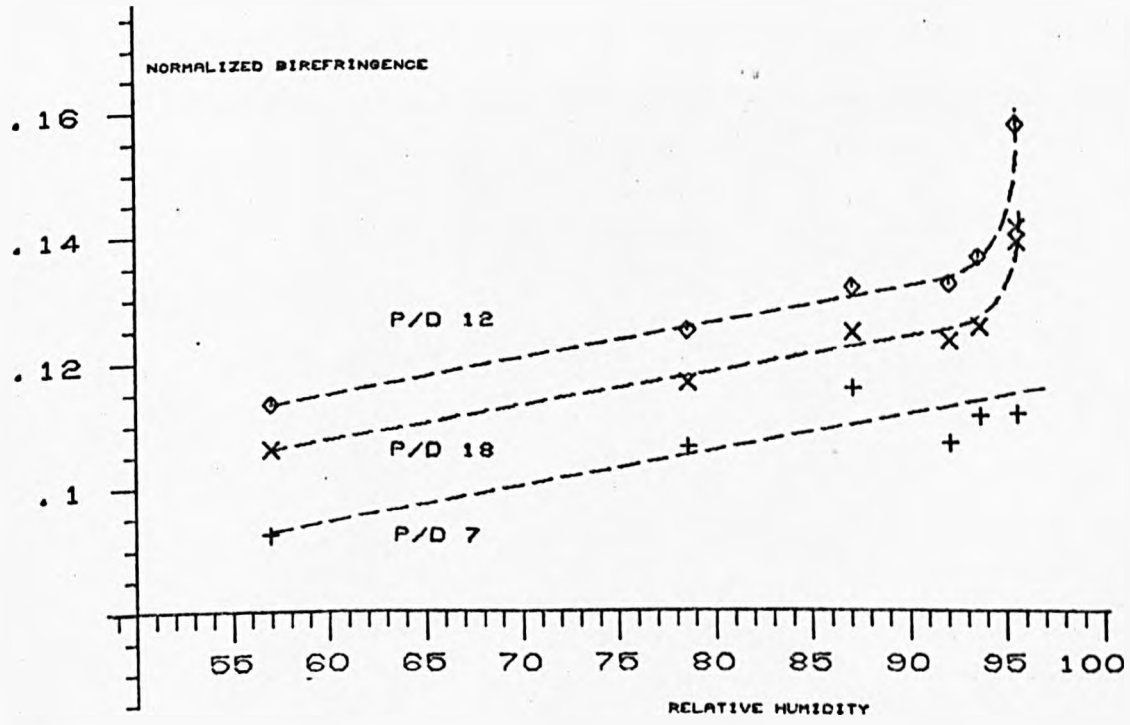

B. LOW IONIC STRENGTH 0.01 M NACL

FIG. 5.13.

In conclusion, the present discussion has shown that having taken into account the dilution effect, the change of the form birefringence due to increased intermolecular separation and the change of the degree of orientation in the fibre, the remaining features of the birefringence are mainly a function of the tilt of the anisotropic units - the nucleotide bases and the drugs. It has been pointed out that the enhanced birefringence of the drug-DNA fibres arises from the preferential orientation of the drug chromophores. With anthracyclines, and possibly with ethidium, it has been inferred that the drug molecules remain essentially perpendicular to the fibre axis at all humidities.

REFERENCES

1. N.H. HARTSHORNE, A. STUART; Crystals and the polarising microscope. (1970), Edward Arnold, London, 4th edition.
2. W.E. SEEDS; Thesis (1951), London University.
3. A.N. WINCHELL; Elements of optical mineralogy - an introduction to microscopic petrography; part I (1949), John Wiley, New York.
4. V.N. TSVETKOV; Polymer Sci. U.S.S.R. (1963), 4, 1456.
5. S. TAKASHIMA; Biopolymers (1968) 6, 1437-1452.
6. T. PORUMB, E.F. SLADE; J. Magn. Reson. (1976) 22, 219-226.
7. WIENER; Abh. Sachs. Ges. (Akad.) Wiss. (1912) 32, 507.
8. J.L. SARQUIS, R.E. HARRINGTON; J. Phys. Chem. (1969) 73, 1685.
9. T. PORUMB, E.F. SLADE; Eur. J. Biochem. (1976), 65, 21-24.
10. T. PORUMB, E.F. SLADE; "Fibre - an ESR lineshape synthesis computer programme", Quantum Chemistry Exchange Programs, University of Indiana, QCEP 295 (1976).
11. V.A. BLOOMFIELD, D.M. CROTHERS, I. TINOCO JR.; Physical chemistry of Nucleic Acids; (1974) Harper Row, New York.
12. R.E. HARRINGTON; (in) Encyclopedia of Polymer Science and Technology, Vol. 7, p.100.
13. M. FALK, K.A. HARTMAN, JR., R.C. LORD; J. Amer. Chem. Soc. (1963) 85, 387.
14. W.J. PIGRAM, W. FULLER, M.E. DAVIES; J. Mol. Biol. (1973) 80, 361-365.

CHAPTER 6

X-RAY DIFFRACTION RESULTS FROM DRUG-POLYNUCLEOTIDE FIBRES

6.1 Introduction

X-Ray diffraction patterns from DNA fibres

Several control X-ray diffraction patterns from double stranded polynucleotide fibres are shown in Fig. 6.1. The cross shaped distribution of the diffracted intensities in these patterns is characteristic for helical molecules (Ref. 1 and Ref. 2). The diffracted intensity is confined to layer lines, the spacing of the layer lines being related to the reciprocal of the helix pitch. The repeating of the monomeric units (the base-paired nucleotides) along the helix axis generates further cross shaped series of reflections centred on the meridian of the pattern. The spacing of the reflections along the equator is related to the side by side packing of the helices in the fibre and can be used to calculate the intermolecular separation. Further analysis using the diffracted intensities and molecular model-building studies are required to determine the molecular structure. Usually, the individual structures of the bases and sugar-phosphates are assumed from single crystal studies, so what remains to be determined is their disposition. Such studies have been carried out in connection with the determination of the conformations of a number of naturally occurring nucleic acids and synthetic polynucleotides.

In the B-DNA (Fig. 6.1/b/d; Ref. 3), the bases are stacked on top of one another with orientation nearly perpendicular to the helix axis (the tilt is in the region of 6 - 8^{o}; see synoptic table in Ref. 4). There are ten base pairs per turn of helix and the pitch is 34.6 A for the sodium salt and 33.7 A for the lithuim salt. Thus, each residue is

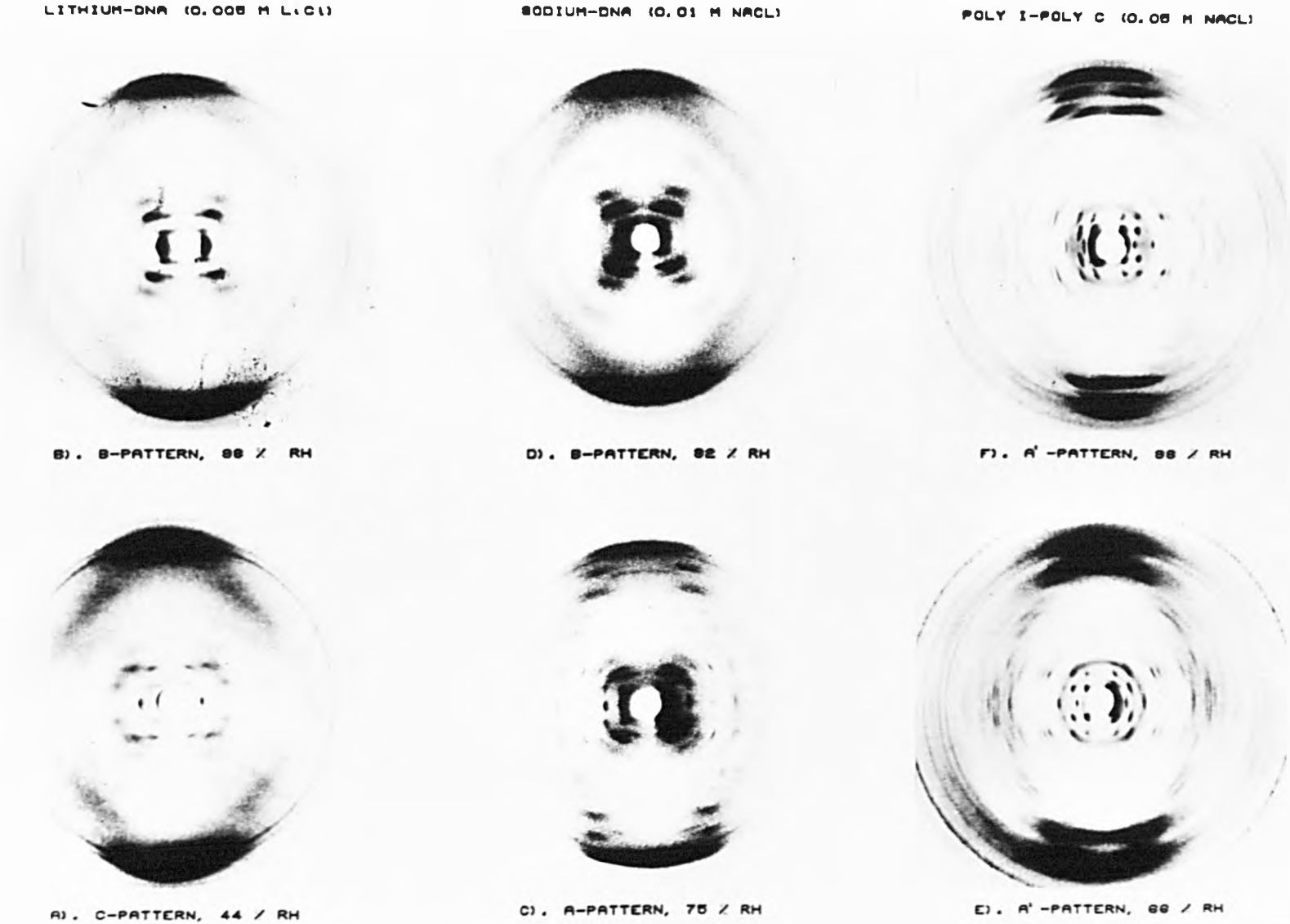

FIG. 6.1 X-RAY DIFFRACTION PATTERNS FROM POLYNUCLEOTIDE FIBRES.

related to the previous one by a 3.46 - 3.37 A rise and 36^{o} rotation.

In the A-DNA (Fig. 6.1/c; Ref. 3), the bases are moved away, by ~$4A^{o}$ and tilted by 20^{o} with respect to the helix axis. The helix is 11-fold, with a pitch of 28.15A. The structure of the double helical RNA can only be of the A-type (Fig. 6.1/eef; Ref. 5 and Ref. 6).

In the C-DNA (Fig. 6.1/a; Ref. 4 and Ref. 7), the helix is non-integral, with 9 1/3 base pairs per turn and a pitch of about $31A^{o}$. As in the B form, the sugar conformation is C_3 - exo (in A-DNA it is C_3 -endo) and the bases retain their near-perpendicularity to the helix axis. The B and C forms of the DNA are usually semicrystalline, whereas the A-type structures are always crystalline.

In the present study, the X-ray diffraction technique was used to monitor the changes in the helical parameters and molecular packing of the DNA brought about by the presence of the drug in the fibre. The variation of these parameters was studied as a function of the drug content (P/D ratio) and relative humidity.

In this work only sodium-DNA was used, the gels being usually obtained from solutions of ionic strength around 0.01 M NaCl. At this ionic strength, the DNA fibre would normally undergo a transition between the B form existing at high humidities, to the A form, appearing below ~80% relative humidity (Figs. 6.1/c/d; Ref. 8). Such a transition takes place between the two structures without passing through intermediate forms, although both structures may be present simultaneously in the same fibre. However, it was found that a number of DNA fibres (both with and without drug) displayed the normal B patterns at high humidities, but did not undergo the expected B to A transition upon lowering the humidity. Instead, a gradual decrease of the pitch was recorded (reaching ~28.5A around 50% relative humidity), while the diffraction photographs retained the semicrystalline features and the strong meridional reflections

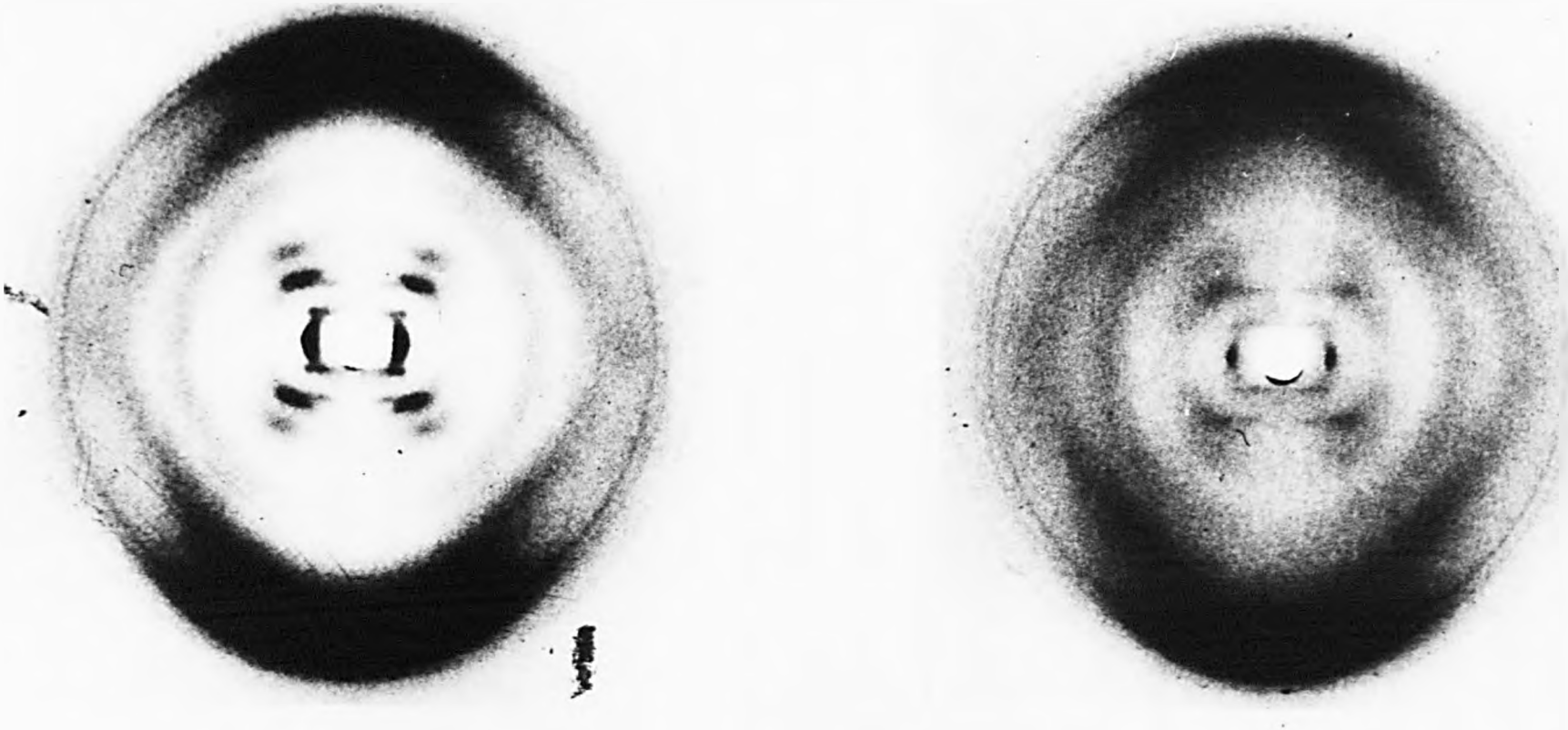

B PATTERN, 92 % RH

LOW PITCH PATTERN, 66 % RH

FIG. 8.2 X-RAY DIFFRACTION PATTERNS FROM A DNA FIBRE (0.01 M NACL).

characteristic for a B-DNA pattern (a typical diffraction pattern is shown in Fig. 6.2). The variation of the parameters of such a fibre with the relative humidity is shown in the plot from Fig. 6.3. The measured values were reproducible for a number of cycles in which the humidity was varied between the two extremes (the probable maximum errors are estimated to be $\pm$ 4%).

The pitch of the low humidity form represents a 5A decrease (about 15%) from the value of the B-DNA pitch, or a decrease of 1 - 2A from that of the C-DNA. This behaviour was not obtained from DNA fibres of the same material in which the ionic strength was greater than 0.05 M NaCl.

The occurrence of the species presented above reflects the general tendency of the DNA to adopt conformations of lower ptich under conditions of decreased hydration. However, an important characteristic of this form is that the transition from high to low pitch values is gradual, and takes place over a range of humidities at which intermediate pitch values are obtained.

Neville and Davies (Ref. 9) reported similar diffraction patterns for acridine-DNA fibres at low humidities and suggested that they were caused by the presence of the drug. However, the present results show that the low pitch form can be obtained both from the control DNA and the drug fibres (Fig. 6.4), thus it seems that its occurrence is correlated with the particular ionic strength employed.*

The exact mechanism by which the low pitch conformation arises is not known. This DNA form may be treated as a helix containing

---

* It may be significant that fibres of nominally the same ionic strength, made with DNA from two different preparations, behaved differently (see Section 6.3); the low pitch form was obtained in the case in which the DNA was prepared by a purification procedure (Section 2.1) repeated three times, whereas in the other case the purification was performed only once. It thus appears that in addition to the ionic strength, it is also the past history of the DNA sample that may be implied in the occurrence of the low pitch structure.

HELICAL PITCH AND INTERMOLECULAR SEPARATION

OF A DNA FIBRE

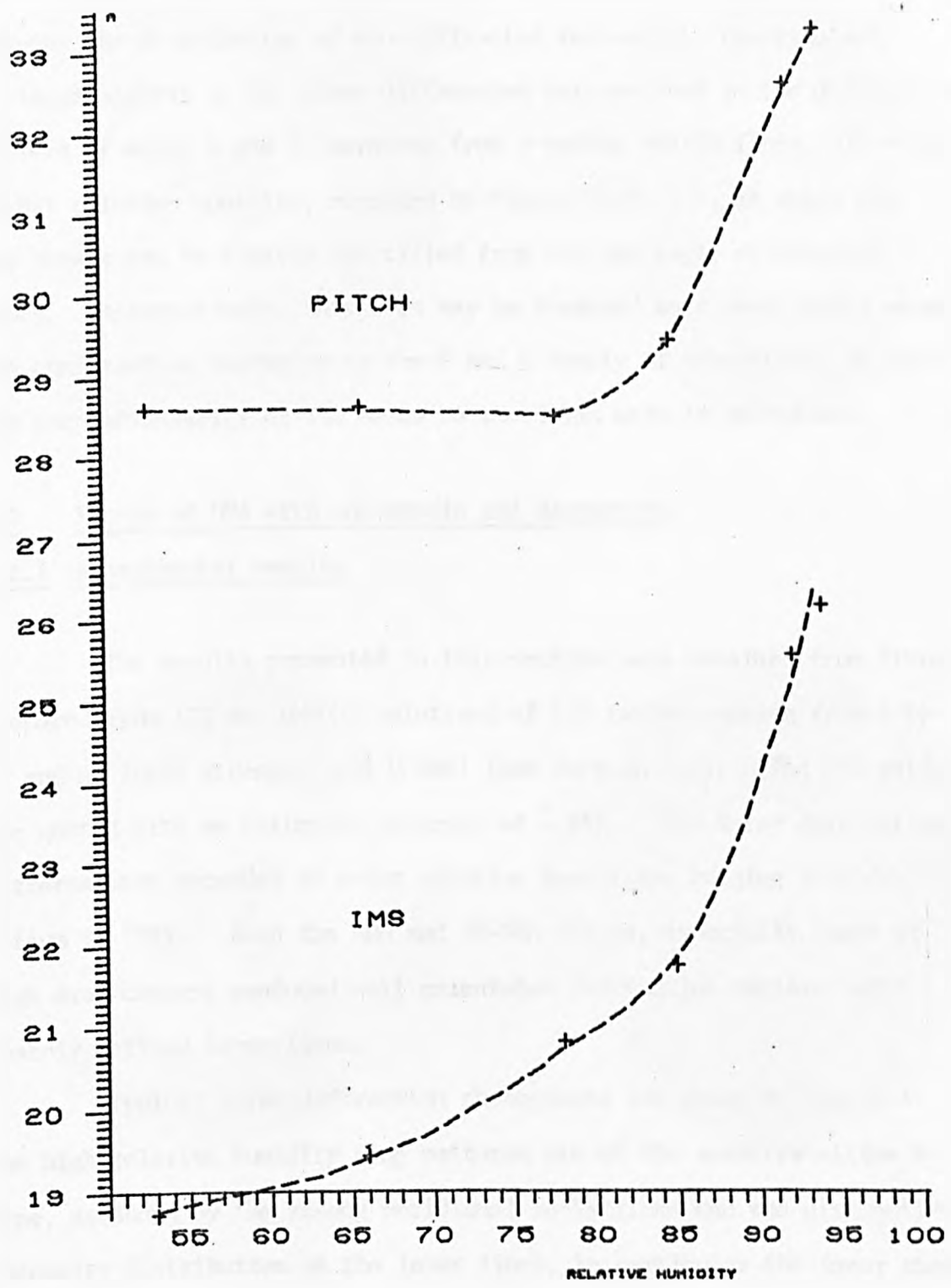

FIG. 6.3. THE VARIATION OF THE PARAMETERS OF A LOW-PITCH DNA FIBRE AS A FUNCTION OF RELATIVE HUMIDITY. IONIC STRENGTH 0.01 M NA CL . (X-RAY DIFFRACTION PATTERN, IN FIG. 6.2)

alternating regions of A and B type resulting from an indecisive B to A transition. Such as interpretation is supported by the similarity between the distribution of the diffracted intensities (particularly at large angles) in the above diffraction patterns and in the diffraction pattern of mixed A and B character from a sodium DNA-EB fibre, P/D = 25, at 92% relative humidity, reported by Pigram (Ref. 10), in which the two phases can be clearly identified from the low angle diffraction spots. Alternatively, this form may be regarded as a more highly wound DNA conformation belonging to the B and C family of structures, in which the perpendicularity of the bases to the helix axis is maintained.

6.2 Fibres of DNA with adriamycin and daunomycin

6.2.1 Experimental results

The results presented in this section were obtained from fibres prepared from ADM and DM-DNA solutions of P/D ratios ranging from 4 to 50 and at ionic strength 0.01 M NaCl (see Section 2.3). (The P/D ratios are quoted with an estimated accuracy of $\pm$ 4%). The X-ray diffraction patterns were recorded at seven relative humidities ranging from dry helium to ~98%. Both the ADM and DM-DNA fibres, especially those of high drug content produced well orientated diffraction patterns with sharply defined layer lines.

Typical X-ray diffraction photographs are shown in Fig. 6.4. The high relative humidity drug patterns are of the semicrystalline B-type, as shown by the strong meridional reflections and the distinctive intensity distribution on the layer lines, in particular the inner sharp spots on the second layer. The low humidity pattern obtained from fibres of P/D ratios less than 10 (eg. P/D = 5 in Fig. 6.4), retained the same B-type appearance, whereas the fibres of P/D ratios larger than 10, including the control DNA, produced patterns which resembled the low pitch DNA

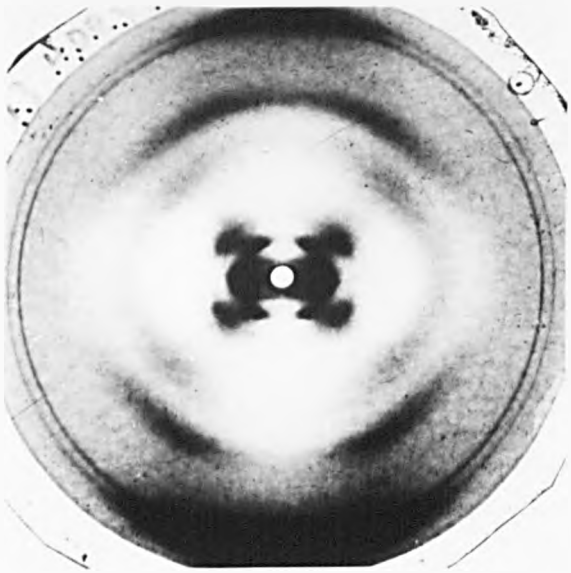

P/D 5, 92 / RH

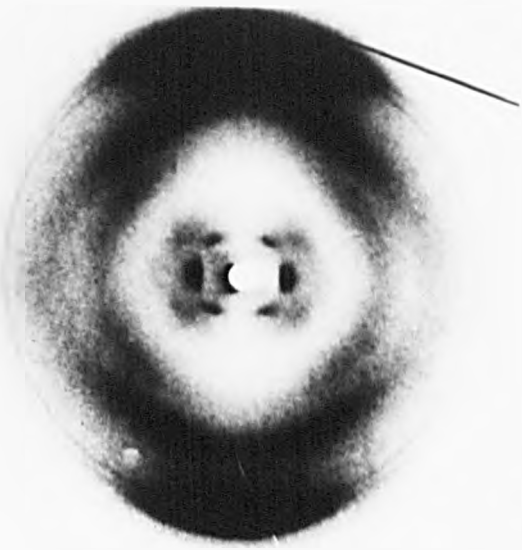

P/D 5, 33 / RH

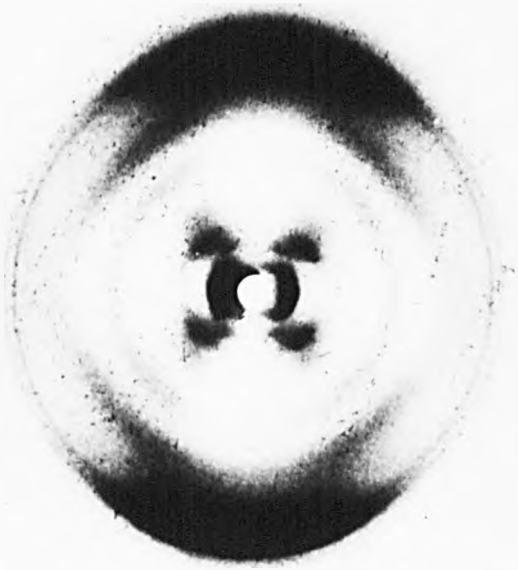

P/D 20, 92 / RH

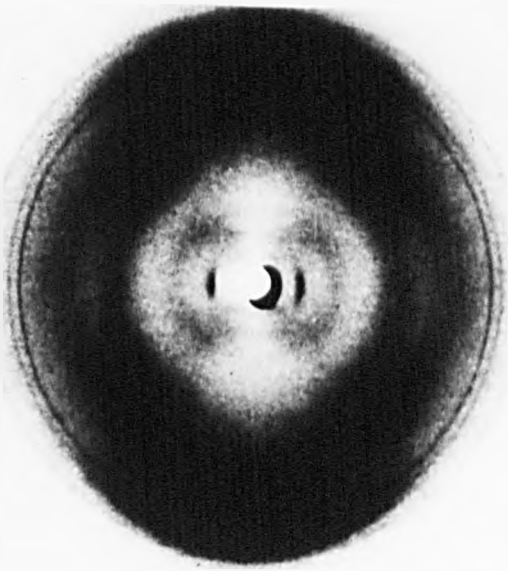

P/D 20, 58 / RH

FIG. 8.4 X-RAY DIFFRACTION PATTERNS FROM ADM-DNA FIBRES (0.01 M NA CL)

described earlier (Section 6.1).

For all fibres, the helix pitch and the intermolecular separation underwent progressive, reversible changes as a function of the relative humidity, while the meridional reflection retained its position at 3.4Å.

The variation of the intermolecular separation with the relative humidity is shown in Fig. 6.5. The rapid increase of the intermolecular separation above ~80% relative humidity resembles the variation of the fibre diameter, mentioned earlier (Section 5.3.1). The points enveloped by the two curves in Fig. 6.5/a belong to ADM fibres of various drug contents. The fibres with more drug tended to have a lower intermolecular separation, as seen explicitly in Fig. 6.5/b, in which the intermolecular separation is plotted against the D/P ratio. The intermolecular separation values were the same for ADM and DM fibres under similar conditions.

Fig. 6.6 is a plot of the pitch of DM-DNA fibres of different D/P ratios as a function of relative humidity. A typical curve starts with a plateau in the low humidity region, followed by an increase of pitch in the region of ~80% relative humidity and another plateau at high humidities.

Fig. 6.7 is another way of plotting the same data, using the intermolecular separation rather than the relative humidity as a measure of the hydration within the fibre. As a result, the low humidity region is contracted, and what appeared as a plateau in the previous plot no longer looks so, whereas the plateau on the high humidity side is emphasized. At very high humidities, after having reached a maximum, there is a tendency of the pitch of the ADM-DNA fibres to drop. This effect is not observed with DM-DNA fibres.

The maximum and minimum pitch values obtained from each fibre are plotted against the nominal D/P ratio in Figs. 6.8 and 6.9. The

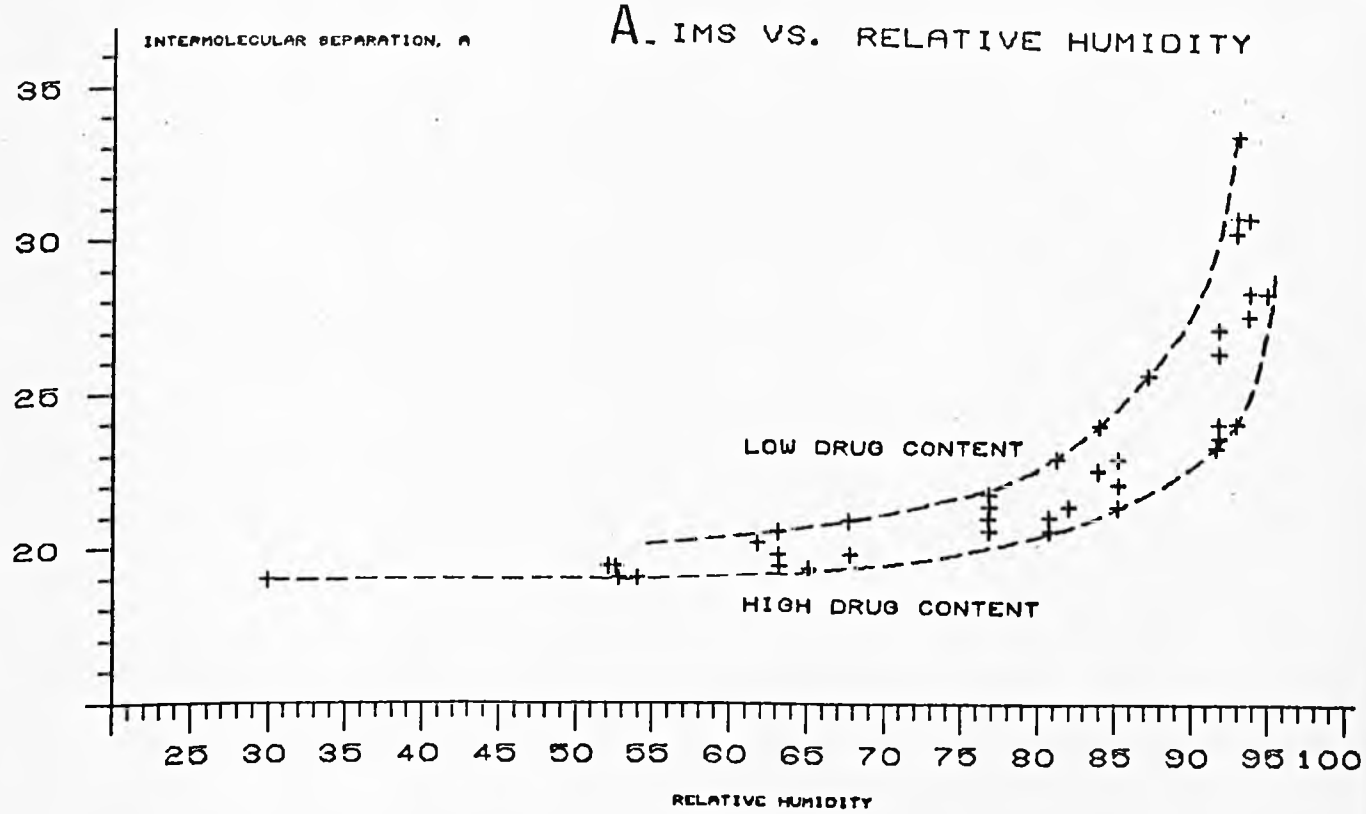

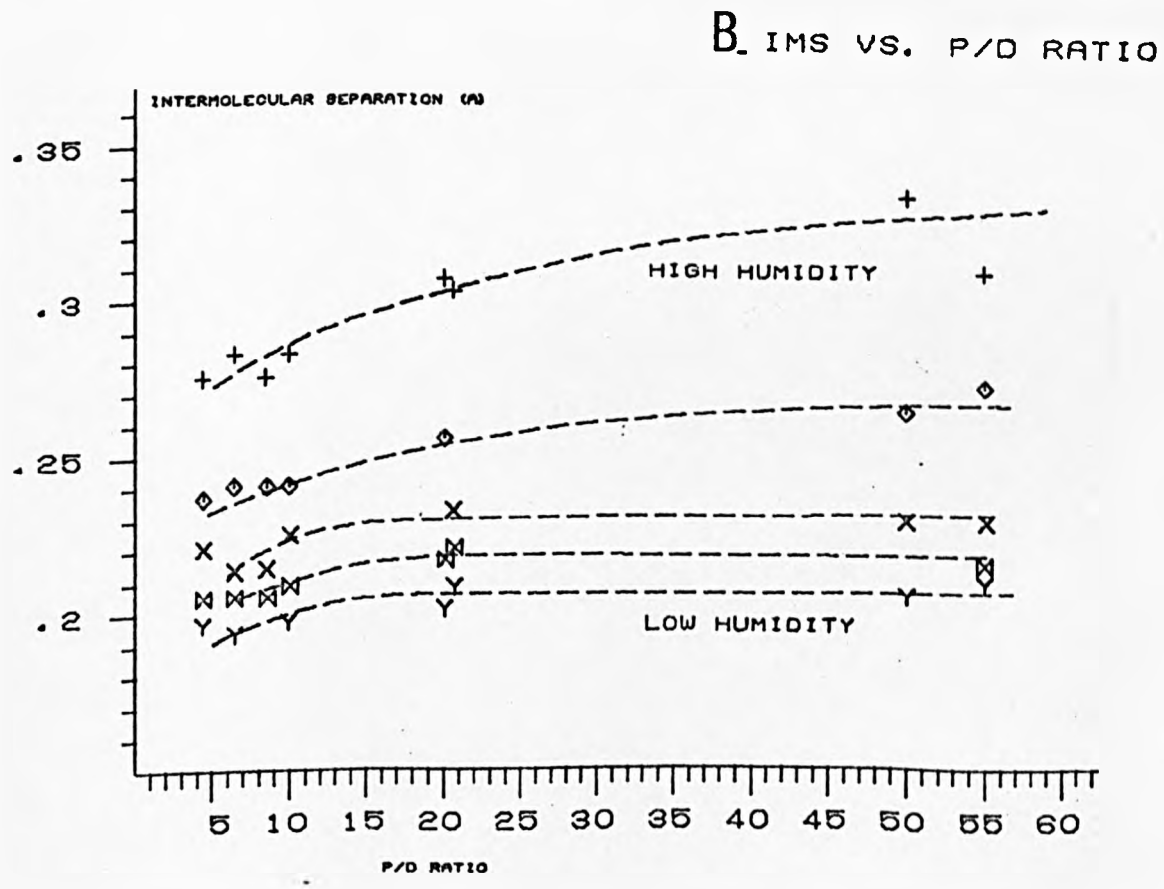

FIG. 6.5. INTERMOLECULAR SEPARATION (ADRIAMACYN-DNA FIBRES)

FIG. 6.6 HELIX PITCH VS. RELATIVE HUMIDITY DAUNOMYCIN-DNA FIBRE

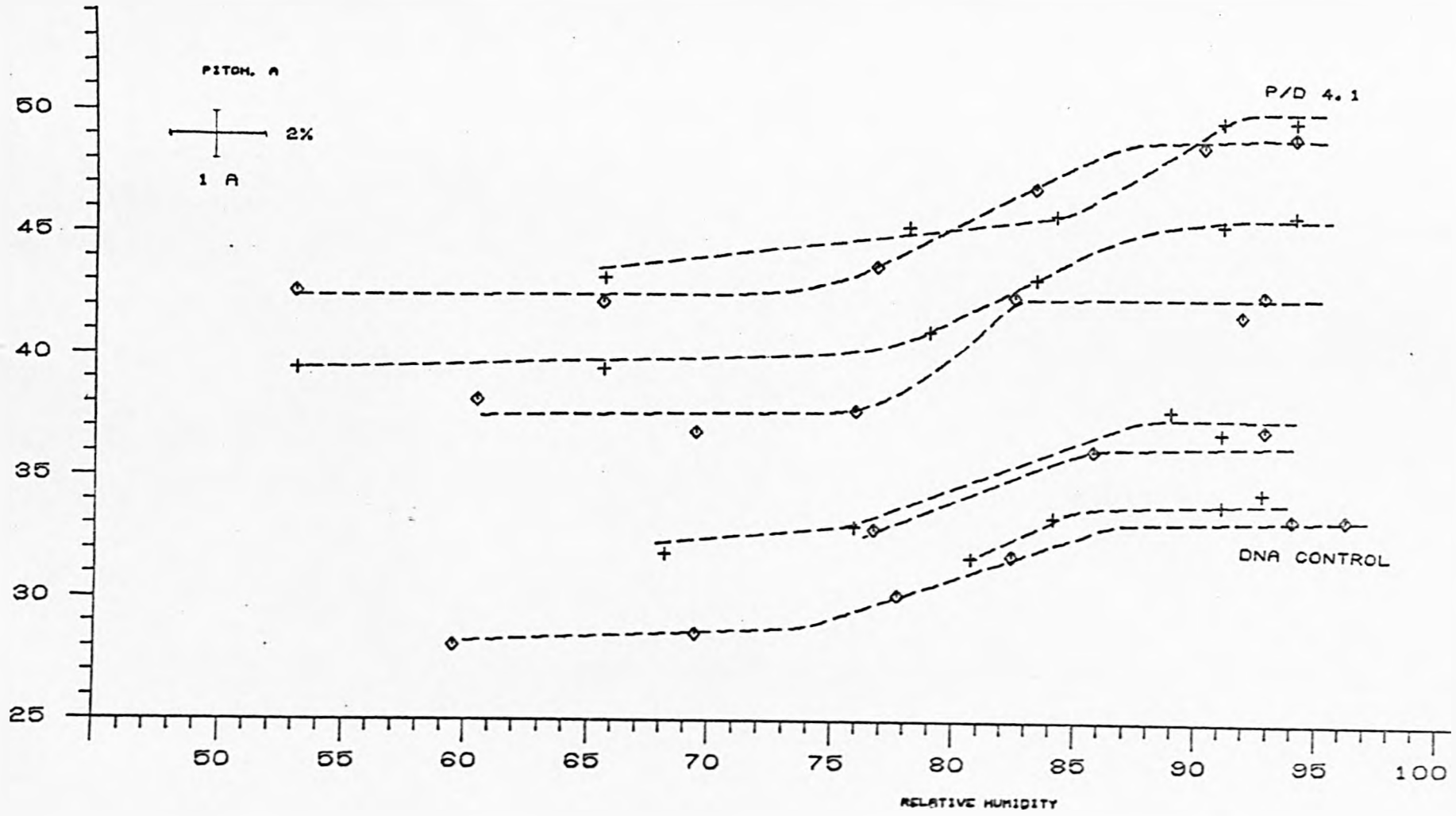

FIG. 6.6. HELIX PITCH VS. RELATIVE HUMIDITY, DAUNOMYCIN-DNA FIBRES
P/D RATIOS = 4.1, 5.1, 7.8, 10.1, 15.4, 20.0, 50.0;

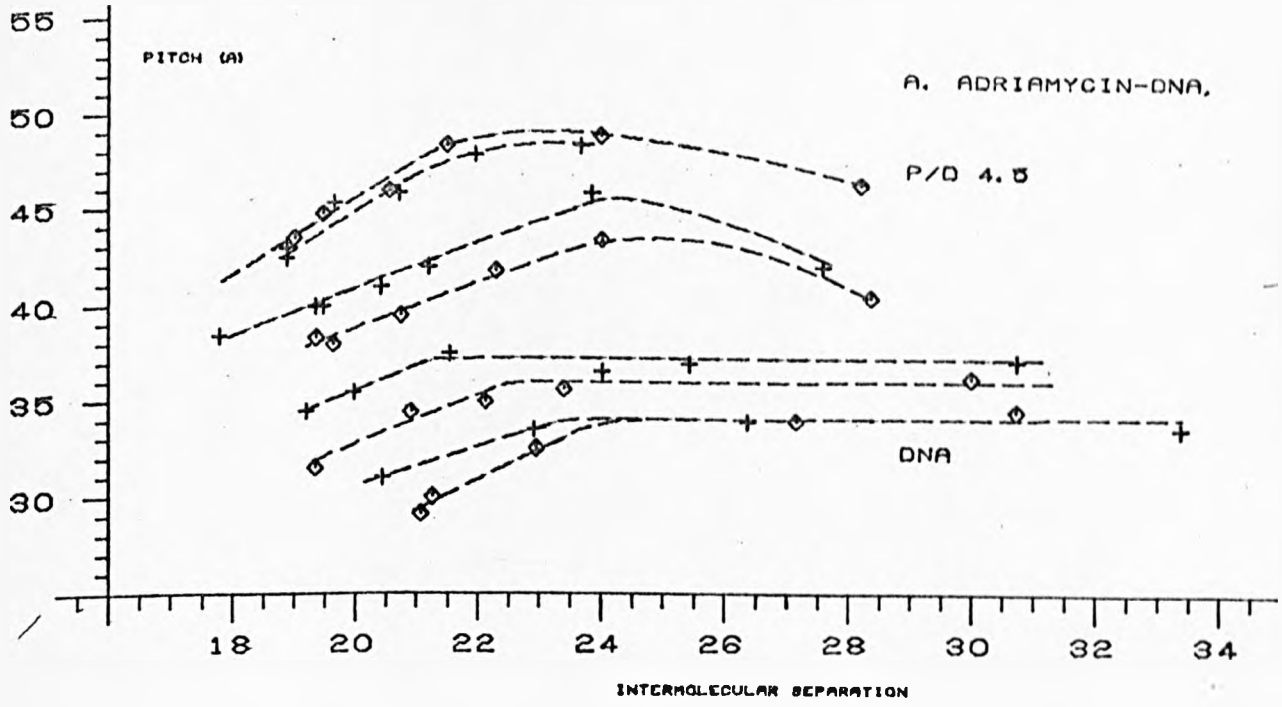

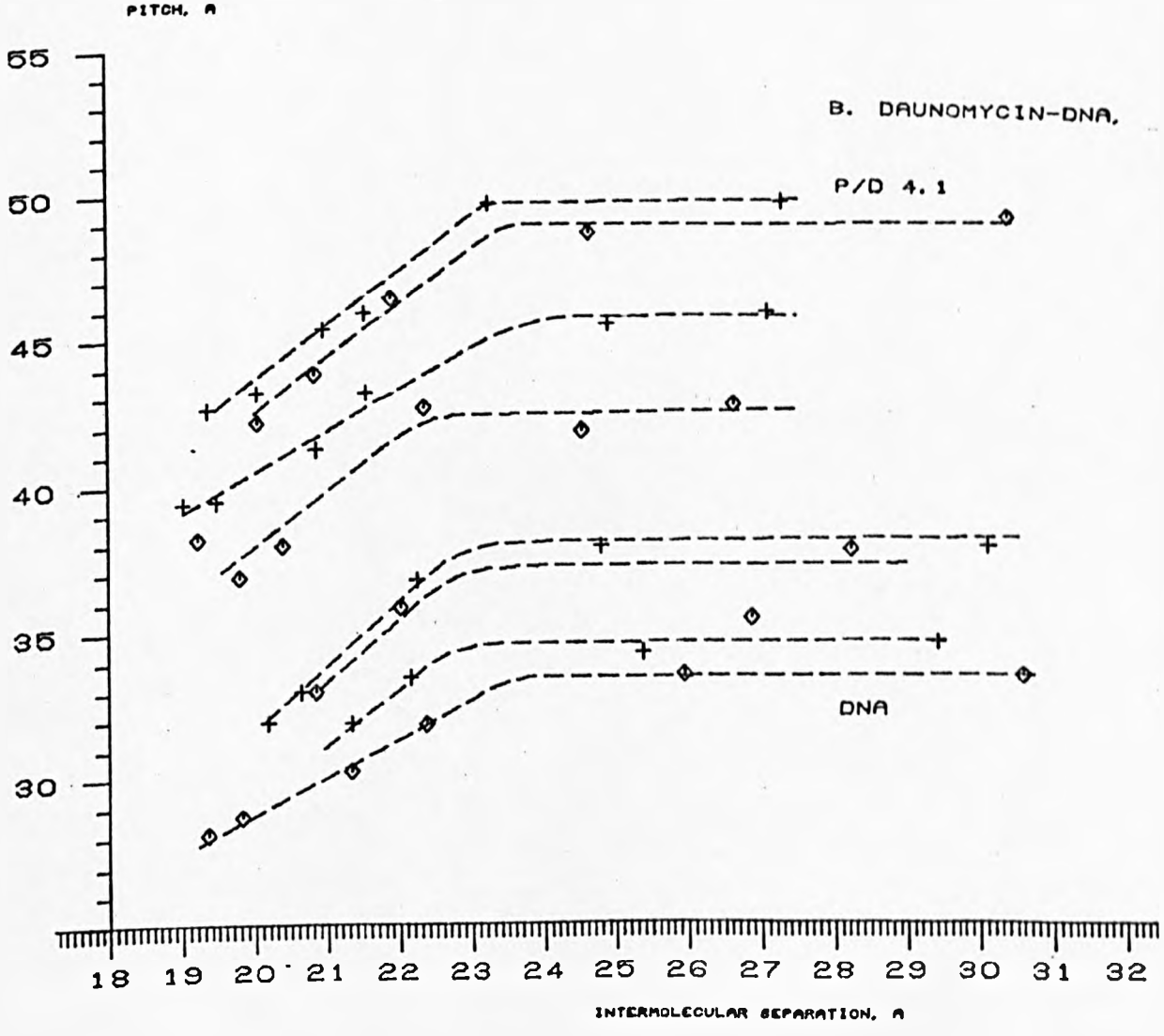

FIG. 6.7. PITCH VS. INTERMOLECULAR SEPARATION (ANTHRACYCLINE FIBRES)
A. ADRIAMYCIN-DNA, P/D= 4.5, 5.6, 8.6, 10.9, 18.8, 20.4, 50.0;
B. DAUNOMYCIN-DNA, SAME P/D RATIOS AS IN FIG. 6.6.

experimental points follow curves which originate at the values corresponding to the pitch of the control DNA fibres, namely ~34A at high humidities and ~28.5A at low humidities.

In order to compare the pitch values corresponding to the two drugs under similar humidity conditions, the parameters measured from two fibres of ADM and DM of the same P/D ratio were plotted in Fig. 6.10. As it can be seen, the maximum pitch value is slightly larger for DM than ADM, but the transition to the dry state is sharper in the case of DM, as a result of which the two curves cross over.

6.2.2 Discussion of the experimental results

6.2.2A The interpretation of the variation of the helix pitch as a function of relative humidity. A B-type structure in which the 3.4A translation per residue persists, while the helix pitch increases and the intermolecular separation decreases proportionally to the amount of drug present indicates intercalation (Ref. 9, Ref. 11, Ref. 12 and Ref. 13; see also Chapter 1).

According to Fuller (Ref. 11), the relationship between the helix pitch and the intercalated drug may be described by the formula:

$$L = \frac{L_o + 3.4\ N/M}{1 + (\emptyset/360)(N/M)} \quad , \qquad (6.1)$$

where L_o is the helix pitch of the DNA in the absence of drug, N is the number of base pairs in one turn of the undistorted helix, $\emptyset$ is the angle of winding of the helix at the site of intercalation (negative for unwinding), and M is the number of base pairs per molecule of bound drug (2M = P/D).

The theoretical curve calculated on the basis of the B-DNA parameters (see Section 6.1) and an unwinding angle of 12^o (as suggested by model-building studies - Ref. 11 and Ref. 15) is plotted

FIG. 6.8 PITCH VS. D/P (ADM-DNA FIBRES)

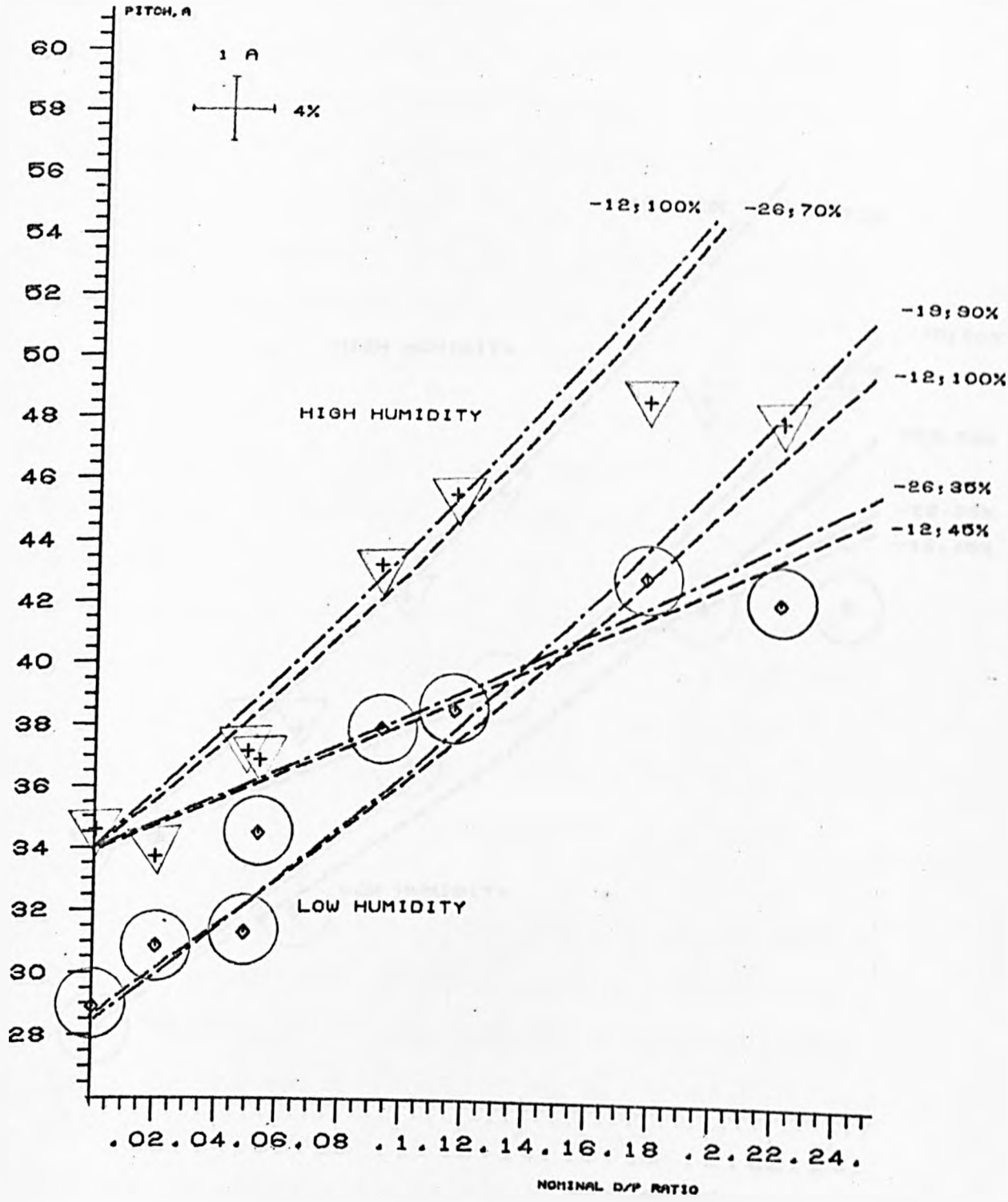

FIG. 6.8 ADRIAMYCIN
MAXIMUM (HIGH HUMIDITY) AND MINIMUM (LOW HUMIDITY) PITCH VALUES PLOTTED AGAINST NOMINAL D/P RATIOS. THE THEORETICAL CURVES WERE CALCULATED FOR THE UNWINDING ANGLES AND FRACTIONS OF INTERCALATED DRUG INDICATED .

FIG. 6.9 PITCH VS. D/P (DNM-DNA FIBRES)

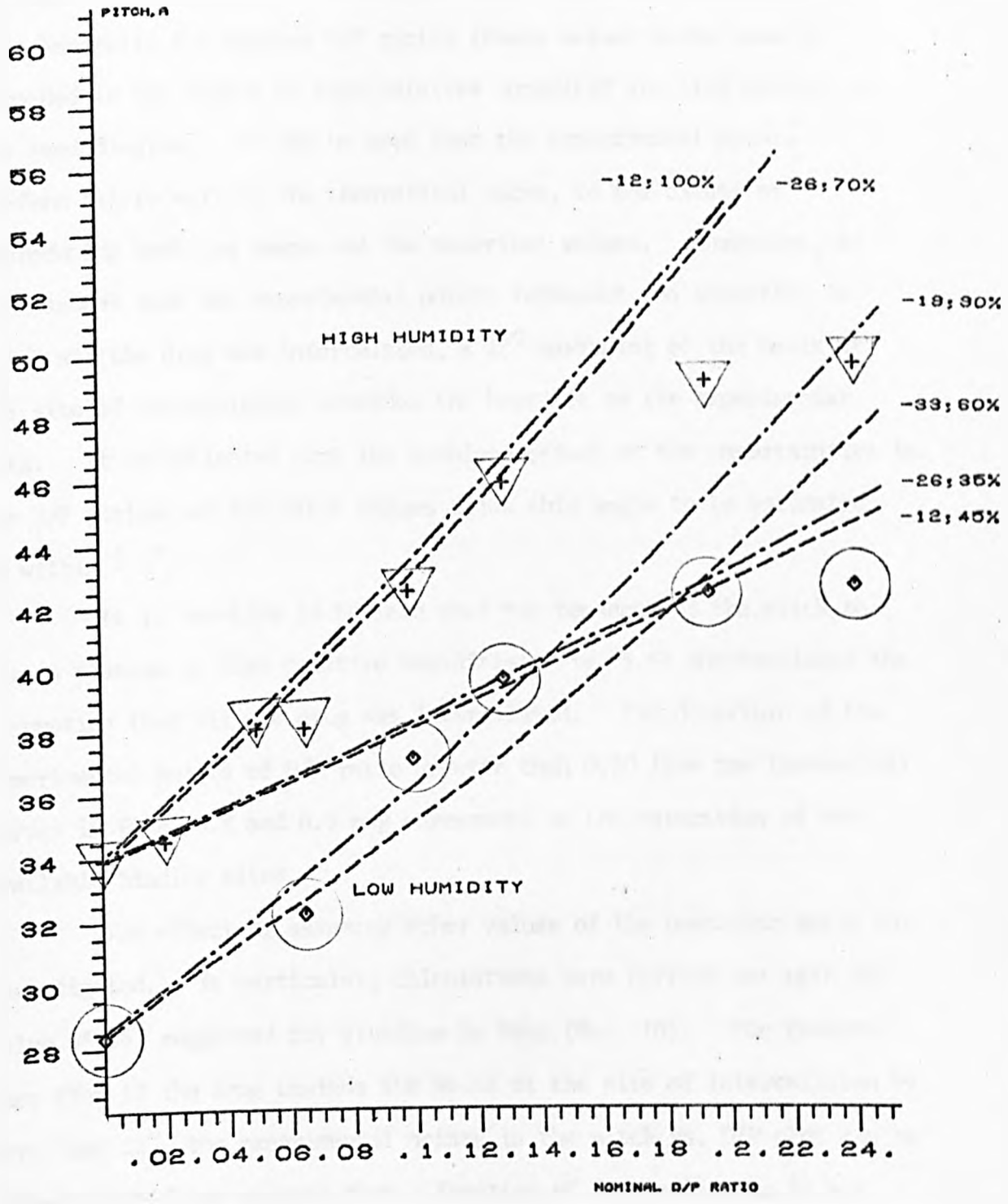

FIG. 6.9. DAUNOMYCIN

MAXIMUM (HIGH HUMIDITY) AND MINIMUM (LOW HUMIDITY) PITCH VALUES PLOTTED AGAINST NOMINAL D/P RATIOS. THE THEORETICAL CURVES WERE CALCULATED FOR THE UNWINDING ANGLES AND FRACTIONS OF INTERCALATED DRUG INDICATED .

in Figs. 6.8 and 6.9. The maximum values of the pitch recorded experimentally for various D/P ratios (these values being usually recorded in the region of high relative humidity) are also plotted in the same diagram. It can be seen that the experimental points conform fairly well to the theoretical curve, to the extent of reproducing both its shape and the numerical values. Therefore, if one assumes that the experimental points represent the situation in which all the drug was intercalated, a 12^{o} unwinding of the helix at the site of intercalation provides the best fit to the experimental data. It is estimated that the combined effect of the uncertainties in the D/P ratios and the pitch values allow this angle to be estimated to within $\pm 3^{o}$.

It is tempting to believe that the tendency of the pitch to form a plateau at high relative humidities (fig. 6.6) substantiates the assumption that all the drug was intercalated. The departure of the experimental points of D/P ratio greater than 0.20 from the theoretical curves in Figs. 6.8 and 6.9 may correspond to the saturation of the available binding sites.

The effect of assuming other values of the unwinding angle was investigated. In particular, calculations were carried out with the value of 26^{o} suggested for ethidium by Wang (Ref. 16). The results show that if the drug unwinds the helix at the site of intercalation by more than 12^{o}, the experimental points in the pitch vs. D/P plot can be fitted only if one assumes that a fraction of drug molecules is not intercalated; the larger the unwinding angle, the larger this fraction should be. For 12^{o} unwinding this fraction was zero. For an unwinding angle of 26^{o}, the best fit to the high humidity points in the plot from Figs. 6.8 and 6.9 was obtained if one assumed that $30 \pm 5\%$ of the molecules was unintercalated.

It is possible that in this case the plateau at high humidities in the plot of the pitch vs. relative humidity from Fig. 6.6 reflects the attainment of an equilibrium situation between the hydrophobic drive towards intercalation (inherent in the apolar nature of the drug chromophore) and the hydrophilic nature of the polar substituents of the drug molecule.

At this point an attempt will be made to estimate quantitatively the amount of drug leaving the intercalated state upon lowering the humidity. As some of the X-ray diffraction patterns of the drug-DNA fibres (namely those of P/D ratios 20 and 50) displayed at the low humidities the characteristics of the low pitch DNA form, such an estimate will depend critically on the way in which one treats the appearance of pitch values below the 34A limit of the B-DNA (see Figs. 6.8 and 6.9). It turns out that the problem may be approached along two different lines, with significantly different consequences. A first treatment and its consequences are discussed below and an alternative one is given in Section 6.2.2C.

If one ignores in Figs. 6.8 and 6.9 the low humidity points belonging to fibres with P/D ratios greater or equal to 20, it is possible to fit the remaining low humidity points onto theoretical curves based on the parameters of the B-DNA, assuming the presence of a certain fraction of unintercalated drug. The best fit to the experimental points for unwinding angles of 12^{o} and 26^{o} was obtained if the fraction of unintercalated drug was 55 ($\pm$5)% and 65 ($\pm$5)% respectively; thus, approximately 55% of the drug molecules leave the intercalated state upon lowering the humidity according to the first model, and approximately 35% (in addition to the 30% already unintercalated at the highest RH) according to the second model. These figures represent overestimates of the real situation, in view of the

fact that the low pitch form of the DNA might have contributed towards lowering the pitch values experimentally recorded.

The variation of the pitch with the relative humidity is consistent with the belief that the intercalation is driven by hydrophobic forces (Ref. 17). The fact that the pitch values remain higher than those of the control DNA even at lower humidities, when the hydrophobic drive is minimum, indicates the additional stabilization of the intercalated state by the interaction of the side groups of the drug with the phosphate backbone of the DNA (Ref. 11 and Ref. 18).

Previous model building studies by Pigram et al (Ref. 11) have shown that DM may be intercalated via the large groove of the B-DNA helix, the intercalated configuration being stabilized by the formation of an electrostatic bond between the amino group of the drug and the first phosphate group away from the intercalation site. Present model building studies have shown that ADM may be intercalated in a way similar to DM, but in the case of ADM an additional hydrogen bond can also be formed between the extra hydroxyl group of the drug and the phosphate group situated next to the intercalated chromophore.

The possibility of the intercalated ADM forming an additional stabilizing bond with the DNA backbone may account for the longer persistence of ADM in the intercalated state upon decreasing the humidity, as it can be noticed by referring to Fig. 6.10.

The presence of the hydroxyl substituent can also explain why the high humidity plateau corresponding to ADM occurs at a lower pitch value than that corresponding to DM: under conditions of high hydration, the polar, hydrophillic OH group will cause an increased affinity of the drug towards the solvent. Thus, the hydrophobic drive towards intercalation will be reduced, with the result of a proportionally lower number of drug molecules becoming intercalated, with the consequence of

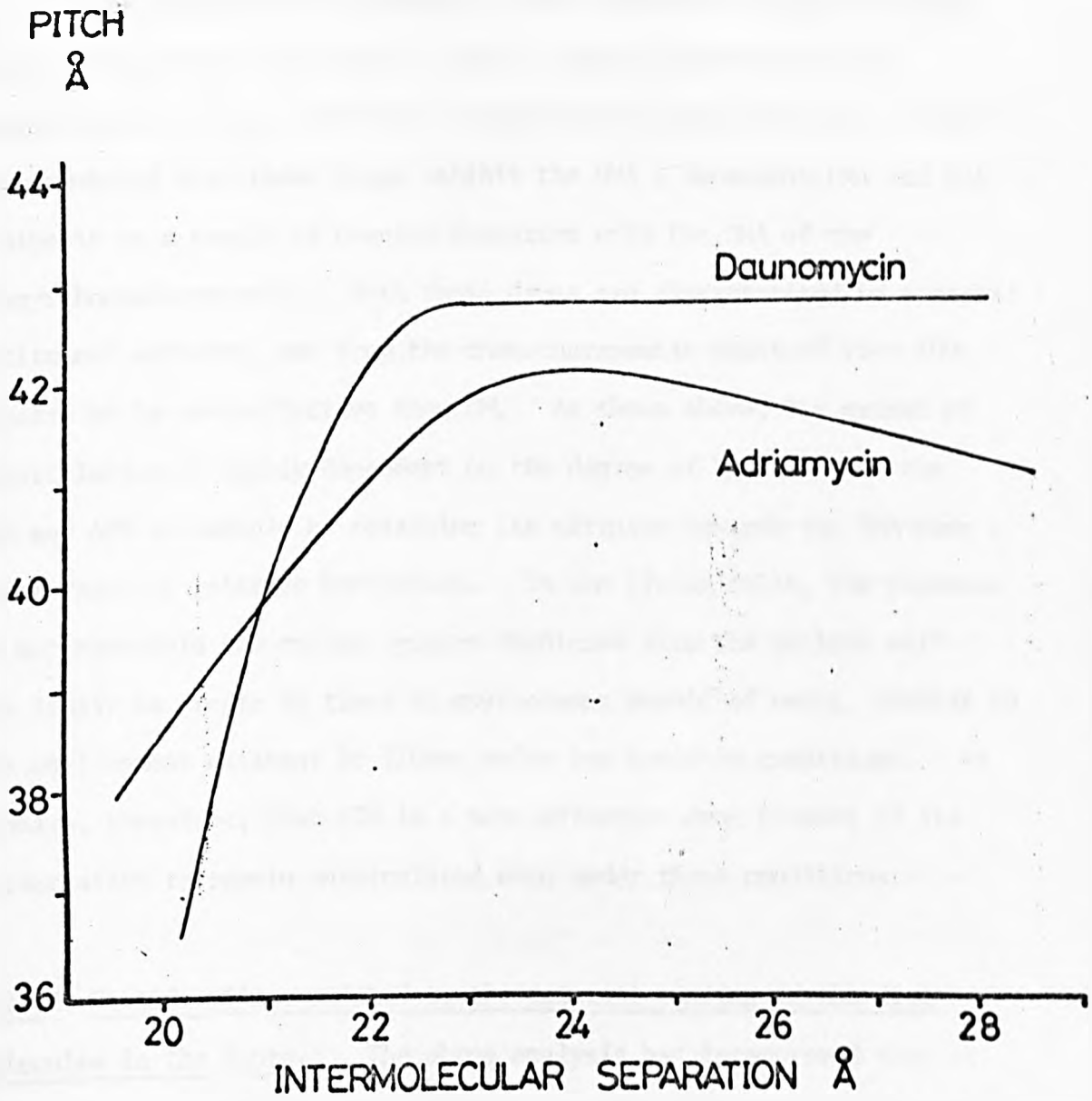

FIG. 6.10. PITCH VS. INTERMOLECULAR SEPARATION, AOM & DM FIBRES, P/D-10

a lower pitch. Support for this interpretation comes from the observed drop of the pitch values of the ADM fibres at the highest humidities (Fig. 6.7), behaviour which is not observed with DM.

The significant difference in the behaviour of the two drugs on lowering the humidity (Fig. 6.10) has direct relevance to the understanding of the difference in their biological activity. It will be remembered that these drugs inhibit the DNA - dependent DNA and RNA synthesis as a result of complex formation with the DNA of the deoxyribonucleoprotein. Both these drugs are characterized by a marked antitumour activity, and from the chemotherapeutic point of view ADM appears to be more effective than DM. As shown above, the extent of intercalation is highly dependent on the degree of hydration of the DNA and ADM is capable of retaining its affinity towards the DNA over a wider range of relative humidities. In the living cells, the presence of nucleoprotein and enzyme systems complexed with the nucleic acid are likely to create at times an environment devoid of water, similar to the environment existent in fibres under low humidity conditions. It appears, therefore, that ADM is a more effective drug because of its potentiality to remain intercalated even under these conditions.

6.2.2B Considerations related to the external binding of the drug molecules in the fibre. The above analysis has interpreted the variation of the helical pitch with the relative humidity in terms of a fraction of drug molecules becoming unintercalated at low humidities. In connection with Fig. 6.5, it is at first sight surprizing to see that even at the lowest humidity, when the centre-to-centre distance between helices is of the same order of magnitude as the sum of their radii, the helices of large drug content, such as P/D = 5, pack closer than those of low drug content, despite the presence of a considerable

amount of nonintercalated drug.

To a certain extent, the reduced intermolecular separation in the drug-DNA fibres reflects the reduction in the average helix diameter, as a result of the unwinding of the helix by the intercalated molecules (Ref. 11 and Ref. 13). At the same time, the charged side groups of the intercalated drugs are expected to cause considerable screening of the electrostatic repulsion between the DNA helices, thus allowing the helices to pack even closer. It is possible that the nonintercalated drug would have a similar screening effect and, provided the bulk of the molecule is confined to the helical groove, this would not prevent the close packing of the DNA molecules.

It should be mentioned that the optical properties of the fibres - the birefringence (Chapter 5) and the dichroism (Chapter 7), would require that all the drug molecules retained their oreintation approximately perpendicular to the helix axis at all humidities. Such a situation could arise if the unintercalated drug molecules adopted a well defined external mode of binding which imposed this particular orientation of the chromophores relative to the helical axis.

It could be envisaged that the external binding of the drug would involve the same ionic and hydrogen bonding interactions between the side groups of the drug and the DNA backbone as in the case of the intercalated drug. Very preliminary model building tests have shown that, in principle, the drug molecule could be attached in either groove of the DNA helix, while retaining its hydrogen bonded link(s) with the phosphate backbone and maintaining the approximate perpendicularity of the chromophore to the helix axis.

6.2.2C Considerations related to the possibility of intercalation into the low-humidity form of the DNA. According to one of the interpretations mentioned in Section 6.1, the low pitch form of the DNA, occurring at low humidities, may be regarded as a version of the B-DNA in which the bases maintain their perpendicular orientation to the helical axis but the winding angle per residue is increased. Indeed, the ~28.5A pitch can arise from a structure in which there are ~8.4 base pairs per turn of helix, related by a rise per nucleotide of 3.4A and a rotation of about 43^{o}, i.e. 7^{o} larger than in the B-DNA.

It could be envisaged that the drug molecules, rather than leaving the intercalated state upon lowering the humidity, remained intercalated, and the observed variation of the helix pitch was the result of the conformational change undergone by the DNA between its B conformation and the low pitch form.

Theoretical calculation were carried out on the basis of Eqn.(6.2),using the low pitch DNA parameters, various unwinding angles and assuming various proportions of intercalated drug. It was found that in this case the low humidity points (Figs. 6.8 and 6.9), including those of low D/P ratio which were ignored in the previous analysis, could be fitted by assuming much smaller fractions of unintercalated drug than required previously.

For example, if the unwinding angle of the low pitch helix was 12^{o}, all the drug molecules could be intercalated even at the low humidity. This situation, therefore, sets the lower limit to the possible unwinding angles. It is difficult to appreciate how significant is the fact that the calculations based on a 12^{o} unwinding angle are consistent with 100% intercalation both under the previous treatment of the high humidity pitch values and the present treatment for the low humidity ones.

However, it is tempting to believe that the geometry of the intercalation site would tend to be similar, whether the intercalation took place into the low pitch DNA form or into the ordinary B-DNA. In this context, one can regard the binding as consisting of the drug first inducing a local conformational change towards the B form, followed by intercalation. For example, a local unwinding of the helix at the site of intercalation of 19^{o} (i.e. 12^{o} plus an additional 7^{o} to account for the higher degree of winding up of the low pitch helix) would bring the base pairs adjacent to the intercalated drug in the same relative orientation as following 12^{o} unwinding of the B-form. The theoretical curves (Figs. 6.8 and 6.9) based on 19^{o} unwinding agree with the experimental results if the fraction of intercalated drug was in the region of 90 ($\pm$ 5)%. Assuming the model in which the B-DNA is unwound by 26^{o} at high humidity, a 33^{o} unwinding of the low pitch form (i.e., $26^{o} + 7^{o}$) would require an additional 10% of the total number of drug molecules becoming nonintercalated, making the total amount of free drug to 40%. Thus, the change in the fraction of intercalated drug would be again of the order of ~10%, as in the first example.

It is difficult to assess the merits of this interpretation over the model presented in the first sub-section; the advantage of the present treatment is that it takes into consideration all the experimental points, particularly those from fibres of low drug content which produced pitch values below those of the B-DNA.

As under this treatment the change in the fraction of intercalated drug caused by lowering the humidity is small, the birefringence measurements mentioned above can be interpreted without having to assume the preferred orientation of the unintercalated chromophores perpendicular to the fibre axis. It will be shown in Chapter 7 that the fibre dichroism results can be interpreted quantitatively to suit either model.

6.3 X-ray diffraction results obtained with EB-DNA fibres

An X-ray diffraction study similar to that presented above for ADM and DM was carried out with EB. It covered the range of P/D ratios between 5.6 and 18 and the ionic strength was 0.01 M NaCl.

Typical X-ray diffraction patterns from EB-DNA fibres at high and low humidities are shown in Fig. 6.11. They indicate a lower regularity of the DNA structure than obtained with anthracyclines. Contrary to the tendency noticed with the anthracyclines, the fibres with increased EB content produced worse X-ray diffraction patterns than those of low drug content.

The diffraction patterns recorded under conditions of high relative humidity had recognizable B-type features. The definition of the patterns became worse upon decreasing the humidity.

The coordinates of the centres of the diffraction spots on the equator and the second layer lines in each pattern were used to calculate the intermolecular separation and the helical pitch. By repeating the measurement of the same pattern a number of times, it was estimated that the accuracy achieved in determining these parameters was within $\pm$ 4% (standard deviation). A plot of the helix pitch against the intermolecular separation is shown in Fig. 6.12. Diffraction patterns similar to those from Fig. 6.11, but with layer lines less well defined have been reported previously (Ref. 12 and Ref. 10). The pitch values at 92% relative humidity measured from four diffraction photographs by Pigram (Ref. 10) are of the same order of magnitude as the values obtained in this study.

The fibres with P/D ratios 10, 12, 18 (Fig. 6.12a) belong to a set of complexes for which the control DNA fibres underwent the normal B to A transition on lowering the humidity. The X-ray diffraction patterns of the corresponding drug-DNA fibres became diffuse

P/D 8.8.92 / RH

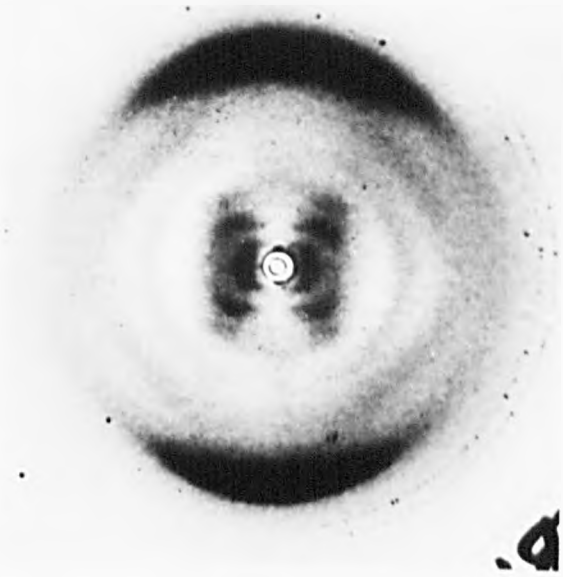

P/D 12, 92 % RH

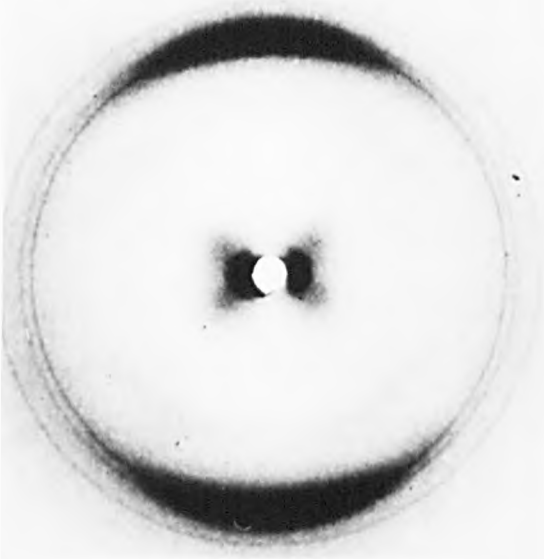

P/D 5.6.92 / RH

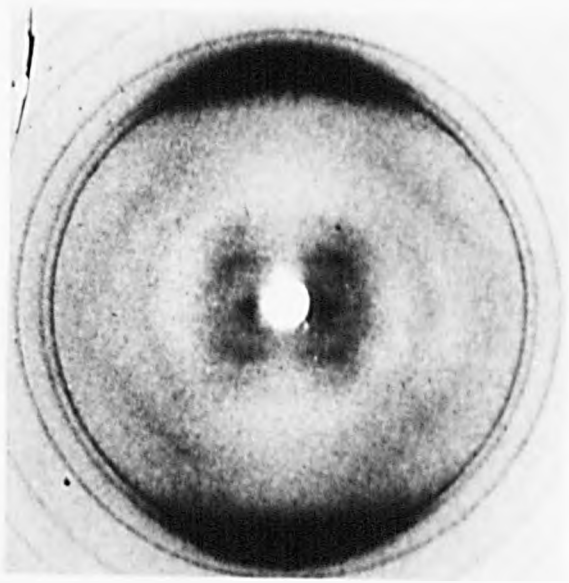

P/D 11, 75 / RH

FIG. 6.11 X-RAY DIFFRACTION PATTERNS FROM CS-DNA FIBRES (0.01 M NA CL)

for humidity below 75%.

The fibres with P/D ratios 8.8 and 11 (Fig. 6.12/b) were prepared from the same DNA which was used for the anthracycline-DNA fibres (Section 6.2). From the X-ray diffraction patterns of these fibres, recorded under conditions of low relative humidity (below 75%), pitch values intermediate between that of the B-DNA and that of the low pitch DNA were obtained. With fibres which produced low pitch patterns at low humidity, the pitch increased continuously over the entire range of humidities (Fig. 6.12/b), whereas with the fibres of the previous set (Fig. 6.12/a), the pitch tended to reach a plateau at high humidities. It looks as if the absence of a plateau in the variation of the pitch in Fig. 6.12/b is due to the additional effect of the progressive contraction of the DNA on lowering the humidity (mentioned in Section 6.1 with reference to Fig. 6.3).

The increased pitch values obtained with all the fibres at high humidities confirm that EB is an intercalating drug. The maximum pitch values obtained from the EB-DNA fibres are of the same order of magnitude as those obtained from the ADM and DM fibres of the corresponding P/D ratios and thus can be fitted to the same theoretical curves to within 5 - 10% (see Section 6.2.2).

It will be recalled that following a study of the variation of the supercoils in closed circular DNA, the anthracyclines were found to unwind the helix at the site of intercalation by half as much as EB (Ref. 19). However, the present X-ray diffraction data do not seem to reflect a significant difference between the maximum pitch values obtained with EB and the anthracyclines.

Further interpretation of these observations is not possible without a knowledge of the fraction of drug actually intercalated at the high humidity in the fibres containing these drugs.

In both plots from Fig. 6.12, corresponding to the two sets of EB-DNA fibres, the increase of the helical pitch upon increasing the relative humidity started with pitch values around those of the

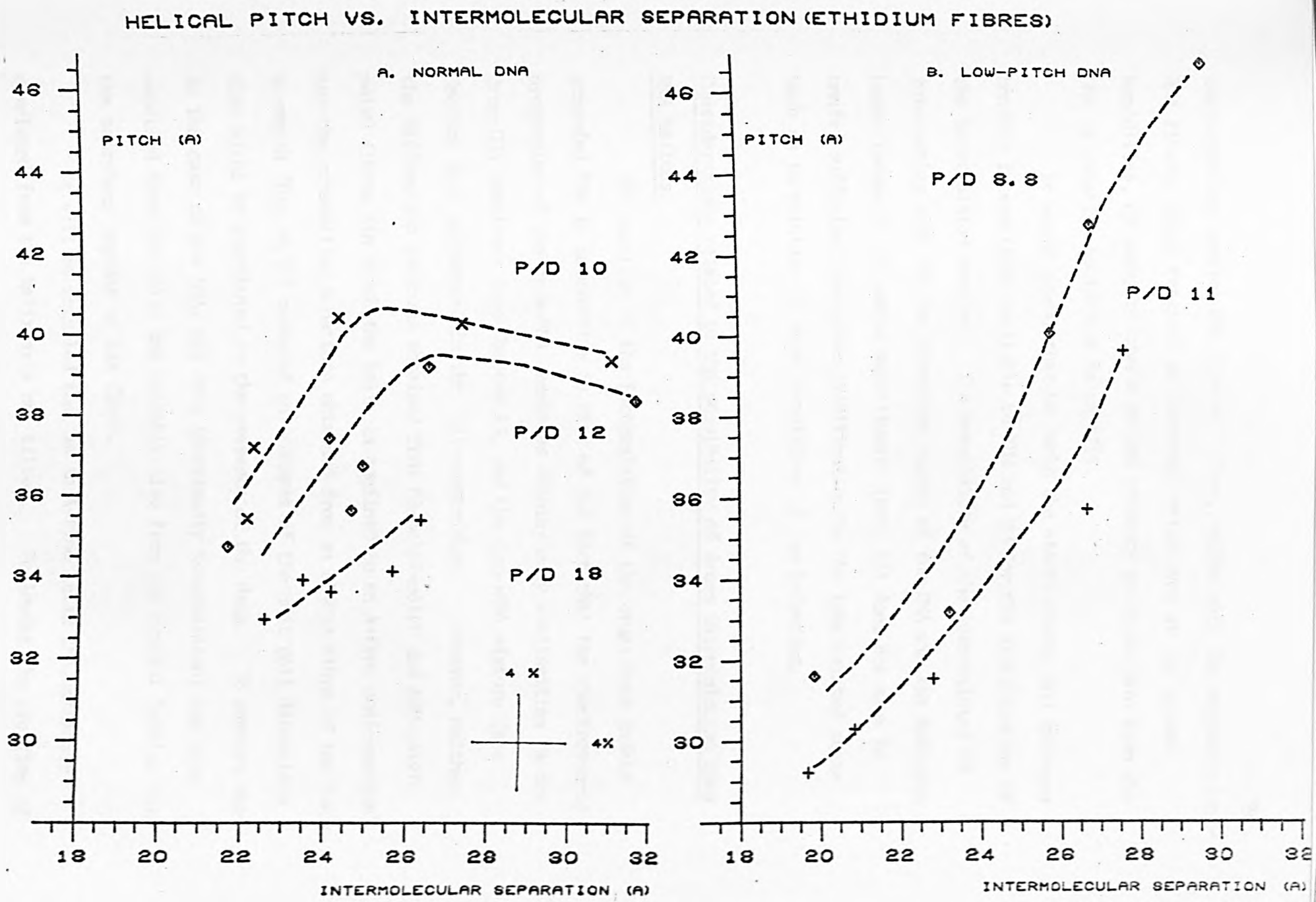
HELICAL PITCH VS. INTERMOLECULAR SEPARATION (ETHIDIUM FIBRES)
A. NORMAL DNA
B. LOW-PITCH DNA
PITCH (A)
INTERMOLECULAR SEPARATION (A)
P/D 10
P/D 12
P/D 18
P/D 8.8
P/D 11
4 X
4X
46
44
42
40
38
36
34
32
30
18
20
22
24
26
28
30
32

FIG. 6.12.

corresponding control DNA fibres. Thus, unlike with the anthracycline-DNA fibres, which retained an increased pitch even at the lowest humidities, EB seems to have a marked tendency to dissociate from the DNA at relative humidities below ~75%.

It would appear that EB lacks the electrostatic and hydrogen bonding interactions available to ADM and DM for the stabilization of the intercalated complex. The possibility of the intercalated EB interacting with the two phosphate chains of the DNA via the hydrogen bonds formed by its amino substituents (Ref. 12) does not seem to confer sufficient energetic stabilization to the intercalated state such as to maintain it under conditions of low hydration.

Considerations related to the possibility of drugs intercalating into RNA helices

The question of the intercalation of the drugs into double stranded RNA is interesting in view of the fact that the spectroscopic properties of the drug-RNA complexes display many similarities to the drug-DNA complexes (see Chapter 1), and the drug-RNA mixture (see Section 4.1) sedimented in the ultracentrifuge. However, neither the diffraction patterns obtained from EB-polyI-polyC and ADM-polyI-polyC fibres (in which the helix is confined to an A-type conformation), nor the crystalline A pattern obtained from an EB-DNA fibre of low ionic strength (Fig. 6.13) revealed any changes of the unit cell dimensions that might be attributed to the presence of the drug. It appears that in the case of the DNA, the drug (previously intercalated) has been expelled from the helix and probably also from the crystal lattice into the amorphous regions of the fibre.

It will be recalled that in an A-type helix the bases are displaced from the helix axis and tilted. Following the creation of an intercalation gap into this helix, consisting in an untwisting of the

ADM - POLY I.POLY C (0.05 M NA CL)

P/D 5, 92 / RH

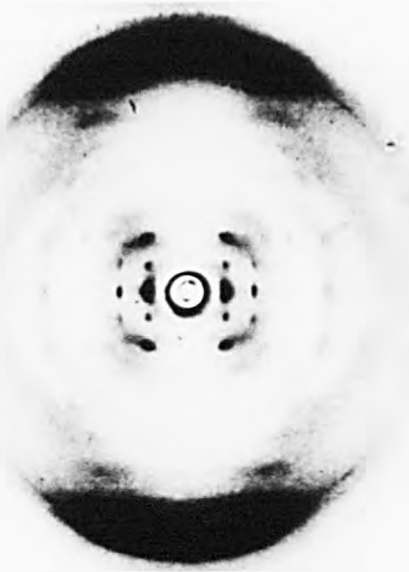

EB - DNA (0.001 M NA CL)

P/D 16, 92 / RH

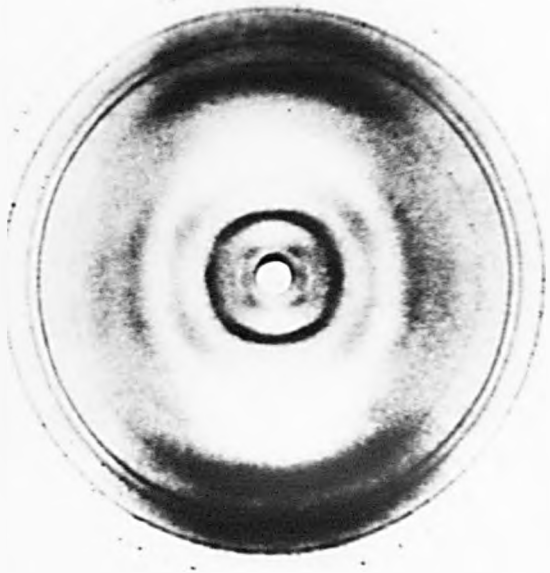

EB - POLY I.POLY C (0.05 M NA CL)

P/D 5, 75 / RH

FIG. 6.13 X-RAY DIFFRACTION PATTERNS FROM DRUG - POLYNUCLEOTIDE FIBRES IN WHICH THE HELIX ADOPTED AN A-TYPE CONFORMATION.

helical backbone and the separation of two base pairs, the axes of the RNA segments above and below the intercalation site would loose their colinearity. (For an analogy, see also Crick's hypothesis of the kinky DNA helix - Ref. 20). Even if in solution the intercalation of the drug was accepted as a possibility, such a change of direction of the helical axis would be opposed by the packing constraints within fibres. Thus, the energetic advantage gained from crystallinity may well result in abolishing the binding of the drug, as was also the case with the EB-DNA fibre mentioned above.

Possibly an insight into the drug-RNA interaction could be gained from a comparative sutdy of the radial intensity distribution in gel X-ray diffraction patterns, as under these conditions the packing constraints are less severe.

REFERENCES

1. W. COCHRAN, F.H.C. CRICK, V. VAND; Acta Cryst. (1952), 5, 581.
2. A. KLUG, F.H.C. CRICK, H.W. WYCKOFF; Acta Cryst. (1958), 11, 199.
3. S. ARNOTT, D.W.L. HUKINS; Biochem. Biophys. Res. Commun. (1972), 47, 1504-1509.
4. S. ARNOTT, E. SELSING; J. Mol. Biol. (1975) 98, 265-269.
5. S. ARNOTT, F. HUTCHINSON, M. SPENCER, M.H.F. WILKINS, W. FULLER, R. LANGRIDGE; Nature (1966), 211, 227-232.
6. S. ARNOTT, D.W.L. HUKINS, S.D. DOVER; Biochem. Biophys. Res. Commun. (1972) 48, 1392-1399.
7. D. A. MARVIN, M. SPENCER, M.H.F. WILKINS, L.D. HAMILTON; J. Mol. Biol. (1961), 3, 547-565.
8. P.J. COOPER, L.D. HAMILTON; J. Mol. Biol. (1966) 16, 562-563.
9. D. M. NEVILLE, JR., D.R. DAVIES; J. Mol. Biol. (1966), 17, 57-74.
10. W. J. PIGRAM; Thesis (1968), London University.
11. W. J. PIGRAM, W. FULLER, L.D. HAMILTON; Nature New Biol. (1972) 53, 17-19.
12. W. FULLER, M.J. WARING; Ber. Bunsenges. Phys. Chem. (1964), 68, 805-808.
13. L.S. LERMAN; J. Mol. Biol. (1961), 3, 18-30.
14. W. FULLER; Genetic Elements (Shugar, D., ed.) pp. 17-39, Academic Press, 1966, London.
15. W.J. PIGRAM, W. FULLER, M.E. DAVIES; J. Mol. Biol. (1973), 80, 361-365.
16. J.C. WANG; J. Mol. Biol. (1974), 89, 783-801.

17. L.S. LERMAN; J. Cell. and Comp. Physiol. (1964), 64, sup. 1, 1-18.

18. E. CALENDI, A. DI MARCO, M. REGGIANI, B. SCARPINATO, L. VALENTINI; Biochim. Biophys. Acta. (1965), 103, 25.

19. M.J. WARING; Prog. Mol. Subcell. Biol. (1971), 2, 216-231.

20. F.H.C. CRICK, A. KLUG; Nature (1971), 255, 530-533.

CHAPTER 7

THE OPTICAL DICHROISM OF DRUG - DNA FIBRES

7.1 Theoretical considerations

7.1.1 Introduction

The visible absorption bands of the planar drugs usually correspond to $\pi\pi^*$ transitions which take place within the planes of the drug chromophores (Ref. 1 and Ref. 2). A condition for the absorption of polarized light is that the direction of vibration of the electric vector of the radiation should be parallel to the electronic transition dipole of the molecule. Thus, if the drugs are intercalated into the DNA, light will be preferentially absorbed when its direction of polarization is perpendicular to the helix axis. For a fibre, one defines the dichroic ratio, D, as the absorbance for polarization perpendicular to the fibre axis, $A_\perp$, divided by the absorbance for polarization parallel to the fibre axis, $A_{\parallel}$:

$$D = A_\perp / A_{\parallel} \quad , \qquad (7.1)$$

It may be expected that D will vary according to the extent of intercalation of the drug in the fibre and will also be sensitive to the general degree of alignment of the DNA helices and the orientation of the un-intercalated drug.

In the previous chapter, the results obtained by monitoring the extent of intercalation by the X-ray diffraction technique were discussed and, in particular, quantitative predictions were made of the fractions of intercalated drug at the highest and lowest relative humidities. In the subsequent treatment these fractions will be denoted by f_{max} and f_{min} respectively. In this chapter, the

dichroic ratio technique will be used quantitatively to check the validity of these predictions and to obtain further information about the state of the un-intercalated drug in the fibre. For this purpose, a theoretical simulation of the dichroism of the drug-polynucleotide fibres as a function of the orientation of the drug chromophores relative to the helix axis and the degree of misalignment of these helices was developed.

7.1.2 Theoretical simulation of the fibre dichroism

Fraser has calculated the dependence of the dichroic ratio on the angles of the (infra-red) transition dipoles relative to the helix axis for the case of a perfectly orientated fibre (Ref. 3). The present theoretical simulation extends that treatment to take into account the various degrees of misalignment of the helices within the fibre.

The simulation is based on similar principles and was carried out using an extension of the same computer programme as used for the calculation of the fibre birefringence (see Section 5.2). In previous studies (Ref. 3, Ref. 4 and Ref. 5), the departures from perfect alignment were treated in terms of a model according to which a fraction of helices were perfectly oriented whereas the others were randomly disordered. In the present model, the drug molecules were assumed to be rigidly bound to the polynucleotide helices which, in turn, were assumed to have a gaussian distribution of orientations about the fibre axis (Eqn. 5.12). The absorption of polarized light is proportional to the square of the cosine of the angle between the direction of polarization of the light and the direction of the electronic transition dipole within the chromophore (Ref. 3). A cylindrical averaging was performed at the level of both fibre axis and polynucleotide helix, in

which the contributions of each molecule to the absorbance of light polarized perpendicular and parallel to the fibre axis were accumulated separately. The two quantities were then divided into one another to yield the dichroic ratio D.

The results are presented in Fig. 7.1, in which the dichroic ratios calculated for fibres of various degrees of misalignment are plotted against the angle between the transition dipole and the plane perpendicular to the helix axis. The dichroic ratio of a perfectly orientated fibre varies between zero and infinity, reproducing Fraser's results (Ref. 3). All the curves cross over on the D = 1 line for a tilt angle of $35^{o}16'$. It should be noted that the angle of the transition dipole to the plane normal to the DNA helix does not have to be equal to the angle of tilt of the chromophore (defined in Section 5.2.2, by reference to Fig. 5.2) For an arbitary orientation of the transition dipole within the chromophore, this angle will usually be lower than the angle of tilt.

The practical use of the above simulation requires the knowledge of the orientation of the electronic transition dipole in the chromophore. However, the number of molecules for which the directions of the transition dipoles have been determined is very limited, and even if quantum mechnaical calculations have been performed (Ref. 1 and Ref. 2), these directions are not known with certainty. Under these circumstances, it was decided to consider the absorption of light being isotropic in the plane of the chromophore. It will be seen below that for small angles of tilt of the chromophore this was a reasonable approximation.

Fig. 7.2 shows the theoretical curves calculated on the basis of the above assumption, representing dichroic ratio as a function of

OPTICAL DICHROISM

OF FIBRES OF VARIOUS MISALIGNMENTS

(ABSORPTION DUE TO A SINGLE TRANSITION DIPOLE IN THE PLANE OF THE CHROMOPHORE)

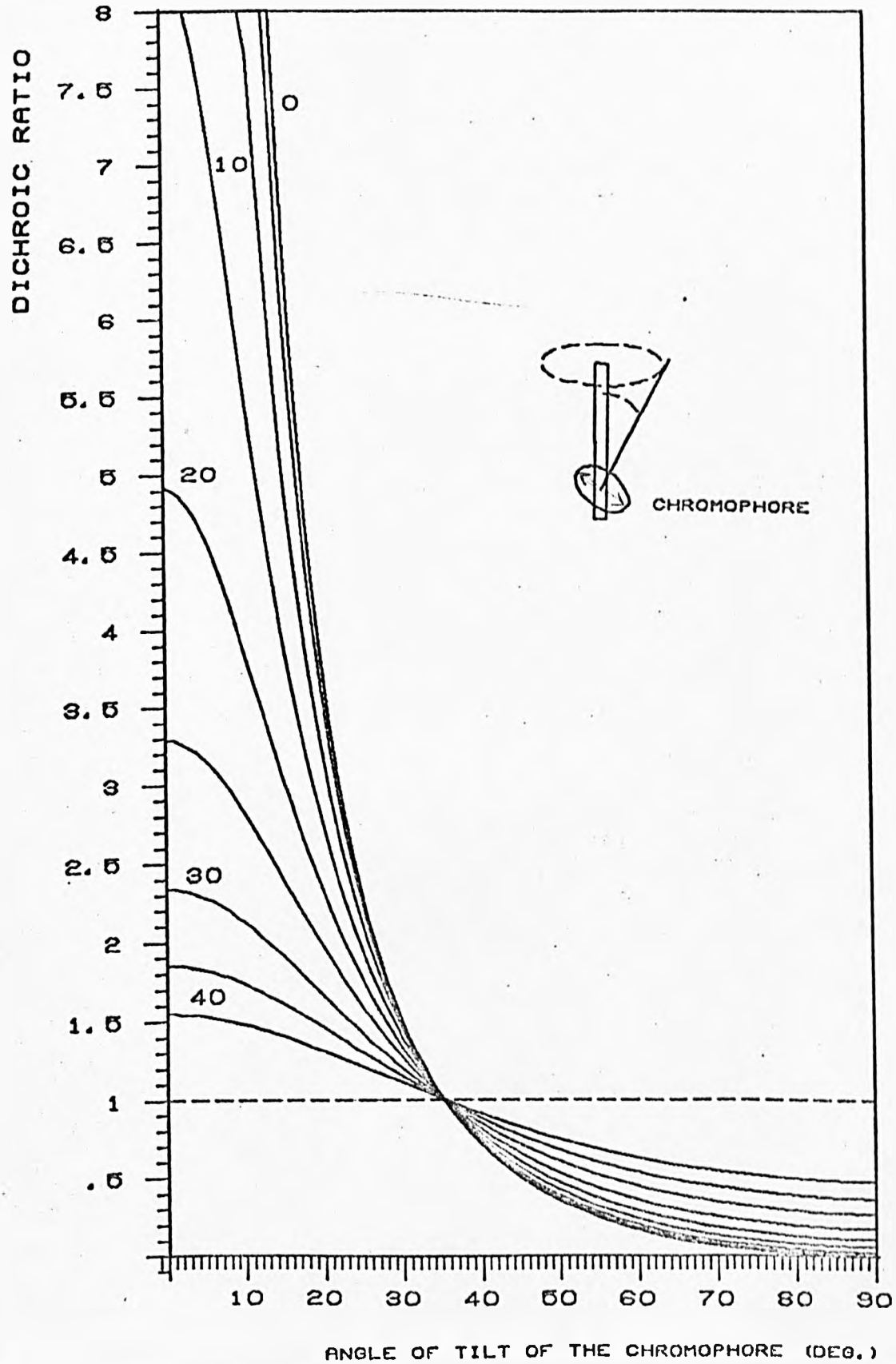

FIG. 7.1. COMPUTER SIMULATION OF THE DICHROISM OF A DRUG-POLYNUCLEOTIDE FIBRE. THE DICHROIC RATIO IS PLOTTED AGAINST THE ANGLE OF TILT OF THE TRANSITION DIPOLE IN THE DRUG CHROMOPHORE RELATIVE TO THE PLANE NORMAL TO THE HELIX AXIS. THE GAUSSIAN PARAMETER OF MISALIGNMENT IS INDICATED ON EACH CURVE .

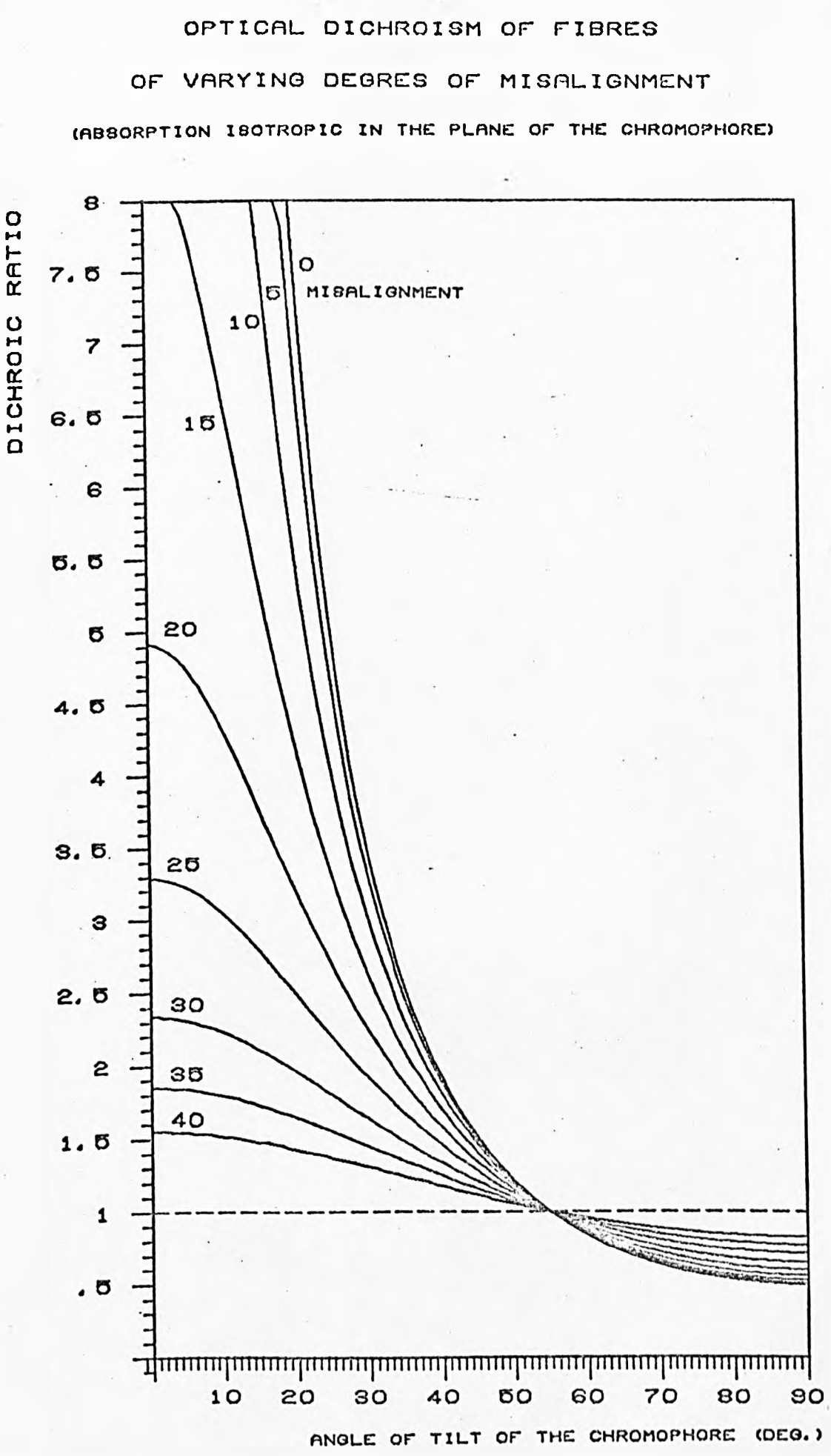

FIG. 7.2. COMPUTER SIMULATION OF THE DICHROISM OF A DRUG-POLYNUCLEOTIDE FIBRE - ISOTROPIC APPROXIMATION .

the tilt of the chromophore relative to the plane perpendicular to the helix axis. In view of what was mentioned above, the isotropic approximation may be regarded as equivalent to the absorption being due to a single transition dipole in the plane of the chromophore, making an angle with the plane normal to the helix axis intermediate between zero and the angle of tilt of the chromophore.

In the isotropic case, the dichroic ratio varies between 0.5 and infinity and the crossover occurs on the D = 1 line at $54^{o}44'$. As expected, for zero tilt the curves intersect the D- axis at the same values as obtained under the previous treatment (Fig. 7.1). Thus, for small values of the tilt angle the predictions made on the basis of either model will be very similar. For larger angles of tilt, such as 10^{o} and 20^{o} and a gaussian parameter of misalignment of 20^{o}, the dichroic ratio values predicted on the basis of the isotropic model are 13% and 33% larger than the respective values predicted on the basis of the first model.

7.1.3 An analysis of the dichroism in terms of two bound drug species

The case in which a fraction of drug molecules is either randomly oriented or assumes a preferential orientation relative to the fibre axis, different to that of the remaining molecules will now be considered.

If the drug molecules in the fibre are oriented and if A_{11} and A_{1} are the absorbances measured with light polarized parallel and perpendicular to the fibre axis, then the expression:

$$A = (1/3)\ (A_{11} + 2A_{1}) \qquad (7.2)$$

gives the isotropic value of the absorbance, which would be recorded on the same specimen using unpolarized light, and which is the same as

the value that would be recorded (for any direction of polarization of the light) if the absorbing chromophores were randomly disordered.

Using Eqns. (7.1) and (7.2), it is easy to show that if the drug molecules are distributed between two phases (eg. intercalated and outside bound), each characterized by a distinct orientation relative to the helix axis, the dichroic ratio (D) is given by the following expression:

$$D = \frac{f\,(D_{int} - D_{out}) + D_{out}\,(2D_{int} + 1)}{(2D_{int} + 1) - 2f\,(D_{int} - D_{out})} \quad , \qquad (7.3)$$

where f is the fraction of drug molecules present in the first phase and D_{int}, D_{out} are the dichroic ratios one would measure if all the drug molecules belonged to the first and second phase respectively.* The dichroic ratios D_{int} and D_{out} can be related to the angles of tilt of the chromophores and their degrees of misalignment using the theoretical simulations from Figs. 7.1 and 7.2. The Eqn. (7.3) may be used to predict a value for the fibre dichroic ratio on the basis of a particular given model, or may be solved for one of the parameters f, D_{int}, D_{out} if the others are known.

In principle, one may write a relation of the type (7.3) for the experimental dichroic ratio obtained at any relative humidity; in particular for the maximum (D_{max}) and minimum (D_{min}) values obtained at high and low relative humidities respectively:

$$D_{max} \sim (f_{max}, D_{int}, D_{out}) \qquad (7.3')$$

$$D_{min} \sim (f_{min}, D_{int}, D_{out}) \quad . \qquad (7.3'')$$

The corresponding fractions of intercalated drug f_{max}, f_{min} may be obtained from the analysis of the X-ray diffraction data. Thus, the system of two equations (7.3') and (7.3''), containing two unknowns (D_{int}, D_{out}), can be solved to yield a unique solution in terms of the

---

* The case when the unintercalated drug is randomly orientated may be obtained by taking $D_{out} = 1$.

experimental quantities D_{max}, f_{max}, D_{min}, f_{min} obtained at two different humidities. One obtains:

$$D_{out} = \frac{f_{min} D_{min} (2D_{min} + 1) - f_{max} D_{max} (2D_{max} + 1)}{f_{min} (2D_{min} + 1) - f_{max} (2D_{max} + 1)} , \quad (7.4)$$

which, used in conjunction with Eqn. (7.3) yields the second unknown, D_{int}. The implicit assumption made on solving this system of equations was that D_{int} and D_{out} remained the same at both humidities, that is to say that for each mode of binding the orientations of the chromophores relative to the helix axis and the misalignment associated with these orientations did not change with the humidity.

7.2 Experimental results

7.2.1 General

Due to the large absorbance of the nucleic acid - drug fibres of high drug content, the optical dichroism work was confined to the study of specimens of P/D ratios greater than about 20. In order to obtain spectra from fibres of higher drug content, longitudinal fibre sections were obtained, as described in Section 2.5.

Figs. 7.3 and 7.4 show typical absorption spectra recorded with light polarized perpendicular and parallel to the fibre axis from an ADM-DNA fibre and fibre section. The spectra are similar to those obtained from the same complexes in solution (see Section 4.2.2). From the positions and relative intensities of the peaks it can be deduced that most of the drug is in the intercalated state, with the exception of the freshly-cut section (Fig. 7.4), the spectrum of which is not red shifted and displays the characteristics of the free, unbound drug (compare to Fig. 4.7; see also the discussion in connection with Fig. 5.12 in Section 5.3.3).

FIBRE ABSORPTION SPECTRA AT TWO POLARIZER ORIENTATIONS

(FULL LINE: POLARIZATION PERPENDICULAR TO FIBRE AXIS,
DASHED LINE: POLARIZATION PARALLEL TO FIBRE AXIS)

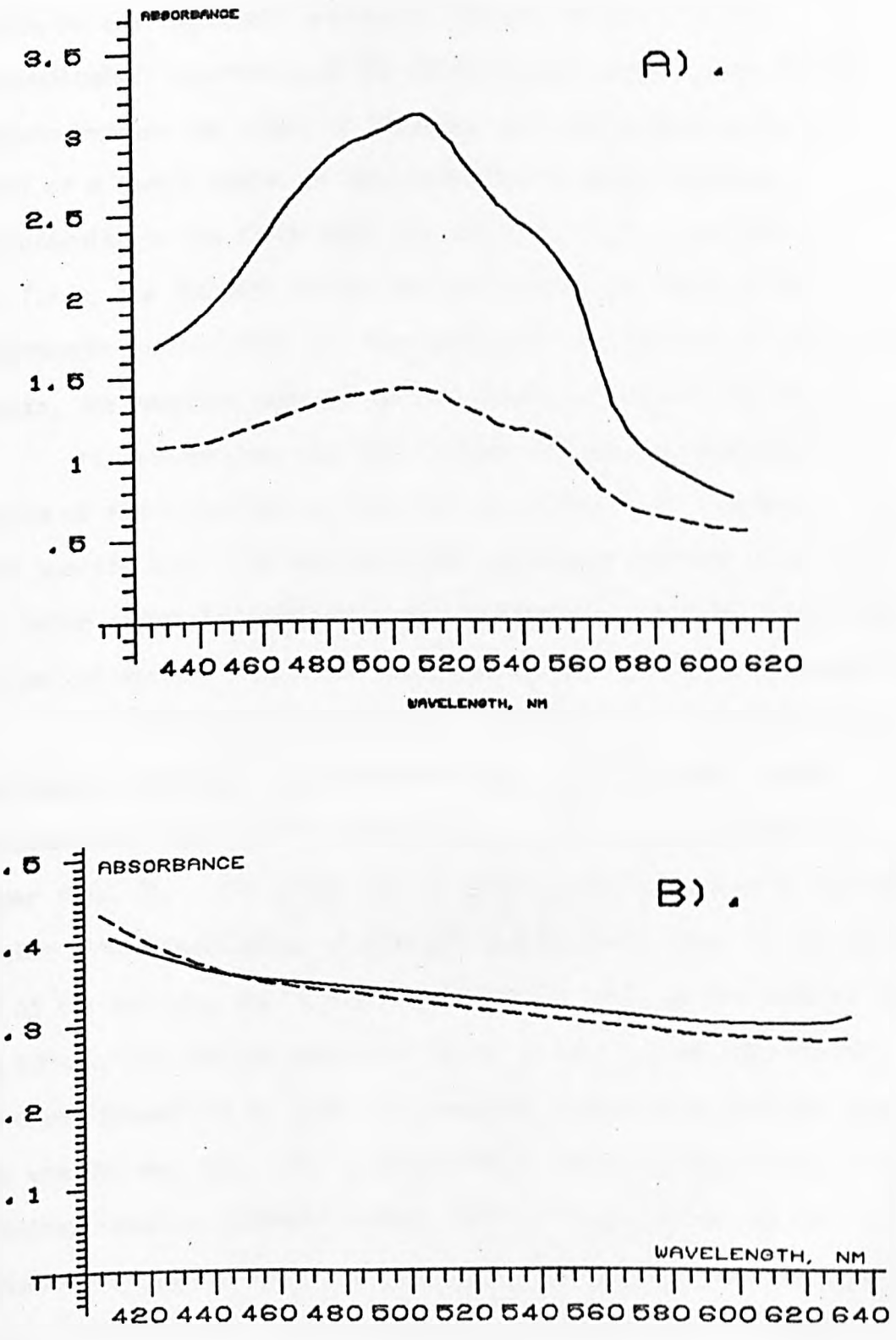

FIG. 7.3. FIBRE ABSORPTION SPECTRA: A. ADRIAMYCIN-DNA FIBRE (P/D=50) AT 92% RELATIVE HUMIDITY. B. CONTROL DNA FIBRE AT 92% RELATIVE HUMIDITY

Upon increasing the relative humidity, the general tendency of the absorbance of both fibres and fibre sections is to decrease, due to the dilution effect caused by the swelling of the DNA. This effect is visible in the "parallel" absorption spectra from Fig. 7.4/b. The "perpendicular" absorbance of the fibre section (Fig. 7.4/a) did not decrease because the effect of dilution was counterbalanced by the effect of a larger number of drug molecules becoming oriented perpendicular to the fibre axis (see Section 7.2.3). As seen in Fig. 7.4/c, the dichroic ratios obtained taking the ratio of the corresponding values from the "perpendicular" and "parallel" absorption spectra, are constant over the entire absorption band of the drug.

It is estimated that the dichroic ratios calculated from spectra of fibre sections are accurate to within $\pm$ 2%. However, with fibre spectra (Fig. 7.3) one faced the additional problem of the base-line being translated vertically and inclined due to light scattering and the cylindrical lens effect produced by the fibre (see Section 3.5).

A correction for the vertical translation of the spectra was performed by drawing a horizontal baseline through a point of the spectrum where the drug did not absorb, eg. 600 nm, as suggested by Fraser (Ref. 3). The values of the dichroic ratios quoted in the next section were determined at wavelengths sufficiently close to the 600 nm end of the spectrum (eg. 550 nm, the shoulder band, in the case of ADM, and 520 nm, the maximum absorbance peak, in the case of EB), so that the error introduced by using a horizontal, rather than inclined base-line was not serious. The dichroic ratios obtained upon using inclined baselines would be slightly larger, but such a procedure was not considered of being beneficial because of the arbitrary way such base-lines could be drawn. In general, it is estimated that the fibre dichroic ratios were obtained with an accuracy of better than $\pm$ 8%.

ABSORPTION SPECTRA AND DICHROIC RATIOS OF AN ADM-DNA FIBRE SECTION.

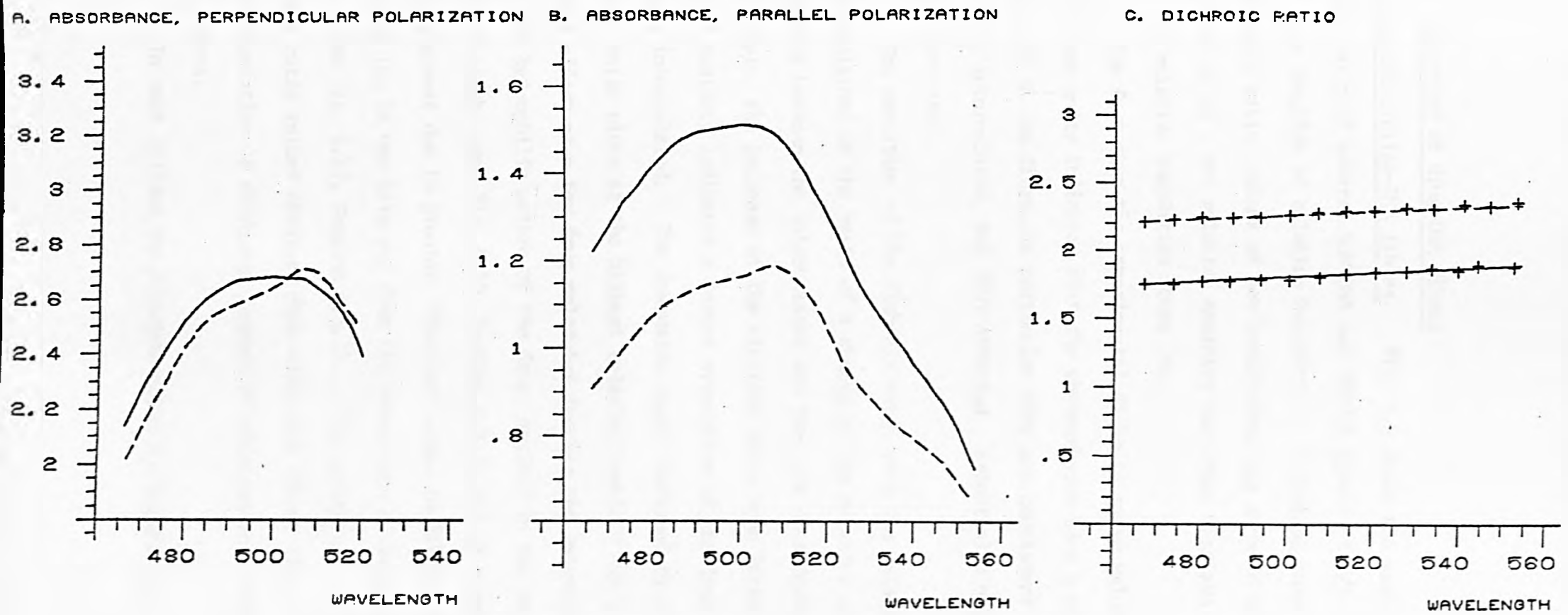

FIG. 7.4. DICHROISM OF AN ADRIAMYCIN-DNA FIBRE SECTION (P/D-5.6) AT ROOM HUMIDITY (FULL LINE) AND 85% RELATIVE HUMIDITY (DASHED LINE).

7.2.2 Dichroism of drug-DNA fibres

7.2.2A Anthracycline-DNA fibres. Fig. 7.5 shows the variation of the dichroic ratio of several ADM-DNA and DM-DNA fibres of P/D ratio equal to 50 as a function of relative humidity. A typical curve starts with low dichroic ratio values at low humidities, has a rapid increase in the region of 80 - 90% relative humidity and often displays a downwards slant for relative humidities above 90%.

The fact that the experimental dichroic ratio values are greater than unity indicates that the chromophores have a preferential orientation in the fibre, in particular they are consistent with the drug being intercalated, and thus oriented essentially perpendicular to the fibre axis.

The variation of the dichroic ratio with the relative humidity may be explained on the basis of a change in the relative distribution of the drug between the intercalated and free (or outside-bound) states. In principle, the increase of the dichroic ratio upon increasing the relative humidity indicates a larger proportion of the drug molecules becoming intercalated. The downwards slant displayed by several dichroic ratio plots at the highest relative humidity may be the combined effect of a few drug molecules leaving the intercalated state (viz. the hydrophilic nature of the drug, noticed in the variation of the helix pitch - see Fig. 6.10, Section 6.2.2, and of a greater degree of misalignment due to greater 'fluidity' under conditions of high hydration (as it was inferred from the appearance of some birefringence plots - see Fig. 5.13, Section 5.3.3). The variability of the dichroic ratio values obtained from different fibres (Fig. 7.5) may be the manifestation of different degrees of misalignment of the DNA in these fibres.

In what follows the interpretation outlined above will be

DICHROISM OF ADM-DNA & DM-DNA FIBRES

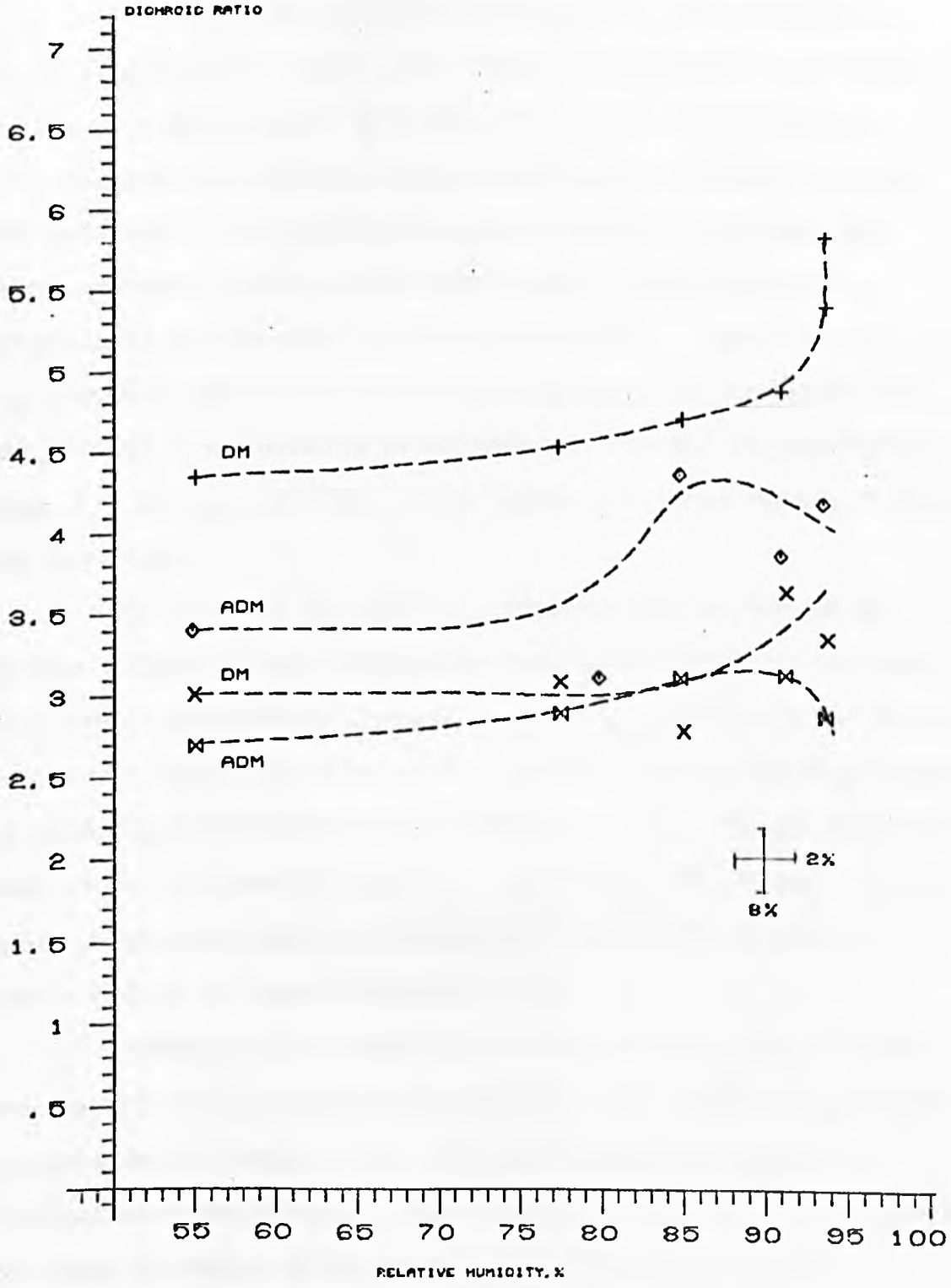

FIG. 7.5. DICHROIC RATIO VS. RELATIVE HUMIDITY OF SEVERAL ADM-DNA AND DM-DNA FIBRES, P/D-50 .

tested quantitatively in conjunction with the data derived from the X-ray diffraction studies (Section 6.2.2).

It will be recalled that according to the first treatment of the X-ray diffraction results, the change in the pitch of the DNA helix was due to a variation (of the order of 35 - 55%) of the fraction of drug molecules intercalated, whereas according to the second treatment, the variation of the helix pitch was mainly due to a conformational change undergone by the DNA while the change in the fraction of intercalated drug was small (of the order of 10%). Two values for the unwinding angle at the site of intercalation were considered (12^{o} and 26^{o}) and it was possible to estimate the fractions of intercalated drug, f_{max} and f_{min}, existing at the highest and lowest relative humidities in each case.

The values of f_{max} and f_{min}, togather with the maximum and minimum dichroic ratios obtained from each curve in Fig. 7.5 were used to calculate the theoretical values D_{int} and D_{out}, which are the dichroic ratios that would be recorded if all the drug molecules were intercalated or outside-bound respectively (see Section 7.1.3). The results of the analysis are tabulated in Fig. 7.6. Each of the four columns of the table contains the results corresponding to one of the numerical predictions of the X-ray diffraction study.

Considering the intercalated species and assuming a 5^{o} value for the tilt of the intercalated chromophore, the gaussian misalignment parameter corresponding to the calculated dichroic ratio D_{int} was obtained using the theoretical simulation from Fig. 7.2*. This parameter describes the degree of alignment of the helices in the fibre.

The value of D_{out}, corresponding to the non-intercalated drug,

---

* As mentioned in Section 6.1, the bases in the B-DNA are not oriented strictly perpendicular to the helix axis. For a tilt of the drug of 0^{o}, as opposed to the value of 5^{o} considered above, the corresponding gaussian parameters obtained on the basis of the dichroic ratios would be about 1^{o} larger.

may be interpreted in two ways. On one hand it may be assumed that the drug is loosely attached to the exterior of the DNA with an orientation approximately perpendicular to the helix axis, as suggested by the birefringence results (Section 5.3.3). Thus, the misalignment parameter corresponding to D_{out} should reflect both the misalignment of the helices in the fibre and the additional orientational freedom enjoyed by the outside-bound drug. On the other hand, it may be assumed that the drug is rigidly bound, thus retaining the same gaussian parameter of misalignment as the DNA. In this case, the corresponding angle of tilt of the chromophore relative to the helix axis may be obtained.

The results from Fig. 7.6 will be discussed separately for the two modes of treating the X-ray diffraction data.

I The treatment predicting a large variation in the fraction of intercalated drug

If the unwinding angle is 12^{o} (the first column in the table), the gaussian parameters of misalignment of the intercalated drug (and thus of the DNA) should be in the range of 18^{o} - 25^{o}. Considering the externally bound drug, if it is preferentially oriented perpendicular to the DNA helix, its gaussian spread of orientations should have a half-width 4^{o} - 5^{o} larger than that of the DNA; alternatively, if it is rigidly bound, its angle of tilt relative to the DNA helix should be equal to about 20^{o}. (These figures, rounded up, are shown in the table under the corresponding dichroic ratio values).

It should be noted, in the one hand, that the misalignment parameters of the DNA vary from one fibre to another, thus accounting for the spread of the experimental dichroic ratios obtained from different fibres, as already envisaged in the qualitative discussion

at the beginning of this section. The difference between the gaussian parameters characterizing the "best" and "worst" fibre is 7^{o}. At the same time, the values of the gaussian parameters are of the right order of magnitude compared to the half-width of the angular spread of the reflections in the X-ray diffraction patterns. On the other hand, the parameters which describe the orientation of the outside-bound drug relative to the DNA, namely the additional orientational freedom measured by the increment of the misalignment parameter, or the predicted binding angle, are remarkably consistent from one fibre to another.

Similar considerations hold if the unwinding angle was assumed to be equal to 26^{o} (the second column in the table).

As an average of the two cases, i.e. if the unwinding angle had an arbitrary value, intermediate between 12^{o} and 26^{o}, the gaussian parameter of misalignment of the DNA would be of the order of $20^{o} \pm 5^{o}$; the non-intercalated drug would either be loosely bound, essentially perpendicular to the DNA helix, with an additional orientational freedom of $7^{o} \pm 3^{o}$, or would be rigidly bound to the DNA with a tilt angle of 20^{o} - 25^{o}. Of course, the actual mode of external binding could be a hybrid of these two extreme situations, which set the boundaries to the acceptable angles of tilt and degree of "wobbling" of the chromophore.

II The treatment predicting a small variation in the fraction of intercalated drug.

According to this treatment, the fraction of intercalated drug at the highest humidity is the same as before, but the fraction of molecules intercalated at the low humidity is considerably higher than under the previous treatment.

For the 12^{o}-unwinding case (the third column in the table)

one obtains the same misalignment parameters for the DNA helices as under the previous treatment. Considering the non-intercalated drug, the fact that the values of D_{out} for all the fibres are close to unity clearly indicates that under this treatment the drug should be free, randomly oriented.

Finally, in the 26^{o}-unwinding case (the fourth column in the table), the D_{int} values are too high to be acceptable. For example, the value $D_{int} = 61$ implies a gaussian parameter equal to $\sim 5^{o}$. It is doubtful that under these circumstances the meridional reflections in the X-ray diffraction patterns would be recorded, since a 5^{o} tilt of the helices might not be large enough for the non-zero region of the Fourier transform corresponding to the meridional reflection to intersect the sphere of reflection. Therefore, under this treatment, the possibility of having an unwinding angle of 26^{o} (which was acceptable for the interpretation of the X-ray diffraction results) is rejected on the basis of the optical dichroism data. However, this treatment assuming only a small variation in the fraction of intercalated drug is applicable if the unwinding angle is close to 12^{o}, in which case it is predicted that the unintercalated phase, representing about 10% of the total number of molecules, is randomly orientated.

7.2.2B Ethidium - DNA fibres. The X-ray diffraction results presented in Section 6.3 have shown that, depending on the value assumed for the unwinding angle (12^{o} or 26^{o}), the fraction of EB molecules intercalated at the highest humidity (f_{max}) is, as with the anthracyclines, of the order of 100% - 70%. However, unlike the anthracyclines, all the EB molecules leave the intercalated state at low humidities ($f_{min} = 0$).

For an EB-DNA fibre of P/D ratio equal to 50 the variation of the dichroic ratio as a function of the relative humidity is shown in

Fig. 7.7. The maximum and minimum values were used in conjunction with the above values of the fractions of intercalated drug to calculate the theoretical dichroic ratios D_{int} and D_{out}.

The D_{int} values, in the range of 3.2 - 3.5, indicate a gaussian parameter of misalignment of the DNA helices of the order of 25^{o}. The value of D_{out} = 2.7 may be interpreted as arising from the drug molecules bound externally to the DNA helix, with a similar tilt as that of the intercalated drug and a gaussian parameter approximately 3^{o} larger than that of the DNA. It seems, therefore, that the outside mode of binding of EB is a specific and fairly rigid one, in which the chromophore adopts an orientation approximately perpendicular to the helix axis.

7.2.3 Dichroism of fibre sections

Fig. 7.8 shows the variation of the dichroic ratio of several ADM-DNA fibre sections as a function of the relative humidity.

The values of the dichroic ratios of the freshly-cut sections at room relative humidity are low, in the range of 1.7 - 2.0; a first increase of the relative humidity of the environment of these sections results in an irreversible increase of their dichroic ratio values. The variation of the dichroic ratio for subsequent cycles of the section through relative humidities not larger than 85% is reversible, qualitatively similar to that displayed by the fibres. The 85% value of the relative humidity represents the stage when the tendency of the section to swell begins to set up tensions in the specimen because the change of the dimensions of the section is mechanically prevented by the matrix formed by the embedding material. The dichroic ratios measured at relative humidities above 85% are lower (see Fig. 7.8/a), but a subsequent restoration of the relative humidity to a value below 85% results in a larger dichroic ratio than previously obtained at the

same humidity. Repeating this procedure, increasingly higher dichroic ratio values are obtained, approaching the values recorded from fibres (see Fig. 7.8/b).

It should be mentioned that similar dichroic ratio values (of the order of 1.7) have been reported for oriented films of acridine-DNA complexes by Neville and Davies (Ref. 6) and Kurucsev (Ref. 7). Dichroic ratios of the same magnitude have also been obtained from the UV absorption band corresponding to the DNA bases from films of pure DNA (Ref. 7).

The low dichroic ratios obtained from sections and films, as compared to fibres, indicate a lower degree of alignment of the DNA in these specimens. It seems that repeated cycling of the section through high and low relative humidities helps improving this alignment.

The even lower dichroic ratio values of the freshly-cut sections as well as the blue shifted spectra of these specimens, resembling the spectra of the free drug, indicate that most of the drug in these specimens is unbound, probably forced to dissociate from the DNA during the process of embedding of the fibre. The increase of the dichroic ratio during a first humidifying cycle is consistent with the drug becoming bound again, either intercalated or assuming an external mode of binding with a preferential oreintation to the DNA helix.

A very approximative analysis of the numerical data from the first-humidifying curves of a number of fibres was performed in terms of two components: a free phase, completely dissociated from the DNA and a bound phase, incorporating both the intercalated and externally bound drug. If one assumed that the fractions of bound drug at the highest and lowest relative humidities were 1.0 and 0.4 respectively (the second value being suggested by a comparison of the slopes of the

birefringence plots in Fig. 5.12), then the data were found consistent with the bound species being attached approximately perpendicular to the helix axis with a misalignment parameter of the helix of 30^{o}, and the unbound species adopting a tilt of -30^{o} (the same as the angle of ascent of the helical groove) and the same misalignment parameter.

The results of this calculation suggest that if the drug molecules are completely dissociated from the DNA, as was suggested above, the drugs would tend to fill the helical grooves assuming an angle of tilt equal to the angle of ascent of the helix.

It is considered that this could also be the case with drug-RNA fibres. Indeed, it was found that the dichroic ratios obtained from synthetic RNA (polyI-polyC) fibres with EB and ADM were in the range of 1 - 2, which are consistent with the drug being accommodated along the helical grooves of the polynucleotide.

X-ray diffraction predictions for the fraction of intercalated drug		Treatment I, predicting large variation in the fraction of intercalated drug				Treatment II, predicting small variation in the fraction of intercalated drug			
		Unwinding angle 12° f_{max} = 100% f_{min} = 45%		Unwinding angle 26° f_{max} = 70% f_{min} = 35%		Unwinding angle 12° f_{max} = 100% f_{min} = 90%		Unwinding angle 26° f_{max} = 70% f_{min} = 60%	
Experimental dichroic ratio values		Calculated Values		Calculated Values		Calculated Values		Calculated Values	
D_{max}	D_{min}	D_{int}	D_{out}	D_{int}	D_{out}	D_{int}	D_{out}	D_{int}	D_{out}
5.80	4.35	5.80 (misal.18°)	3.6 (misal.23°) (tilt 20°)	8.0 (misal.15°)	3.4 (misal.25°) (tilt 25°)	5.80 (misal.18°)	1.1 (misal≥40°) (tilt 53°)	61.0 (misal. 5°)	1.5 (misal≥40°) (tilt 43°)
4.35	3.40	4.35 (misal.21°)	2.9 (misal.26°) (tilt 20°)	5.6 (misal.18°)	2.8 (misal.27°) (tilt 25°)	4.35 (misal.21°)	0.91 (tilt 55°)	17.5 (misal. 9°)	1.3 (tilt 48°)
3.15	2.70	3.15 (misal.25°)	2.4 (misal.29°) (tilt 20°)	3.7 (misal.23°)	2.4 (misal.29°) (tilt 25°)	3.15 (misal.25°)	1.0 (tilt 55°)	5.8 (misal.18°)	1.3 (tilt 48°)

FIG. 7.6 SYNOPTIC TABLE OF X-RAY DIFFRACTION AND DICHROIC RATIO RESULTS

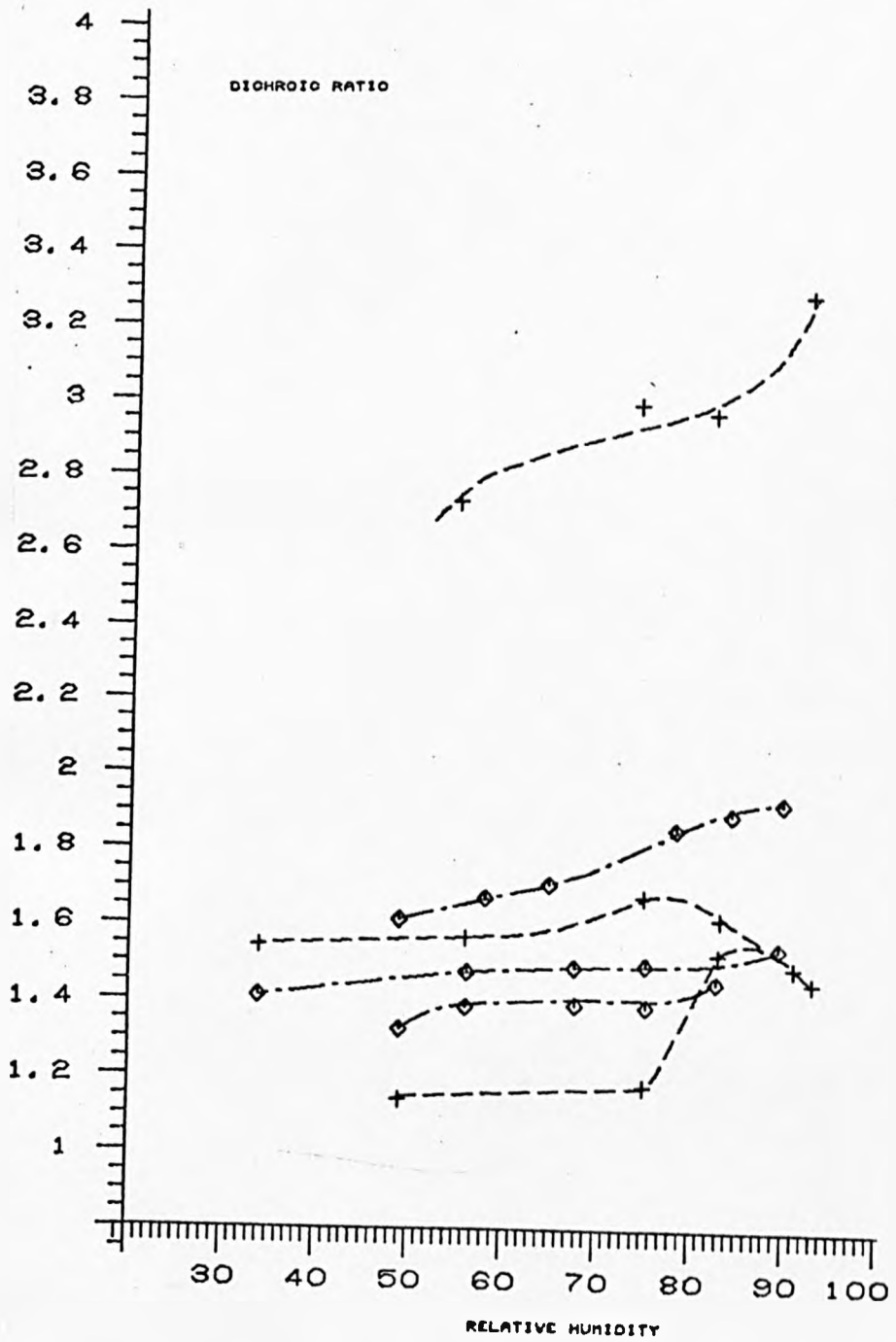

FIG. 7.7. DICHROISM OF EB-DNA FIBRES AND FIBRE SECTIONS
UPPER CURVE: EB-DNA FIBRE, P/D=50 ; LOWER CURVES: FIBRE SECTIONS WHICH UNDERWENT SEVERAL CYCLES OF INCREASING THE RELATIVE HUMIDITY: DASHED LINE, P/D=7; CHAIN LINE, P/D=12 .

FIG. 7.8 DICHROISM OF ADM-DNA FIBRE SECTIONS

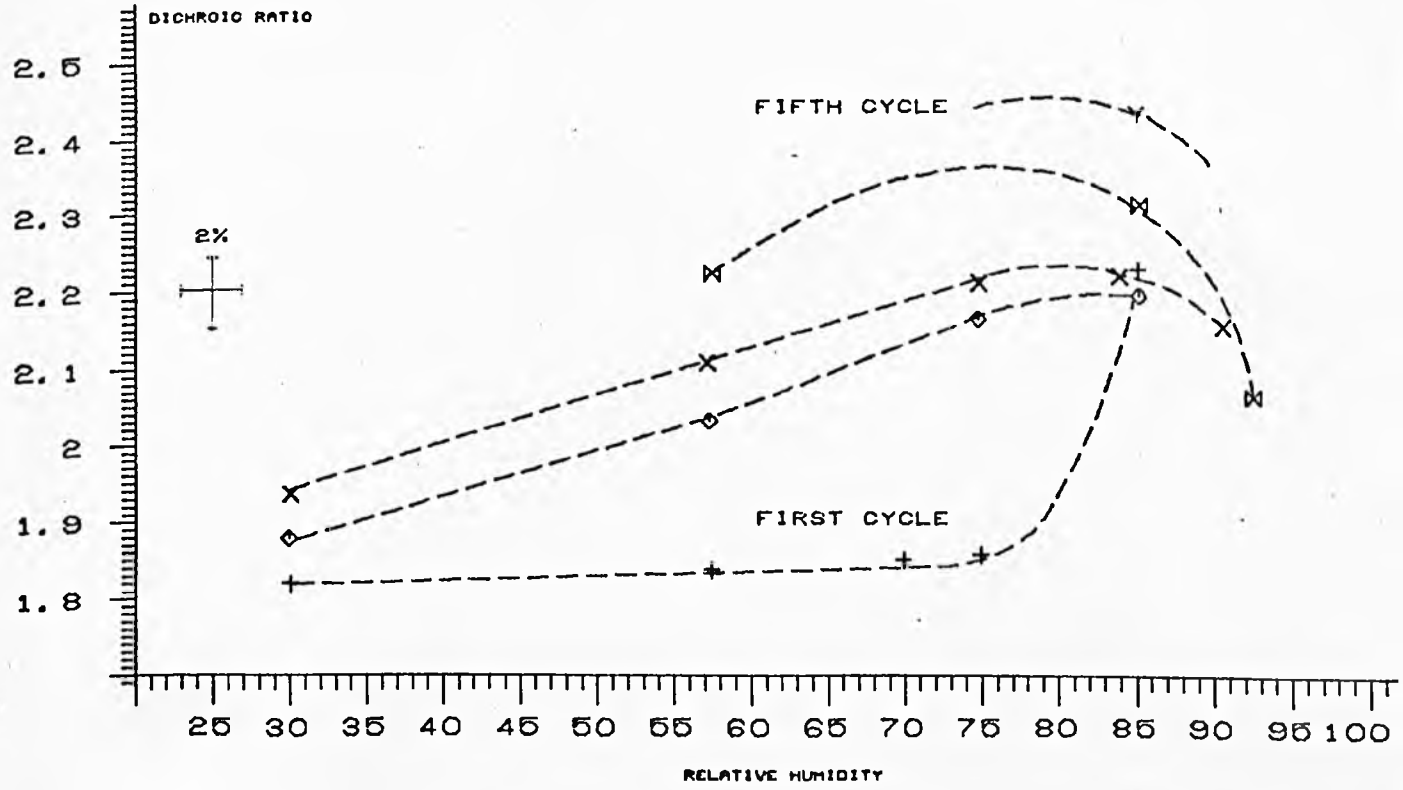

FIG. 7.8/A. REPEATED CYCLING OF AN ADM-DNA FIBRE SECTION (P/D=10.9) AT HIGH AND LOW RELATIVE HUMIDITIES .

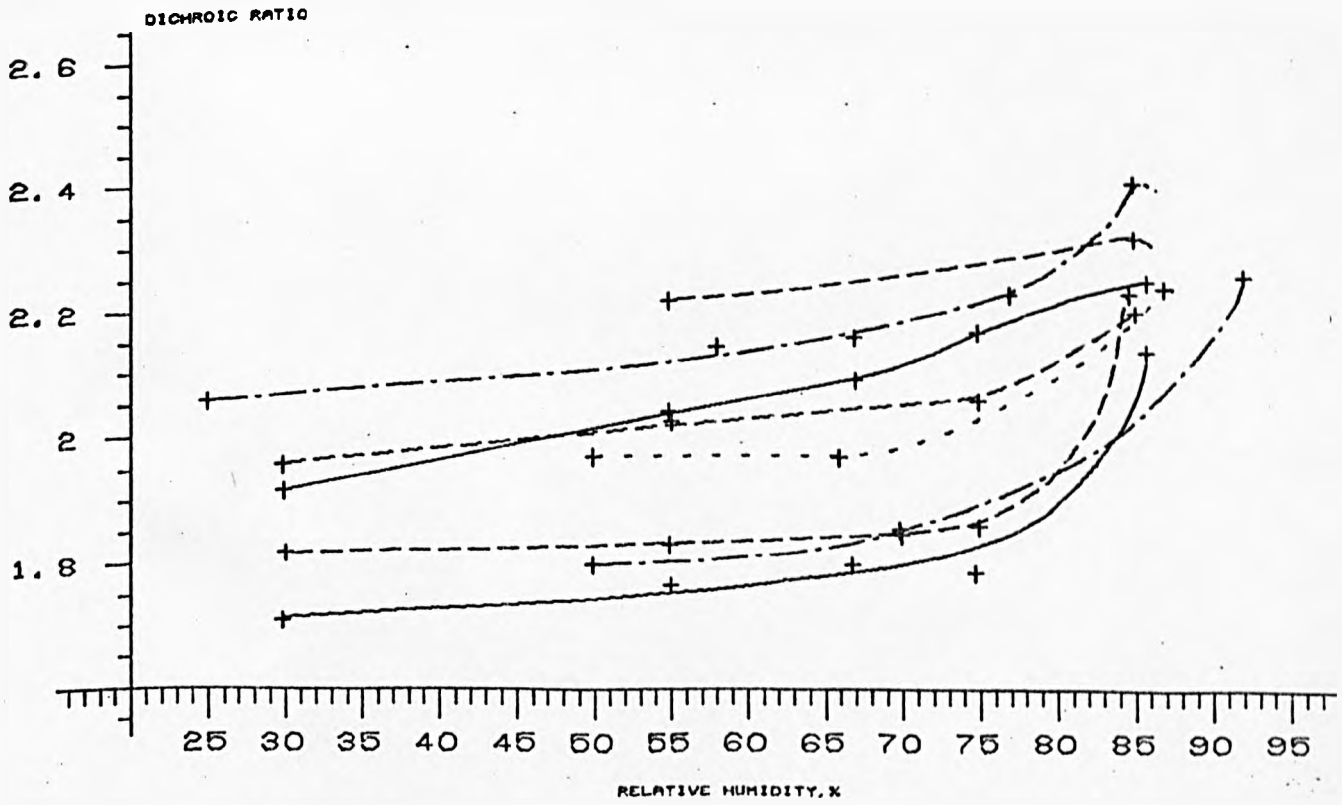

FIG. 7.8/B. DICHROISM OF OTHER FIBRE SECTIONS; FULL LINE: P/D=8.6; CHAIN LINE: P/D=5.6; DASHED LINE: P/D=10.9; DOTTED LINE: P/D=18.8.

REFERENCES

1. P.J. GIACOMONI, M. LE BRET; FEBS Lett. (173) 29, 227-230.

2. L.I. INGRAHAM, H. JOHANSEN; Archives of Biochemistry and Biophysics (1969), 132, 205-209.

3. R.D.B. FRASER; J. Chem. Phys. (1953) 21, 1511.

4. J. PILET, J. BRAMS; Biopolymers (1973), 12, 387-403.

5. J. PILET, J. BRAMS; Nature New Biology (1972), 236, 99-100.

6. D.M. NEVILLE, JR., D.R. DAVIES; J. Mol. Biol. (1966), 17, 57-74.

7. T. KIRUCSEV, J.R. ZDYSIEWICZ; Biopolymers (1971), 10, 593-599.

CHAPTER 8

CONCLUSIONS

The interactions of the drugs ethidium bromide, adriamycin and daunomycin with the deoxyribonucleic acid were extensively studied, in solution by absorption spectroscopy and in oriented fibre specimens by X-ray diffraction, linear dichroism and birefringence.

Considering the X-ray diffraction study (Chapter 6), the previous investigations on intercalation (Ref. 1 and Ref. 2) have been extended by showing that the pitch of the DNA helix varies as a function of relative humidity in a step-wise fashion between two plateau regions. This variation reflects a change in the distribution of the drug molecules between the intercalated and non-intercalated states; a distribution which is determined by the magnitude of the hydrophobic drive towards intercalation, that is, on the degree of hydration in the fibre. The plateau region at low humidities reflects the slow variation of the hydration of the helices, paralleled by similar slow variations of the other microscopic and macroscopic properties of the fibre, the intermolecular separation, fibre dimensions and birefringence (Chapter 5). The high humidity plateau reflects either the situation in which all the drug molecules present in the fibre are intercalated, or a state in which no nett increase in the fraction of drugs intercalated is possible. Such a situation would arise if the effect of the forces opposing the intercalation (forces which derive from the hydrophilic nature of the substituents to the drug molecule) became large enough, so that the effect of the hydrophobic forces was counterbalanced. Due to this uncertainty in the maximum fraction of drugs bound, an absolute determination of the unwinding angles of the DNA helix at the site of intercalation was not possible. However, the

quantitative interpretation of the pitch values has provided the figure of 12^{o} ($\pm 3^{o}$) as the lower limit to the unwinding angles. This figure corresponds to the first possibility, i.e, when all the drug molecules are intercalated at the highest humidity. The 12^{o} value fitted the data for both ethidium bromide and the anthracyclines.

For the study of the optical properties of the specimens, a single-beam microspectrophotometer system was built, with which absorption spectra of small areas of fibres and fibre sections could be recorded. As expected, only fibres of relatively low drug content could be measured directly due to the very large concentration of absorbing material in such specimens. One of the problems encountered with the fibres was the light scattering, which shifted the baseline level in an uncontrollable fashion. However, consistent results were obtained if corrections for this effect were applied by referring the baseline to a region of the spectrum where the drug did not absorb. For specimens of large drug content, the use of fibre sections was adopted. Although the recording of the absorbance of the sections did not raise any of the above problems, it was found that the treatment during the sectioning caused a lower degree of orientation in the specimens. (This could be improved by cycling the section through high and low relative humidities).

By combining quantitatively information obtained using X-ray diffraction and optical techniques, the way of looking at fibres in general, and at the state of the drug molecules in drug-polynucleotide fibres in particular, has changed. At one hand the misorientation of the polynucleotide helices in the fibre was considered explicitly; on the other hand, in the case of ethidium bromide and anthracycline-DNA fibres, it is now possible to talk in terms of an intercalated and an externally bound species, rather than in terms of intercalated and free

drug.

The misalignment of the polynucleotide helices in fibres has to be introduced as a parameter in the analysis of the dichroism and birefringence results, the other parameters being the orientation relative to the helix axis of the anisotropic groups (polynucleotide bases or drug chromophores) and, in the case of birefringence, the relative magnitude of the form term. Theoretical simulations of these quantities (presented in Chapters 5 and 7) were based on a fibre model according to which the polynucleotide helices (or bunches of helices) are oriented in a gaussian fashion about the fibre axis. This model is thought to be a more realistic representation than the previous models in which the helices in the fibre were considered to be perfectly aligned, except for a fraction which were randomly oriented. The experimental data was found to be consistent with a misalignment parameter of the helices of the order of 20^{o}, that is to say the majority of polynucleotide helices in the fibre were oriented within a cone of semiangle 20^{o}. It would be interesting to be able to compare this value with independent estimates from the angular extension of the diffraction spots in the X-ray diffraction patterns. However, such estimates are not readily obtainable, especially from the semi-crystalline patterns, and an investigation of this effect is suggested for the future.

The value of the combined X-ray and optical study, in relation to the state of the drug in the fibre, lies in the fact that it provides both a check on the validity of the X-ray diffraction interpretation (referring primarily to the intercalated drug), and information about the non-intercalated species. In the case of ethidium bromide, it was shown that the non-intercalated molecules were externally bound, essentially perpendicular to the DNA helix, with an orientational freedom

of about 3^{o}. It is believed that a similar external mode of binding exists in the case of the anthracyclines, although at present there persists an uncertainty, caused by the existence of two possible interpretations of the X-ray diffraction data (the pitch values) obtained at low relative humidities (see Sections 6.2.2A and 6.2.2C, and a recap in Section 7.2.2A). It is suggested that a further study should be performed to decide which of the two possibilities is correct. If the DNA underwent a distinct B to A transition as the humidity was reduced, this would probably be sufficient to remove the existent ambiguity in the interpretation.

Unlike ethidium bromide, which tends to dissociate completely from the intercalated state at low relative humidities, some of the anthracycline molecules remain intercalated even under conditions of very low hydration. The range of humidities in which the drug molecules remain intercalated is greater in the case of adriamycin than in the case of daunomycin. This behaviour can be accounted for in terms of adriamycin forming an additional hydrogen bond to the DNA backbone, which offers the supplementary stabilization to the intercalated state. As it was pointed out in Section 6.2.2A, this interpretation provides a rationale at a molecular level of the enhanced chemotherapeutic activity manifested by adriamycin as compared to daunomycin.

It is considered that the approach developed in this thesis may be extended to future investigations of polynucleotide structure in general and drug-polynucleotide interactions in particular. A branch of interest might be the investigation of the birefringence of fibres of polynucleotides having various base compositions and salt contents. For this purpose, the fibre model and birefringence simulations presented in Chapter 5 should be used, and possibly made more explicit. The aim

should be to determine the contribution of the form term to the total birefringence of the fibre as a function of relative humidity and, also to obtain the normalizing factor which will place the theoretical simulations on an absolute scale. If the birefringence could be used quantitatively to obtain the parameter of misalignment in the fibre, this would reduce the number of unknown parameters and greatly facilitate the combined analysis of the X-ray diffraction and dichroism data.

Finally, it is considered that the characterization of polynucleotide-drug complexes has provided the basis for new model building studies and Fourier transform calculations in terms of DNA models containing both intercalated and outside-bound drug molecules. These model building studies should aim towards finding a stereochemically acceptable way of attaching the drugs to the DNA, consistent with the requirements for tilt and orientational freedom derived in Chapter 7.

REFERENCES

1. W.J. PIGRAM; Thesis (1968), London University.

2. W.J. PIGRAM, W. FULLER, M.E. DAVIES; J. Mol. Biol. (1973), 80, 361-365.